

Review

Engineering Dry Electrode Manufacturing for Sustainable Lithium-Ion Batteries

Mohamed Djihad Bouguern, Anil Kumar Madikere Raghunatha Reddy, Xia Li, Sixu Deng, Harriet Laryea  and Karim Zaghib * 

Department of Chemical and Materials Engineering, Concordia University, Montreal, QC H3G 1M8, Canada; mohammeddjihad.bouguern@mail.concordia.ca (M.D.B.); harriet.laryea@concordia.ca (H.L.)

* Correspondence: karim.zaghib@concordia.ca

Abstract: The pursuit of industrializing lithium-ion batteries (LIBs) with exceptional energy density and top-tier safety features presents a substantial growth opportunity. The demand for energy storage is steadily rising, driven primarily by the growth in electric vehicles and the need for stationary energy storage systems. However, the manufacturing process of LIBs, which is crucial for these applications, still faces significant challenges in terms of both financial and environmental impacts. Our review paper comprehensively examines the dry battery electrode technology used in LIBs, which implies the use of no solvents to produce dry electrodes or coatings. In contrast, the conventional wet electrode technique includes processes for solvent recovery/drying and the mixing of solvents like N-methyl pyrrolidone (NMP). Methods that use dry films bypass the need for solvent blending and solvent evaporation processes. The advantages of dry processes include a shorter production time, reduced energy consumption, and lower equipment investment. This is because no solvent mixing or drying is required, making the production process much faster and, thus, decreasing the price. This review explores three solvent-free dry film techniques, such as extrusion, binder fibrillation, and dry spraying deposition, applied to LIB electrode coatings. Emphasizing cost-effective large-scale production, the critical methods identified are hot melting, extrusion, and binder fibrillation. This review provides a comprehensive examination of the solvent-free dry-film-making methods, detailing the underlying principles, procedures, and relevant parameters.



Citation: Bouguern, M.D.; Madikere Raghunatha Reddy, A.K.; Li, X.; Deng, S.; Laryea, H.; Zaghib, K. Engineering Dry Electrode Manufacturing for Sustainable Lithium-Ion Batteries. *Batteries* **2024**, *10*, 39. <https://doi.org/10.3390/batteries10010039>

Received: 11 November 2023

Revised: 3 January 2024

Accepted: 17 January 2024

Published: 22 January 2024



Copyright: © 2024 by the authors. Licensee MDPI, Basel, Switzerland. This article is an open access article distributed under the terms and conditions of the Creative Commons Attribution (CC BY) license (<https://creativecommons.org/licenses/by/4.0/>).

1. Introduction

Carbon neutrality and sustainable development are at the forefront of our collective efforts to achieve clean energy. Modern energy networks can only be built with the help of secondary energy storage devices and significantly advanced batteries. In response, a focus has been placed on developing energy-dense, next-generation batteries. This growing need must be addressed by creating recycle-friendly designs. While mitigating the environmental impacts of spent LIBs, these designs promote long-term sustainable resource utilization [1–3]. Since the entrance of Sony into the market in 1990 [4], LIBs have significantly transformed various aspects of our daily lives; LIBs are the primary choice for energy storage devices due to their exceptional energy density, high power output, long cycle life, and reliability [5]. As production expenses keep decreasing and energy costs decline, LIBs are becoming increasingly prevalent in various applications such as electric cars (EVs), systems for storing energy for electrical grids, the progression of innovative grid technology, and the continuous integration of clean energy sources [6]. The global demand for EVs is experiencing a rapid rise, with a corresponding increase in the need for LIB cells [7]. In the United States, battery demand for vehicles grew by around 80%, even though electric car sales increased by only about 55%, in 2022 [8]. According to the World

Economic Forum (WEF), the demand for LIB cells is projected to increase to 2623 GWh/a by 2030 [9]. Additionally, according to Tesla's CEO Elon Musk, the future demand for LIB cells is projected to soar even higher. He envisions the need to reach an unprecedented scale of 10,000 GWh/year [10,11].

Despite LIBs being recognized as environmentally friendly energy storage solutions, their full potential for driving sustainable development has yet to be realized. This is primarily because of the persistent issue of toxic and volatile solvent pollution (N methyl pyrrolidine NMP) during the initial phases of electrode manufacturing. In recent years, there has been an accumulation of evidence highlighting the environmental impact of these solvents [12–14]. In response to these challenges, numerous battery researchers and manufacturers are actively working to eliminate the use of solvents in the electrode fabrication process [15,16]. Recent research has focused on a variety of emerging technologies that have the potential to lower the energy required to produce battery cells. These advancements aim to decrease the overall cost of production and also to reduce the CO₂ emissions associated with the manufacturing process [17]. Efforts to reduce energy consumption during battery fabrication have led to the exploration of suitable solvent (NMP) replacements, which can significantly decrease energy use [18]. Conventional wet electrode processing is a critical technique in the production of LIBs, characterized by its ability to ensure uniformity, scalability, and quality. The process involves the uniform application of a slurry mixture, which includes active materials and conductive additives, onto a current collector. This uniformity is essential for the consistent electrochemical performance of the battery cells. The process is designed for high scalability, allowing for the expansion of production to meet large-scale commercial demands. The use of solvents, such as NMP, is pivotal in achieving a homogeneous mixture, which translates into electrodes with superior adhesion and electrical connectivity. As a proven technology, wet electrode processing has undergone extensive refinement and optimization, making it a reliable and repeatable method within the industry; however, it suffers from many challenges, which we will see later in the disadvantages of the wet process. Several alternatives to conventional wet electrode processing methods are being explored, which include minimizing the use of solvents, recovering alternative solvents, employing aqueous processing, and developing solvent-free processing techniques [19,20].

One of the most promising technologies to overcome the challenges mentioned previously is dry electrode processing. Dry electrode processing is a manufacturing technique for LIBs that eliminates the use of solvents such as NMP. This method bypasses the conventional wet slurry coating process, thereby removing the need for extensive drying stages. Instead, it employs solvent-free methods to create the electrode [21–31]. With the dry process for fabricating higher mass-loading electrodes presenting these advantages, it stands as a novel method for LIB electrode production. This approach offers exceptional operational cost efficiency and energy conservation benefits when contrasted with the traditional solvent-based process. Additionally, it holds the potential to facilitate battery miniaturization, as the absence of solvents extends the upper limit for loading active mass [32–35].

Advancements in battery technology are pushing the boundaries of electrode capacity, with developments now achieving areal capacities beyond 6 mAh/cm². This reduces the number of layers within LIB stacks, resulting in a notable boost in the overall energy density of LIBs, exceeding 250 Wh/kg [36–39]. Simultaneously, this approach reduces the associated manufacturing costs [40,41]. Ensuring battery safety in the context of electrodes prepared via dry processing methods involves careful material selection, process optimization for uniformity, and addressing thermal management challenges. Understanding the differences in safety considerations between wet and dry processing methods is crucial for developing reliable and safe lithium-ion batteries.

These progressive LIBs are characterized by high energy densities and larger dimensions, making safety precautions an essential prerequisite [42–46]. The utilization of the dry process is essential in the continuous efforts to develop next-generation advanced LIBs

characterized by elevated energy density, extended cycling lifetimes, and exceptional safety standards. Contrasting dry electrodes with traditional wet coating methods presents a promising role, with the key advantage lying in their solvent-free operation, as illustrated in Figure 1. In most methods for manufacturing battery electrodes, the dry mixing of materials is a distinct step that often needs help to achieve uniformity, particularly on a large scale. This lack of homogeneity can result in variable battery performance. Furthermore, the process of handling and transferring these mixed powders to subsequent stages can introduce contamination or segregation, potentially compromising product quality. In contrast, melt extrusion stands out as it incorporates the mixing step within the forming process itself. This approach not only ensures the greater uniformity and improved quality of electrode materials but also brings environmental benefits, enhances scalability, and boosts the overall efficiency of the manufacturing process. Therefore, melt extrusion is emphasized as a superior method in this context.



Figure 1. Overview of benefits of using dry processes and the disadvantages of using wet processes in battery production.

1.1. Principal Parameters in Electrode Manufacturing for LIBs

(i) Areal capacity

Advanced batteries with exceptional areal capacity (mAh cm^{-2}) and flexibility are central in energizing the upcoming era of flexible and mobile electronic devices [47]. Most research efforts have been directed toward advancing high-capacity electrode materials, including lithium sulphide for the cathode and silicon for the anode [48–52]. Another option strategy includes improving the electrode structure to maximize the electrode's areal capacity (C/A), thereby increasing energy density; this pertains to cathodes and anodes, where C/A is calculated as $(\text{CSP} \times \text{M/A})$. Here, CSP stands for the electrodes' specific capacity (mAh/g), M represents their mass loading (g/cm^2), and A signifies the electrode's surface area [53–56].

The electrode's areal capacity is a critical factor influencing all cells' specific energy and energy density [57], as shown in the following equation [58]:

$$Eg = \left(\frac{V \cdot \text{mA} \cdot C}{\sum Wi} \right) \quad (1)$$

$$Ev = \left(\frac{V \cdot \text{mA} \cdot C}{\sum Wi / \rho_i} \right) \quad (2)$$

where E_g = specific energy (Wh/kg); E_v = volumetric energy density (Wh/L); V = average cell operating voltage (V); m_A = active material loading (g/cm^{-2}); C = active material capacity (mAh/g); W_i = weight of individual cell components (g/cm^2); and ρ_i = density of individual cell components (g/cm^3).

The areal capacity is a key performance metric for batteries used in practical applications because it directly affects energy density, power density, size, efficiency, cost, and thermal characteristics. Maximizing areal capacity is a complex challenge. High-capacity electrode materials, such as silicon, often experience significant volume changes during charge and discharge cycles. Managing this volume expansion without causing damage to the electrode or the battery cell is a significant challenge. Some approaches have been proposed and utilized to alter the areal capacity of electrodes [59–64]. H. Hong et al. created an electrode with carbon nanoparticles and metal/metalloid particles, using a surfactant and binder for structure, achieving over 450 mAh/g capacity at a 0.1 C charge/discharge rate [65]. The goal of utilizing a dry process in electrode fabrication is to achieve an areal capacity greater than 4 mAh/cm² while also attaining an energy density above 400 Wh/kg [66,67]. This targeted approach, which avoids liquid solvents in manufacturing, seeks to enhance energy storage capabilities.

(ii) Ionic tortuosity

Various factors influence the electrode configuration, including the utilized material's particle size distribution, porosity, pore size distribution, interfacial contact areas (among different material phases), and tortuosity [68–71]. Tortuosity and porosity are two straightforward parameters employed to capture the intricate microstructure of electrodes. However, the definition of tortuosity (τ) can vary across different literature sources. One common interpretation of tortuosity involves calculating the ratio between the shortest path for mass transfer between two specific points within the material and the direct linear distance between those points. In other words, tortuosity quantifies how much longer and more complex a substance's route is compared to the most natural, straight-line path between two points in the porous structure [72–74]. Tortuosity is a crucial input parameter within mathematical representations designed to predict and analyze battery performance [75]. The Bruggeman relationship is commonly employed for tortuosity estimation [76–79]. Within electrochemistry, numerous methods are available for measuring or calculating tortuosity [80].

It is widely recognized that both the distribution of pore sizes and the tortuosity of these pores substantially impact the electrolyte's ionic conductivity. This underscores the interconnected relationship between tortuosity and ionic conductivity in battery systems [81–83]. Several steps in the wet process, such as mixing, solvent evaporation, and introducing a polymer binder, profoundly impact the final material. These processes can lead to profound modifications in the material's morphology and a notable increase in its ionic tortuosity. Such alterations raise concerns regarding the material's structural integrity, as there is a potential for cracking and an increase in porosity, which may affect its performance and durability [84]. The dry process markedly reduces ionic tortuosity due to dry mixing [85].

In the study by Harimohan Erabhoina et al., the authors systematically examined the impact of altering the cathode composition through adjustments in the amounts of active materials, conductive agents, and ion-conducting components. They found that ball milling effectively reduces particle size and increases the homogeneity of the cathode material, enhancing the rapid movement of lithium ions within the electrode material. The scanning electron microscopy (SEM) examination showcased the emergence of intact, non-porous formations, with even the dispersion of conductive graphite across the electrode. In conjunction with a solid polymer nanocomposite electrolyte, this optimized cathode composition delivered higher initial discharge capacities even at elevated temperatures and high current rates [86]. The study underscores the dry process's pivotal role in achieving a harmonious balance between short-range and long-range conductive pathways, enabling high capacity at increased discharge rates.

(iii) Production suitability

The process of battery manufacturing includes these essential steps, together forming the complete production cycle. The preparation of necessary electrode materials proceeds with the skillful assembly of individual cells. It culminates in the intricate electrochemical processes that empower the battery's crucial energy storage and controlled release functions. These interdependent stages ensure the creation of reliable and efficient battery systems. The initial production phase for standard electrodes primarily employs the slurry coating method, a comprehensive process involving key steps such as slurry mixing, coating, drying, reclaiming solvent, calendaring, segmenting, and vacuum drying [87,88]. The numerous constraints associated with contemporary coating methods stem from using liquid-based slurries [89,90].

Laboratory research endeavors for both dry spraying and dry calendaring technologies exhibit the potential to scale up consistently and transition seamlessly into a roll-to-roll production system. These dry coating methods maintain their core principles, offering a dependable and scalable production approach. All dry processing methods that are discussed in this work have effectively reached the pilot-scale production stage, demonstrating their practical feasibility. By leveraging industrial expertise and experience, it becomes possible to identify the key factors and benefits necessary for its successful industrialization [91]. The advantages of the dry process will be discussed in Section 3.

1.2. Disadvantages of the Wet Process

The dominant large-scale manufacturing of LIBs extensively depends on conventional wet processes, which are associated with several significant disadvantages.

(i) Costly manufacturing: In order to mix electrode slurry, NMP is used extensively, which increases the costs with a unit price ranging from USD 1.5–3.0 per liter in large volumes [92,93], and in the manufacturing of a 1 kWh battery pack, a substantial amount of about 4.40 kg of NMP is utilized as the solvent [94,95]. Both the mixing and drying processes, along with NMP recovery, incur considerable expenses [25,91,96].

(ii) Environmentally harmful: A 2017 report projected the production of lithium-ion batteries and linked them to the release of greenhouse gases (GHGs), which were likely to amount to 150–200 kg of CO₂ (equivalent) per kilowatt/hour (CO₂-eq/kWh). These emissions were measured in terms of their global warming potential (GWP), indicating the impact of these emissions on climate change [97]. NMP is a dangerous substance associated with potential reproductive risks [98,99]. NMP, being volatile and flammable, contributes to approximately 1000 kg of CO₂ emissions during the coating and drying process in producing a 10 kWh battery production line [94,100].

(iii) High energy consumption: The production line can manufacture 1.5 million Li-ion cells annually; these cells have a rated voltage of 3.7 volts and an energy content of 20.5 Ah [101]. To create a battery cell with a capacity of 32 Ah, approximately 13.28 kWh of energy is required. However, it is noteworthy that the procedure for drying the electrode, which involves the evaporation and subsequent retrieval of the solvent, consumes around 47% of the total energy used during production [102], approximately 42 kWh of electricity per 1 kWh of battery production in this process [103].

(iv) Extended duration: Drying can be time-intensive, with particular electrodes, e.g., LiFePo₄, requiring a protracted time of 24 h at 120 °C [104]; LiMn₂O₄ is dried for 24 h at 120 °C [105]. The post-drying parameters, including temperature and duration, significantly influence the remaining moisture and the physical and electrochemical properties of LIBs [106]. The length of the after-drying phase ranges from 2 to 16 h. The term is equally critical. A shorter drying time can be insufficient for complete moisture removal, whereas an extended period can lead to other issues, like binder migration, affecting the electrode's structural and electrochemical properties [107].

(v) **Limited coating thickness:** The coating thickness of electrodes in the industry is typically below 100 µm [108]. The wet process (WP) is susceptible to fragility and the formation of powder particle dispersion. For achieving the desired energy density in LIBs, it is essential to have positive electrodes with a thickness ranging from 100 to 200 µm [109]; achieving such thickness is challenging using the WP. During the drying process, crack forming and propagation have been observed in thick aqueous processed cathodes [110].

(vi) **Heightened and uncontrolled porosity:** Open porosity is crucial for effective electrode performance, as it allows the electrolyte to permeate and distribute evenly throughout the electrode structure [111]. The drying stage significantly affects the distribution and concentration of the binder within the electrode structure, which, in turn, influences the porosity of the electrode, heightening porosity through solvent evaporation [112]. In the WP by solvent evaporation, the porosity values of the uncalendared electrodes are measured to be approximately 56% [113].

(vii) **Incompatible with sulfide-based all-solid-state batteries (ASSBs):** Certain solid-state electrolytes, such as sulfides and garnets, can be sensitive to the solvents used in the WP [114,115]. Sulfide-based solid-state electrolytes can react with the solvents, changing their chemical composition and structure and adversely affecting their ionic conductivity and overall performance [116,117].

(viii) **Other electrolytes and electrode materials:** The impact of absorbed solvents on solid electrolyte and electrode materials in wet processes, particularly in the context of scaling up sulfide-based solid-state batteries, presents several significant challenges: high interfacial resistance due to solid particle contact and the combination of slurry solvent and polymeric binder [118]. However, finding a compatible combination that does not react adversely with the sulfide electrolytes is challenging. The solvent and binder must not only be chemically compatible but also need to ensure the uniform dispersion and adherence of the electrolyte particles to the electrode materials.

1.3. Progression Phases and Selective Approaches to Electrode Fabrication

Before delving into the solvent-free procedures, exploring several of the most notable substitute options (to the existing wet processing methods) and their drawbacks is worthwhile; many researchers have proposed techniques, such as the following:

(i) **Reduce solvent:** Adopting an extruder offers notable advantages in terms of scalability and solvent reduction efficiency, demonstrating the potential to decrease the quantity of solvent by as much as 50% in comparison to conventional planetary mixers; this solvent reduction strategy yields dual benefits, as it reduces the solvent content and contributes to a substantial 50% reduction in the constant rate period; this reduction in drying time signifies a significant enhancement in the overall manufacturing process efficiency [119]. This approach presents benefits regarding the decrease in expenses, but it is imperative to recognize that its environmental effects continue to be worrisome.

(ii) **Alternative solvent recovery or the substitution of the solvent:** The quest for substituting NMP as a prevalent solvent is marked by the exploration of several viable alternatives, such as N-Butyl pyrrolidinone [120], Dimethylformamide and Dimethyl sulfoxide [121,122], Diethylamide and Ethyl Lactate [123], Dimethyl isosorbide, and Polar Clean [124]. NMP can be recovered as a liquid rather than gas using suitable washing agents such as acetone or ethanol. These agents should be able to dissolve NMP effectively, and these liquids should facilitate the separation of NMP from other components in the electrodes; acetone can cause the PVDF polymer to swell under particular conditions [125]. A study by Brigitte et al. revealed that substituting NMP with alternative chemicals, such as dimethyl sulfoxide and sulfonate, can significantly reduce pollution; specifically, these alternative chemicals resulted in a 44% and 47% decrease in pollution levels [126]. Although the recovery step enhances the financial viability of the process, it requires energy and significant capital investment [103].

(iii) Aqueous process: There is burgeoning interest in transitioning from NMP to water as the main solvent in processing; water has gained extensive usage as a solvent for both cathode and anode elements [127–130]. This process is considered for electromobility applications and has been applied to fabricate LIB cathodes from various materials, including LiCoO₂ and LiFePO₄ [131]. Although aqueous-based processing is cost-effective, it presents numerous issues, including low wettability [110,132,133] and the corrosion of current collectors, particularly in the case of aluminum [127,129,134,135]. Ni-rich cathode active substances react with water, forming hydroxide and carbonate compounds [136]. Some strategies to alleviate corrosion involve adding phosphoric acid to the slurry, which effectively reduces the alkalinity of the mixture [137–140]. However, many of these solutions are not environmentally favorable, given that substances like phosphoric acid are both toxic and costly [141]. Theoretically, aqueous LIBs cannot work in the presence of O₂, so eliminating oxygen is a crucial prerequisite for high performance [142]. Even sealed aqueous LIBs carry the risk of thermal runaway, a safety concern that needs to be addressed [143].

(iv) Solvent-free (SF): SF procedures have garnered growing attention as an up-and-coming solution to reducing manufacturing costs and enhancing electrode quality. There are methods for fabricating SF electrodes, with the most prevalent approach being **Vapor deposition:** This technique is primarily employed for producing thin-film ASSBs; in this technique, base materials are transformed into vapor and then deposited onto a substrate, with the advantages of electrode quality summarized in some articles and reviews [144–149]. However, the utility of the vapor coating technique is confined to the production of small-sized electrodes, primarily catering to microelectronic components and advanced integrated circuits. The costly equipment, intricate film-formation procedures, elevated energy usage, and limited areal capacity hinder its applicability in EVs. **Three-dimensional (3D) printing:** The notion of 3D printing is evolving, enabling the creation of materials with distinctive morphologies, and it has also found application in the field of batteries [72,150–155]. Three-dimensional printing that is akin to vapor deposition is presently unsuitable for large-scale electrode manufacturing and applies only to specific scenarios like wearable devices and microelectronics. However, 3D printing is only suitable for some industrial patch production adaptation; its potential lies in applications such as microelectronics or flexible, wearable devices [156]. A detailed explanation of the three methods (**dry spraying deposition, binder fibrillation, and extrusion**) will be provided in Section 3.

2. Status of Lithium-Ion Batteries

2.1. Electrodes

The fundamental process for manufacturing electrodes is where the active material, conductive enhancers, and binding agents (binders) (illustrated graphically in Figure 2) are thoroughly mixed in a planetary mixer, forming a homogeneous slurry; slot-die coating machines deposit the prepared slurry onto substrates. The anodes are electrodes where oxidation occurs during battery discharge and serve as the source of electrons; the anode is deposited on copper foil. The cathodes are electrodes, and this is where reduction occurs during battery discharge, which is the active material contained within the slurry deposited onto aluminum foil [157–160]. In order to initiate the exploration of processing technology, the essential focal point is to analyze the impact of the varying mixing sequences of source materials on the attributes of the negative [161] and positive [162] active materials within the electrode; this investigation will encompass an assessment of the mixing method employed [163] and the ratio of content used [164] to determine the electrode quality.

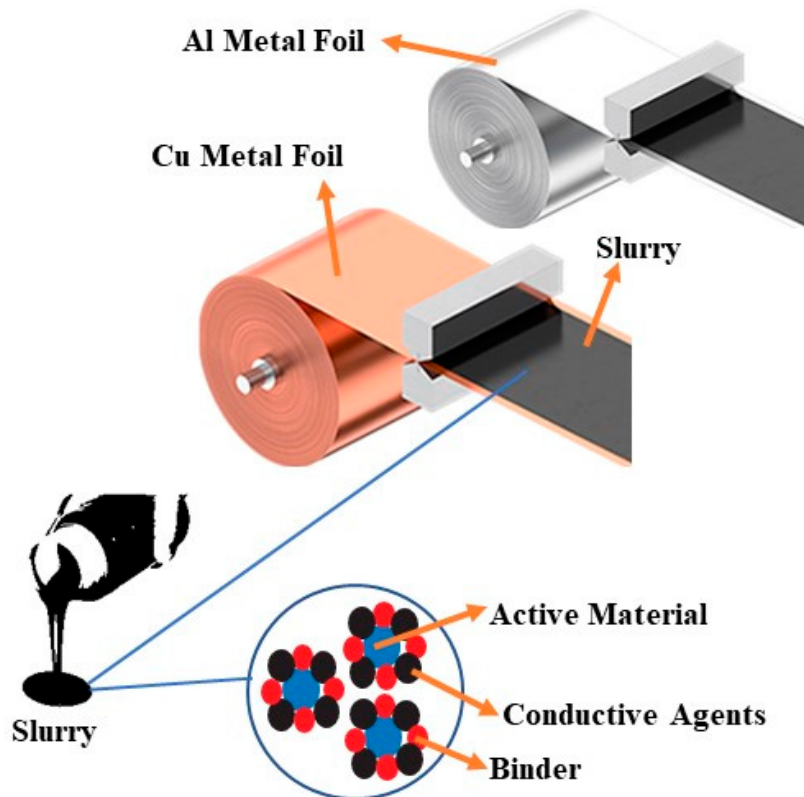


Figure 2. Illustration showcasing the trio of main elements within the LIB electrode.

2.1.1. Cathodes

Cathode materials represent the essential components of LIBs, influencing their performance and characteristics. Typically, they can be categorized into three structures: olivine-type ($\text{Li}(\text{M})\text{PO}_4$), layered ($\text{Li}(\text{M})\text{O}_2$), and spinel-type (LiM_2O_4), with M symbolizing a single or several transition metals [165,166]. Some of the most used cathode-active materials in LIBs are LFP, LCO, NMC, NCA, LMO, and LNMO [167]. Cathode materials are typically polycrystalline, consisting of numerous crystalline grains. However, there has been growing interest in single-crystal cathode materials [168–171]. Among the mentioned cathode materials, LFP is known for its relatively low cost. However, it requires additional processing steps, like applying a carbon layer on the surface to boost its electrical conductivity [172,173]. LFP generally exhibits favorable performance characteristics across various areas, but its energy density is on the lower side when compared to other cathode materials. It is noteworthy that LFP has frequently surpassed or come very close to its predicted capacity of 170 mAh/g [174].

Nevertheless, several of these cathode materials are more expensive. Certain alternative cathode materials, such as those employing layered structures like NCA (250 mAh/g), NMC (220 mAh/g), and LCO (200 mAh/g), exhibit a higher energy density [175–177].

High-capacity cathodes like sulfur (S) and oxygen/air cathodes provide the potential for even greater energy storage [178–183] but may have specific challenges associated with their use [184–187]. NMC cathodes are currently the most commonly used LIBs. The momentum is increasing for NMC cathodes with a high nickel content and enhanced capacity, notably the types 532, 622, and 811. However, cobalt is a valuable and limited resource because of its high cost, and it poses economic and sustainability challenges for the battery industry. In recent times, there has been a growing focus on the exploration and development of cathodes with reduced or zero cobalt content [188–194]. The increasing demand for LIBs, particularly in the electric vehicle and grid-storage markets, is driving a change in the choice of materials, requiring increased energy density and cost-effectiveness [195].

2.1.2. Anodes

Graphite is the predominant anode material in lithium-ion batteries (LIBs), typically 92 wt% due to its numerous advantages, which include natural abundance, affordability, strong cycling stability, a specific capacity of 372 mAh/g, and high electrical conductivity [196–202]. A recent trend among battery manufacturers is to use anodes made from a combination of carbon and silicon, often in the form of SiO_x (silicon oxide); SiO_x offers natural abundance, cost-effectiveness, is eco-friendly [203,204], and exhibits a conductivity of approximately 6.7×10^{-4} S/cm and is often used as a supplementary active material in LIBs to increase the specific capacity of the anode. Using silicon-based materials as conversion materials in the anode (plus conductive materials) allows for a much higher capacity of 3597 mAh/g compared to graphite (372 mAh/g) [205–212].

In comparison, silicon offers a higher capacity and presents challenges such as significant volume changes during charge/discharge cycles, which can lead to mechanical stress and electrode degradation [213–220]. In addition to anode materials, LTO [221,222], when compared to graphite, offers several advantages, such as minimal volume change, enhanced lithium-ion mobility, no lithium plating, and fast charging [223–226]. Moreover, it possesses certain limitations, such as inadequate electrical conductivity ($<10^{-13}$ S/cm) at room temperature, limited capacity, and reduced volumetric energy density [227–233]. On the other hand, graphite, while being a common anode material, has its own set of challenges. It exhibits poor electrochemical performance at low temperatures due to increased resistance [234]. Despite these issues, graphite is still widely used because of its low volume change and high electronic conductivity.

2.2. Electrolytes

In rechargeable battery systems, electrolytes are essential in aiding the movement of ions. Throughout the charging and discharging process, they act as barriers preventing electron flow between the anode and cathode. Even though the electrolyte in an LIB is viewed as electrochemically active depending on the conditions within the battery, its ability to conduct ions and its chemical interactions with the electrodes, which results in the creation of a solid electrolyte interface (SEI), greatly influences the charge rate, cycle durability, and safety of LIBs [235–237]. The electrolytes used in LIBs encompass a variety of types, including organic liquid electrolytes (ethylene carbonate EC), ionic liquid electrolytes, aqueous liquid electrolytes (water as the solvent), inorganic solid electrolytes (ceramics materials), polymer solid electrolytes, and composite electrolytes (ionic liquid + liquid organic); these different electrolytes categories offer distinct characteristics and are suitable for various battery applications [238–242]. The latest development in LIB liquid electrolytes commonly utilizes ethylene carbonate (EC) as the preferred solvent; this choice is attributed to EC's ability to effectively dissolve various lithium salts and its notable dielectric constant, which facilitates superior ionic conductivity [243,244]. Frequently employed lithium salts in batteries include lithium hexafluorophosphate (LiPF₆) [239,245–247] lithium bis (trifluoromethyl sulfonyl) imid (LiTFSI) [248,249], lithium tetrafluoroborate (LiBF₄) [250–253], lithium perchlorate (LiClO₄) [254–256], lithium hexafluoro arsenate (LiAsF₆) [257–260], and lithium bisoxalato borate (LiBOB) [261–264].

The electrolyte widely favored by manufacturers and researchers for use in LIBs is LiPF₆ dissolved in a mixture of binary or ternary solvents comprising (EC) and linear carbonates such as diethyl carbonate (DEC), dimethyl carbonate (DMC), or ethyl methyl carbonate (EMC); these solvents increase the flash point of the electrolyte, enhancing its thermal stability and helping decrease the viscosity of the electrolyte solution [265,266]. In LIBs, a fundamental characteristic of the electrolyte is its ability to have elevated Li⁺ conductivity (σ_{Li}), ensuring the efficient transfer of lithium ions. Concurrently, it should exhibit minimal electronic conductivity to act as an insulator for electrons. For optimal rate performance in LIBs, the electrolyte should demonstrate a conductivity level of 10^{-3} S/cm when measured at an ambient temperature. This elevated Li⁺ conductivity is vital to ensure seamless ion movement between the anode and cathode of the battery

throughout the charging and discharging cycles. This conductivity enables fast and effective Li⁺ diffusion, allowing the battery to deliver desirable rate capabilities and high-power performance [267].

2.3. Separator

Batteries depend on separators to maintain mechanical and electrical separation between electrodes; batteries incorporate separators to thwart any potential short-circuiting between the electrodes effectively. The categorization of separators utilized in LIBs can be streamlined into four fundamental categories, determined by their structure, composition, and corresponding attributes, including a microporous membrane, composite membrane, non-woven mats, and gel polymer electrolyte membranes [268,269]. A comprehensive review has meticulously documented the advantages and disadvantages of each type of separator [270].

The use of polyolefins as a material for microporous separators addresses the shortcomings of traditional separators and satisfies the desired characteristics for LIBs. Polyolefins offer several advantages, including excellent mechanical strength, chemical stability, and thermal resistance. Polymeric materials like polyethylene (PE) and polypropylene (PP) or PE and PP are categorized as polyolefins [271–276]; these membranes are designed to be thin, typically less than 30 μm, and possess a microporous structure [277].

One advantage of using PE as a material in this membrane is its low melting point; PE can serve as a thermal fuse in LIBs when the temperature nears the polymer's melting point, which is 135 °C for PE and 165 °C for PP [278]. To enhance the safety and performance of the membranes, Celgard has developed a tri-layer material known as PP/PE/PP (patent: 1999) [279]. The separator should be as thin (20–25 μm) as possible while possessing the necessary physical strength. Additionally, the separator should exhibit 40–60% porosity to facilitate the efficient movement of ions between the electrodes and a pore size of <1 μm [269,280]. The separator in LIBs can play a significant role in enabling fast charging capabilities; several separator properties, such as electrolyte uptake (absorption) or wettability, contact angle, and surface, as well as the impact of the electrolyte solvent on modified mechanical properties, can influence the charging performance of LIBs [281–283]. Moreover, shrinkage refers to a reduction in size or volume that can occur in certain separator materials under high temperatures; the thermal shrinkage requirement for separators in LIBs is typically specified to be less than 5% after 60 min at 90 °C [284]. In order to improve the performance and characteristics of the separator, one common approach involves applying a silicon dioxide (SiO₂) and aluminum oxide (Al₂O₃) coating to polyolefin materials [285–287].

Additionally, other polymer materials are used for separators in LIBs; Table 1 summarizes the different separator materials and their characteristics and processes, such as being dry or wet (this will be provided in the next paragraph) and electrospinning [288]. Of particular significance is the necessity to comprehend the melting temperature, T_m, and glass transition, T_g, values of the polymers. This is pivotal because these factors impact ion transport within the polymer chains, with T_g and T_m playing a crucial role [289]. Additionally, it must be understood how property mechanics influence the intricate interplay of components within the battery system, and that stability is essential [290–292].

Table 1. Different separator polymer materials and their characteristics in LIBs.

Polymer Materials	Abbreviation	Molecular Formula	Tg (°C)	Tm (°C)	Tensile Strength (MPa)	Separator Properties	Process
Polyolefin: Polyethylene Polypropylene Tri-layer	PE PP PP/PE/PP	(C ₂ H ₄) _n (C ₃ H ₆) _n [293]	-100 -25 [293]	110 170 [293]	12–15 31–41 [294]	-Robust chemical stability; -Excellent electrochemical insulation capabilities; -Exceptional mechanical properties [295–298].	Dry and wet processes
Polyvinylidene fluoride	PVDF	(C ₂ H ₂ F ₂) _n	-35 [299]	171 [299]	45–55	-High temperature resistance; -High crystallinity; -Mechanical strength; -Electrical insulation and dielectric properties [300–302].	Electrospinning
Polyvinyl alcohol	PVA	(C ₂ H ₄ O) _n	85 [303]	230 [303]		-Good wettability; -A network pore structure [304].	Electrospinning
Polytetrafluoroethylene	PTFE	(C ₂ F ₄) _n	110 to 130 [305]	330 [305]	10	-High thermal stability;-Good mechanical strength; -Low electrical conductivity [306].	Electrospinning
Polyurethane	PU	C ₂₇ H ₃₆ N ₂ O ₁₀	formulation	formulation	-	-Help mitigate interfacial degradation; -Enhanced battery performance [307].	Electrospinning
Cellulose	-	(C ₆ H ₁₀ O ₅) _n	-	-	-	-Strong electrolyte affinity; -Thermal stability; -Good wettability [308].	Electrospinning
Polyethylene terephthalate	PET	(C ₁₀ H ₈ O ₄) _n	-	-	-	-Thermal stability; -High tensile strength; -Stable electrochemical performance [309,310].	Electrospinning

2.4. Fabrication of Microporous Separator Materials by Using Dry and Wet Techniques

Thin, porous structures hold significant commercial value. Their predominant application is serving as a separator in energy systems, particularly batteries. Porous compositions can be categorized into two fundamental types: In the first type, pores lack interconnectedness, as seen in foams or cellular plastics. In the second type, intricate and winding paths extend between the surfaces of the structure [311]. The fabrication process of microporous films for LIBs separators, which typically use polypropylene and polyethylene, can be categorized into two main approaches: dry and wet. In the industrial sector, the primary manufacturing focus is on uniaxially stretched dry-processed PP membranes and biaxially stretched wet-processed PE membranes [312], as shown in Figure 3.

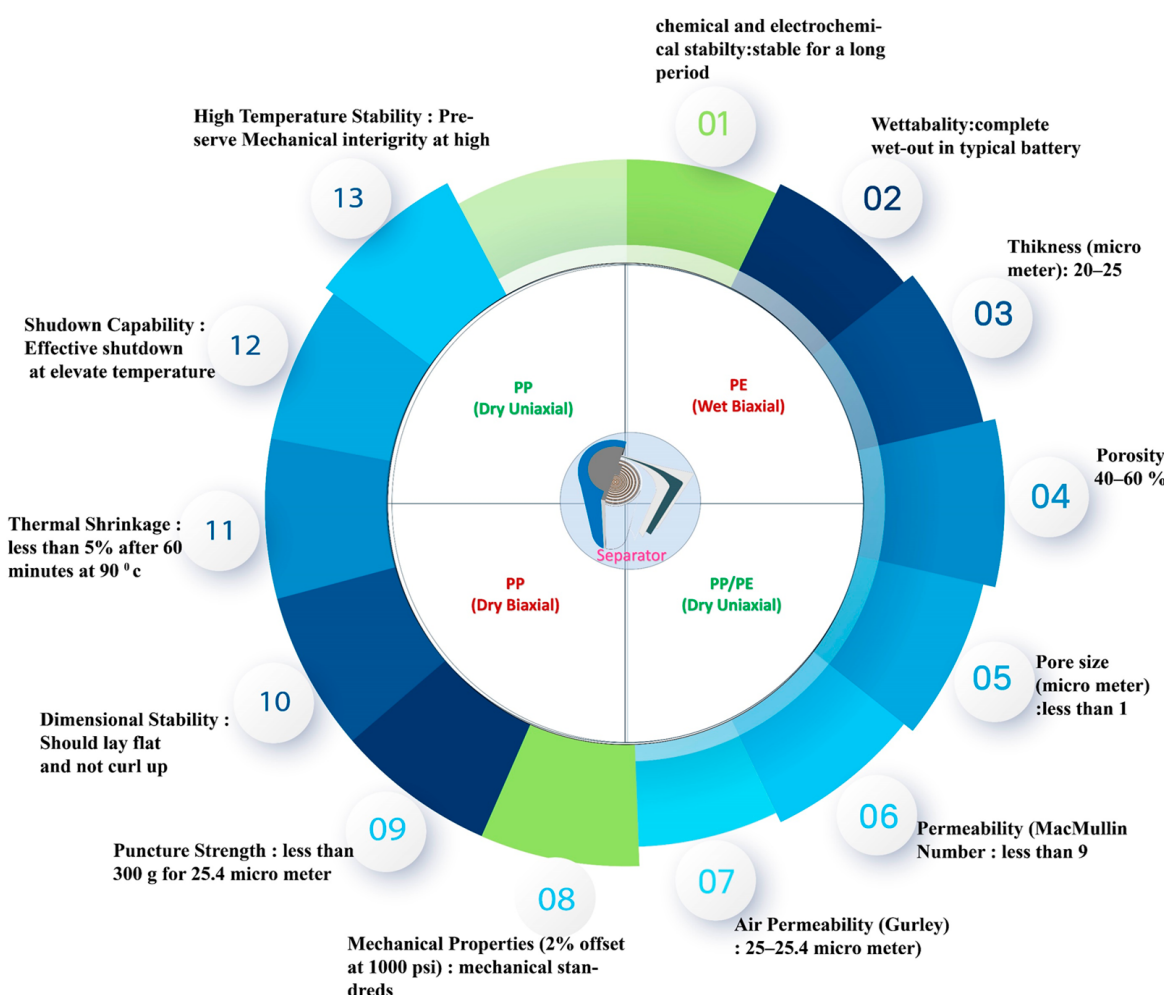


Figure 3. Different types of separators with requirements [313].

2.4.1. Wet Process

The wet process (WP) involves several sequential stages: mixing, melting, extruding, stretching, and eliminating additives (extraction), as shown in Figure 4. The mixture of polyolefin and solvent yields a uniform solution. This solution is extruded through a sheet die, giving rise to a gel-like film in the subsequent phase of separator production; following this, the gel-like sheet is oriented or stretched, typically in two directions. Eventually, the additives are eradicated through volatile solvents, culminating in the production of the final microporous product [314].

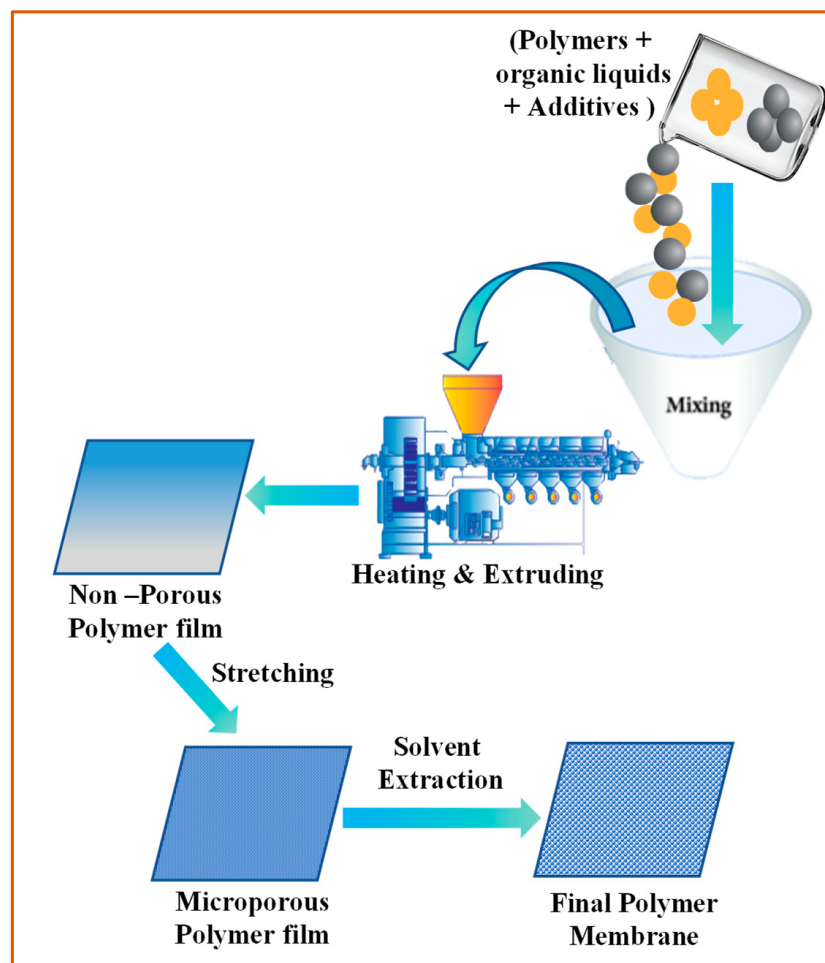


Figure 4. Flow chart of the different approaches involved in the production of microporous separators for the wet process.

PE is the predominant polymer utilized in the WP; the polymer component in the separator formulation can also consist of a blend of PEs with varying molecular weights [315]. The sequence of steps holds significant importance. Research indicates that membranes created via pre-extraction stretching exhibit a smaller average pore size and a more restricted range of pore sizes when compared to membranes formed using the post-extraction stretching process [316].

2.4.2. Dry Process

The dry process (DP) for producing microporous separators can be generally described as a three-step procedure: extruding, annealing, and stretching, as shown in Figure 5 [268]. The commercial PE and PP films produced through the DP can be obtained from Celgard LLC (Charlotte, NC, USA) [277]. Celgard offers products, such as Celgard 2730 and Celgard 2400, which are single-layer PE and PP, respectively. Additionally, Celgard presents separator materials, such as Celgard 2320 and Celgard 2325, which feature a tri-layer PP/PE/PP composition [279,316].

The choice between the dry and wet methods relies on the particular demands of the battery, the application, and the desired pore characteristics. The dry process with oriented slit-like pores may offer advantages in terms of preferential ion transport and enhanced mechanical strength, whereas the wet method with non-oriented interconnected pores can provide a more uniform distribution of pores and potentially better electrolyte uptake [269]; this difference is shown in Figure 6.

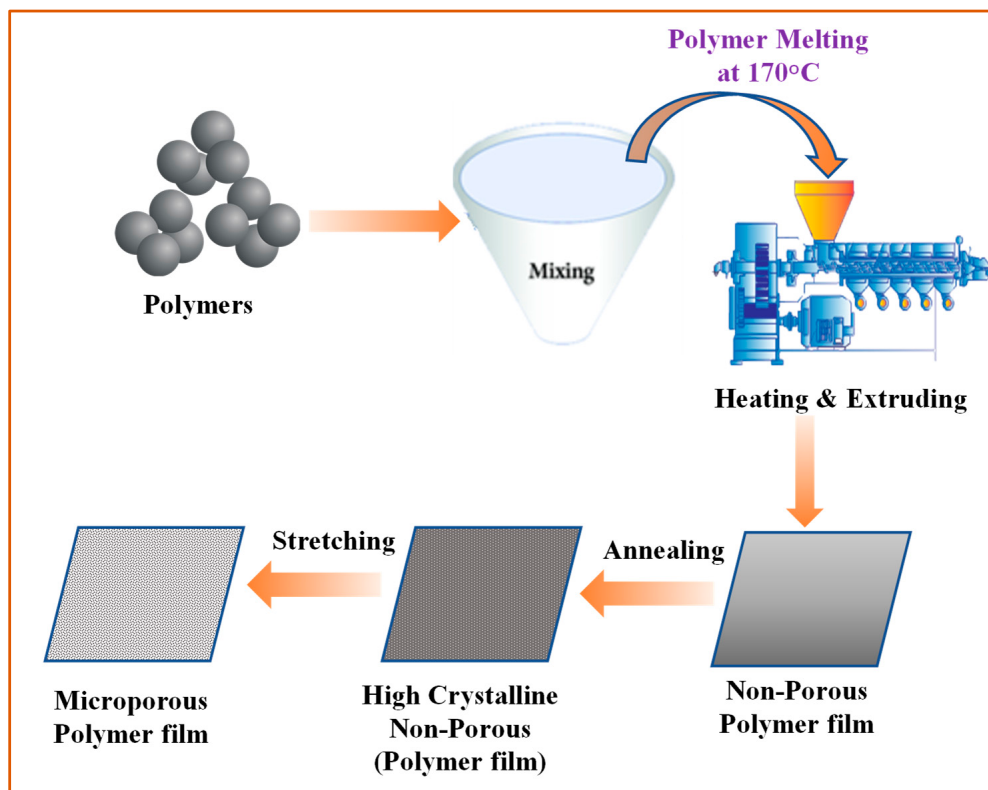


Figure 5. Flow chart of the different approaches involved in the production of microporous separators for the dry process.

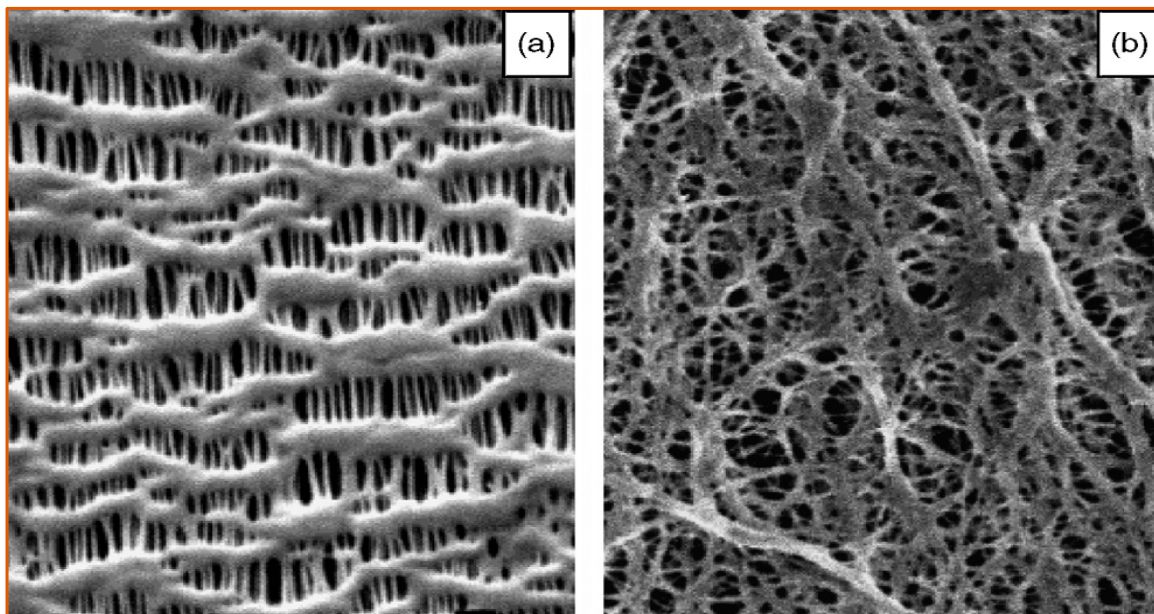


Figure 6. Microstructure of microporous polyolefin membrane made by (a) dry process and (b) wet process, with permission from Zhang et al. [268].

The DP separator passed on PP is well suited for high-power output. It is anticipated for use in EVs due to its reduced production expenses and melting temperature compared to the WP of a PE separator [317]. This difference is shown in Table 2.

Table 2. The difference between the PP and PE separators [294,317].

Dry Process Separator Based on PP	Wet Process Separator Based on PE
Suitable for high-power output in EVs	Potential for EV battery use
Lower manufacturing costs	It involves more steps and materials (solvents), leading to higher manufacturing costs.
Higher melting temperature (beneficial for higher temperature scenarios): 170 °C	Lower melting temperature: 110–135 °C
High tensile strength: 31–41 MPa	Tensile strength: 12–15 MPa
Dielectric constant: 1 MHz 2.2–2.6	Dielectric constant: 1 MHz 2.3

The choice between these two separator types relies on various aspects, considering the distinct necessities of the EV battery, cost considerations, temperature stability, and the balance between power output and energy density. A drawback of the solution method is the substantial volume of residual solvents that must be managed, and their reutilization is typically quite challenging.

3. Dry Electrode Processing for LIBs

The DP procedure aims to reduce the risk of solvent emissions, waste generation, and potential safety hazards by eliminating the need for solvents. This aligns with a growing emphasis on sustainable and environmentally friendly manufacturing practices. In the academic study of Hawley et al., it was found that while wet processing remains prevalent, its challenges, especially in drying, are driving research and development toward DP methods, which represent a promising direction for the future of electrode manufacturing in LIBs. Researchers likely sought to evaluate the viability and potential benefits of adopting the DP in commercial electrode manufacturing processes [318].

3.1. Electrodes

The use of dry-film-production or solvent-free technology in the mass production of LIBs offers numerous advantages, including the following:

(a) Cost reduction: A study conducted by Liu et al. investigated the DP cost savings of solvents, recovery, solvent evaporation, and drying; approximately 48–50.2% of the overall expense for producing electrodes is projected to be spent on solvent recovery, coating, and drying [91]. As a result of applying the DP procedure, it is anticipated that the overall expense will decrease by between 10% and 15% [24].

(b) Consumption of energy and reduction: The WP includes slurry mixing, coating, and drying, and NMP recovery is extremely expensive [91,96,130]. A total of 1 kg of NMP requires 10 kWh of electricity to be recycled [103]. More than 45% of electrode manufacturing costs are attributed to energy consumption [102]. Compared with the DP, there is no solvent recovery and no drying; consequently, much energy and labor time can be saved; for example, the WP takes hours, whereas dry mixing takes only a few minutes during the DP [319,320].

(c) Environmentally friendly product: For a production line with 10 kWh batteries, the CO₂ emissions amount to around 1000 kg during coating and drying [94]. By adopting technologies such as the DP, it is estimated that approximately 4.76 million tons of CO₂ emissions could be saved annually by 2030 [7]. This significant reduction in greenhouse gas emissions demonstrates the potential of the DP to contribute to a more environmentally sustainable manufacturing approach to LIBs. An additional environmental concern in the manufacturing of LIBs is the possible discharge of NMP and the intricate, expensive system required for its retrieval [103].

(d) Enhanced compacted density: The porosities or the fraction of volume unoccupied by solids in the electrode is a factor that significantly influences ion conduction. In the WP, due to solvent evaporation, the porosity will average 56% without calendaring [113]. Due to the absence of solvent evaporation, the DP by dry spray deposition can reduce the electrode porosity by 4–10% [319].

(e) Lowered residuals: The WP cannot wholly remove the residual solvents and other processing agents used during mixing, which can compromise the performance of LIBs [136,321]. The DP procedure eliminates residuals during manufacturing, improving the performance of LIBs.

(f) Heightened mechanical strength: Mechanical strength measures the cathode's ability to withstand mechanical stress or deformation. The dry spray technique with 5% PVDF produces LCO cathodes with a high mechanical strength of 148.8 KPa compared with electrodes prepared by the WP at 84.3 KPa [22]. LCO cathodes, which contain only 1% PVDF as a binder, demonstrated a higher mechanical strength when using the DP compared to the WP; the mechanical strength of the LCO cathode was measured at 93.8 KPa, whereas the WP had a mechanical strength of 83.4 KPa [24]. This indicates that even with a minimum of PVDF as a binder, the LCO cathode exhibited superior mechanical strength compared to the WP electrode.

(g) Saving labour time: The DP reduces the number of labour hours when contrasted with the WP across diverse battery designs. For instance, in the WP, this method entails a demand of 511,871 direct labour hours per year. On the contrary, the DP utilizing the same battery design necessitates a notably diminished number of hours annually: 441,021 [22]. This apparent disparity underscores the operational efficiency of the DP, as evidenced by the reduced labour hours required for the same battery design compared to the WP.

(h) Self-supporting composite electrode without a binder (binder less): Recent advancements in dry LIB electrode technology have developed a unique method that involves dry pressing a combination of LFP active material powder and holey graphene. This process yields a self-supporting composite electrode. Incorporating holey graphene eliminates the need for binders, resulting in a binderless electrode structure [322]. This innovative design maintains a rate capability that is on par with traditional LFP electrodes [323].

As summarized in Figure 7, in the WP process of making electrodes, disorderly binders are layered with thick, porous PVDF [109,113] and use considerable energy during the coating (C), drying (D), and solvent recovery (S) stages. These steps alone account for 47% of the energy consumption, which means that for every 1 kWh battery produced, around 42 kWh of energy is used [91,102,103]. The drying and solvent recovery stages are energy-intensive, contributing significantly to this consumption. Furthermore, these procedures account for between 48 and 50.2% of the electrode production expenses, highlighting their expensive nature [96,128,324–326]. Moreover, there are implications to consider. For instance, producing a 10 kWh battery using the WP emits about 1000 kg of CO₂ into the atmosphere [94,100,327]. This significant environmental impact is further compounded by using solvents in these processes. In contrast, the DP offers marked improvements across these parameters for arrangement binders. It omits the need for drying and solvent recovery, resulting in a 38–40% reduction in energy consumption [114]. This enhanced energy efficiency is accompanied by a decrease in costs, with the elimination of these processes leading to a 14.2–19% reduction in the total electrode manufacturing cost [22]. Environmentally, the DP stands out as a greener alternative, characterized by reduced CO₂ emissions attributable to lower energy consumption and the absence of toxic solvents. Additionally, it offers time savings of 21.6%, a benefit arising from excluding the time-consuming drying and solvent recovery stages [22].

The composition of the slurry mixture and the thickness and porosity of the electrodes are crucial factors influencing their electrochemical efficiency. For instance, electrochemical performance is highly related to the electrode-coating composition, thickness, and mass loading [328]. Achieving improved performance involves maximizing these parameters, as noted in the differences between the dry and wet processes in Table 3.

The process of choosing a binder for electrode formulation requires a delicate balance between a multitude of characteristics and requirements. Among these, the selected binder's molecular weight (MW) emerges as a pivotal factor that profoundly shapes both the electrochemical effectiveness and the structural durability of the electrode within LIBs [329].

Table 3. Electrodes crafted through the wet process and solvent-free techniques, with the composition of the slurry mixture, as well as thickness, porosity, and electrochemical efficiency.

Ref.	Process	Electrode	Materials Wt. %	Thickness (μm)	Porosity (%)	Area Capacity (AC) (mAh/cm^2), Mass Loading (ML) (mg/cm^2)	Discharge Capacity (mAh/g)	Capacity Retention (%)
[22]	Wet	Cathode	NMC111:PVDF:CB 90:5:5	-	30	-	138	84%, after undergoing 50 rounds of charging and discharging at a 0.5 C rate within the voltage range of 2.8–4.3 V
	Dry		NMC111:PVDF:CB 90:5:5	40–130	30	-	138	87%, after 50 cycles at 0.5 C between 2.8 and 4.3 V
	Wet		LCO:PVDF:CB 90:5:5	-	30	-	115	58%, after undergoing 50 rounds of charging and discharging at a 0.5 C rate within the voltage range of 2.5–4.2 V
[319]	Dry		LCO:PVDF:CB 90:5:5	40–130	30	-	114	70%, after 50 cycles at 0.5 C between 2.5 and 4.2 V
	Wet		NMC111:PVDF:CB 19:1:1	32.6	41	7.65 mg/cm ² (ML)	156	60%, after 300 cycles between 3.0 V and 4.3 V at 0.5 C
				52	35	14.27 mg/cm ² (ML)	157	65%, after 300 cycles between 3.0 V and 4.3 V at 0.5 C
[23]	Dry		NMC111:PVDF:CB 19:1:1 wt.	40.5	31	10.07 mg/cm ² (ML)	155	80%, after 300 cycles between 3.0 V and 4.3 V at 0.5 C
	Wet		NMC111:PVDF:CB 90:5:5	55	29–30	2.45 m Ah/cm ² (AC)	145	65%, after 500 cycles at 0.5 C.
	Dry		NMC111:PVDF:CB 90:5:5	55 100 150 200	29–30	2.45 mAh/cm ² (AC) 5.80 mAh/cm ² (AC) 6.52 mAh/cm ² (AC) 9.11 mAh/cm ² (AC)	150 <20 <20 <20 At 3 C.	80%, after 500 cycles at 0.5 C.
[29]	Wet	Anode	Graphite:PVDF:CB 85:10:5	-	-	PVDF 3 mAh/cm ² (AC)	-	-
			Graphite:(FEP or TVH):CB 86:7:7					
	Dry		Graphite:PVDF:CB 85:10:5	-	-	FEP 2.7 mAh/cm ² (AC)	370	99%, after 50 cycles at 0.5 C
			Graphite:(FEP or TVH):CB 86:7:7			TVH 3.5 m Ah/cm ² (AC)	345	97%, after 50 cycles at 0.5 C

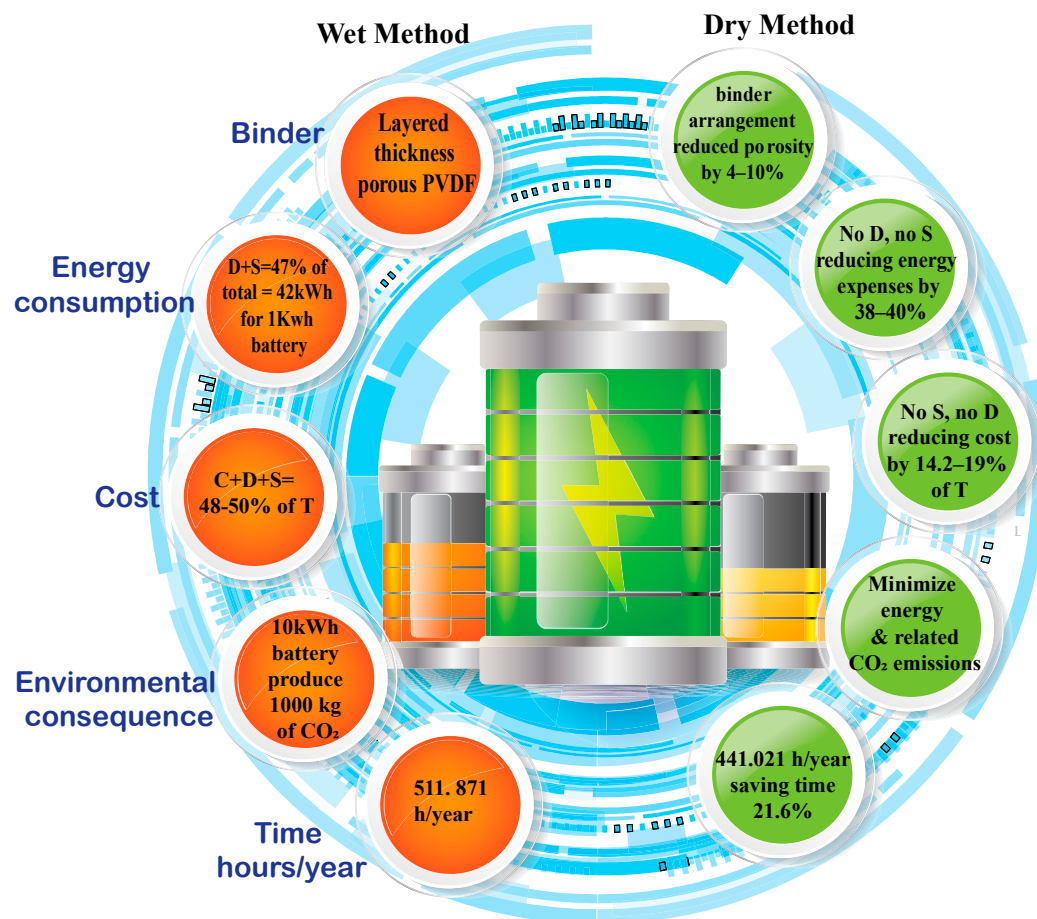


Figure 7. Contrast between the wet process and dry electrode techniques, mentioning some significant parameters like energy consumption, cost, and environmental aspects for C: coating, D: drying, and S: solvent recovery against T: the total cost of electrode manufacturing.

The comparative performance between dry-painted and conventional (likely) wet-coated electrodes in terms of discharge rate performance, discharge capacity, capacity retention, Coulombic efficiency, and rate performance is provided in Figure 8. This influence casts its reach over a range of variables, encompassing the levels of binder and carbon black present, the manipulation of electrode mass loading, the determination of electrode thickness, the technique employed for mixing, the pace at which mixing occurs, and even the intriguing prospect of using less binder in the electrodes. In essence, the interplay of these diverse parameters exerts a notable impact on the properties exhibited by the electrode, especially in the DP, as shown in Figure 8.

Figure 8a shows the discharge rate test results demonstrating that the dry-coated electrodes exhibited superior power output to the wet-coated electrodes within an electrode configuration optimized for high energy density. The electrode loading was set at 5 mAh/cm². The cut-off voltage stood at 4.2 V for charging and 2.8 V for discharging. Figure 8b shows that the cycling performance of the NMC electrode produced via dry spraying surpassed that of the conventional slurry-coated electrode with higher and lower loading, showcasing consistent stability and improved capacity retention. The anode coated with dry powder and FEP mixed at 30 m/s exhibits the most robust cycling performance and enhanced efficiency stability among the various configurations (Figure 8c). Figure 8d demonstrates that the rate capability performance of the DP LFP electrodes surpasses that of the SC LFP electrode. Figure 8e,f show that the dry-painted electrode LCO has excellent cycling stability compared to the conventional LCO electrodes.

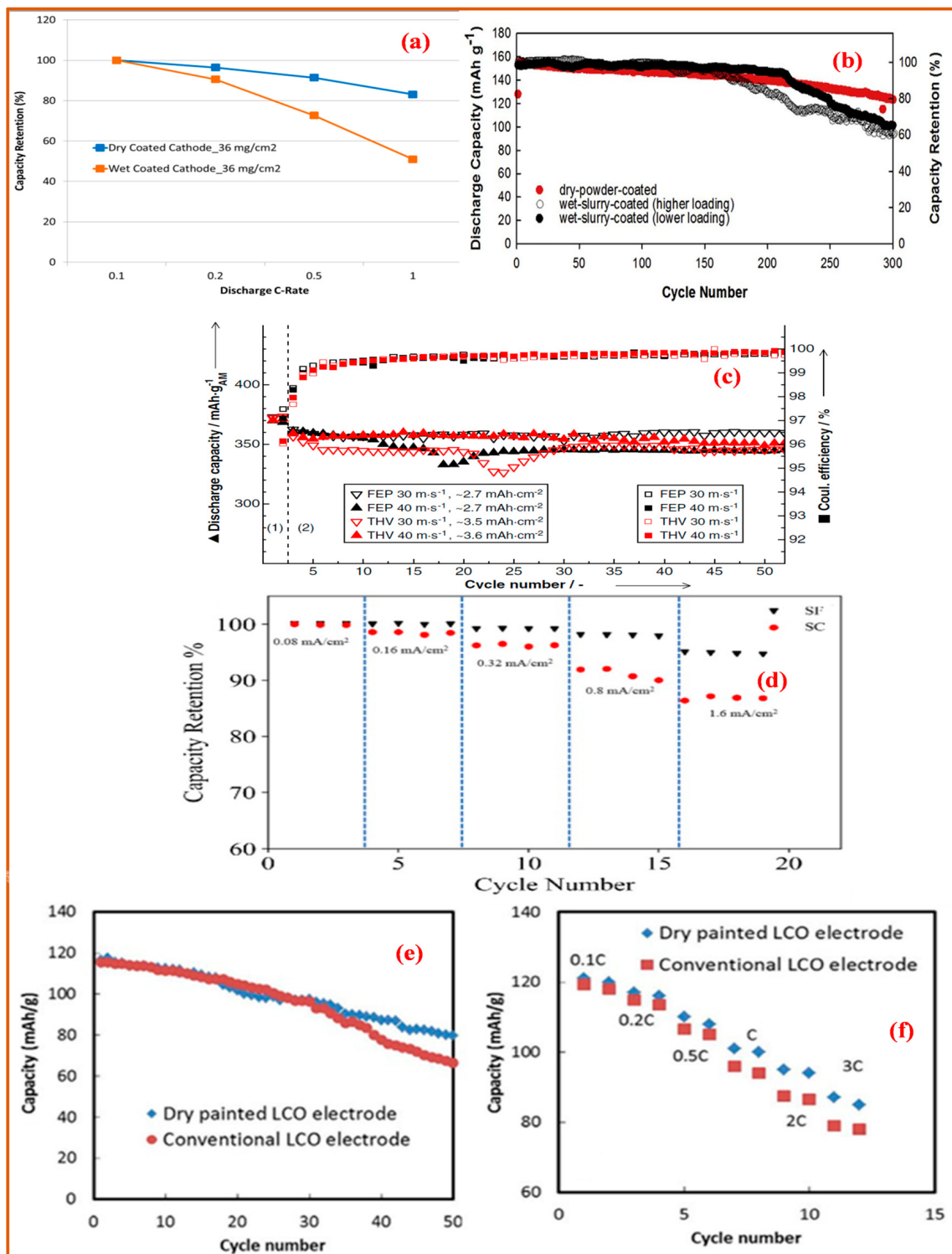


Figure 8. (a) Comparative discharge rate performance between dry-coated and wet-coated NMC111/graphite [28], (b) discharge capacity (on the left) and capacity retention (on the right) curves for an NMC cathode coated with wet slurry and an NMC cathode coated with dry powder in lithium half-cells [319], (c) discharge capacity (▲) and Coulombic efficiency (●) curves for graphite anodes coated with dry powder, varied powder pretreatments, and binder in lithium half-cells [29], (d) SF and SC LFP electrode rate performance across varying current densities [330], (e) comparative cycling performance of dry painted and conventional LCO electrodes, and (f) C-rate performance evaluation of dry painted and conventional LCO [22].

3.2. Dry Mixing and Coating

Dry electrode mixing and coating offer increased production speed, reduced energy consumption, lower environmental impact, and proven electrode performance.

(a) **Dry mixing** is used to homogeneously combine the binder, active materials (AMs), and conductive agents without using solvents; in this process, the solid component is thoroughly mixed to ensure uniform distribution and achieve consistent electrode material composition. Dry mixing using a double-blade mill [331] is a specific method in electrode fabrication for LIBs; the double-blade mill utilizes two blades rotating in opposite directions to achieve a thorough and uniform mixing of the solid components. Dry mixing with a blade mill offers advantages, such as increased efficiency, precise control over the mixing process, and reduced risk of solvent contamination since no liquids are involved [332]. Andreas Gyula et al. discovered that NMC622 electrodes, crafted from well-homogenized powders and enhanced by dry mixing, demonstrate exceptional electrochemical performance, especially in C-rate capability, due to their ideal thickness and porosity [333]. If dry mixing is not conducted optimally, it can lead to issues such as agglomeration, less binder distribution, and the uneven dispersion of AMs and CAs.

Consequently, these problems can adversely affect the electrode coating process; the success of electrode fabrication heavily relies on the quality of dry mixing [334–337]. Various factors impacting the mixing process can significantly influence the resultant mixing outcomes. These factors include the mixing equipment's characteristics, agitation strength, and the material's sequence or properties. Each of these components has a fundamental role in determining the overall effectiveness of the mixing process and the quality of the final mixture [338–340].

(b) **Dry coating:** The dry coating procedure holds significant importance; it involves the direct transformation of electrode materials in powder into a cohesive film without solvents. The dry coating technique depends on factors such as the characteristics of the substrate, the properties of the powder blend, and the desired film attributes. Dry coating is advantageous for avoiding the use of liquid solvents, reducing processing time, and providing a more controlled and reproducible coating; three methods for the dry process are shown in Figure 9a–c.

3.3. Dry Spraying Deposition

Sames has achieved a significant breakthrough in powder electrostatic spraying technology in France. This advancement promises to resolve the challenges stemming from uneven and excessively thick coating methods that arise due to the influence of electric fields. An instrumental development in this field occurred in 2008 when Toyota collaborated with Zeon Corporation (Tokyo, Japan) to create a pioneering electrostatic dictyosome. This sophisticated device leverages an electrode with a powder spray gun to achieve its remarkable capabilities [115].

Dry spraying deposition (DSD) and hot rolling are techniques that can be employed as a part of the dry process for LIB electrode preparation. This method involves depositing active material powders directly onto a current collector substrate to create electrode layers without a solvent-based slurry. LCO electrodes fabricated by DSD are depicted in Figure 10a [22], and NMC111 manufactured by DSD is shown in Figure 10b [319]. DSD offers benefits such as reduced solvent waste, enhanced control over coating thickness, and simplified manufacturing processes. Here is how SDS can be applied in the context of LIB electrode preparation: in a study conducted by Ludwig et al. [22], the electrochemical performance of LIB electrodes was investigated using Electrostatic Spry Deposition (ESD) techniques; the active materials used were LCO or NMC111 combined with PVDF as the binder and carbon black was used as a conductivity enhancer. The electrodes were tested in Li half-cells, and their porosity was maintained at around 30%, with various electrode thicknesses ranging from 40 to 130 μm , indicating the versatility of the SDS process.

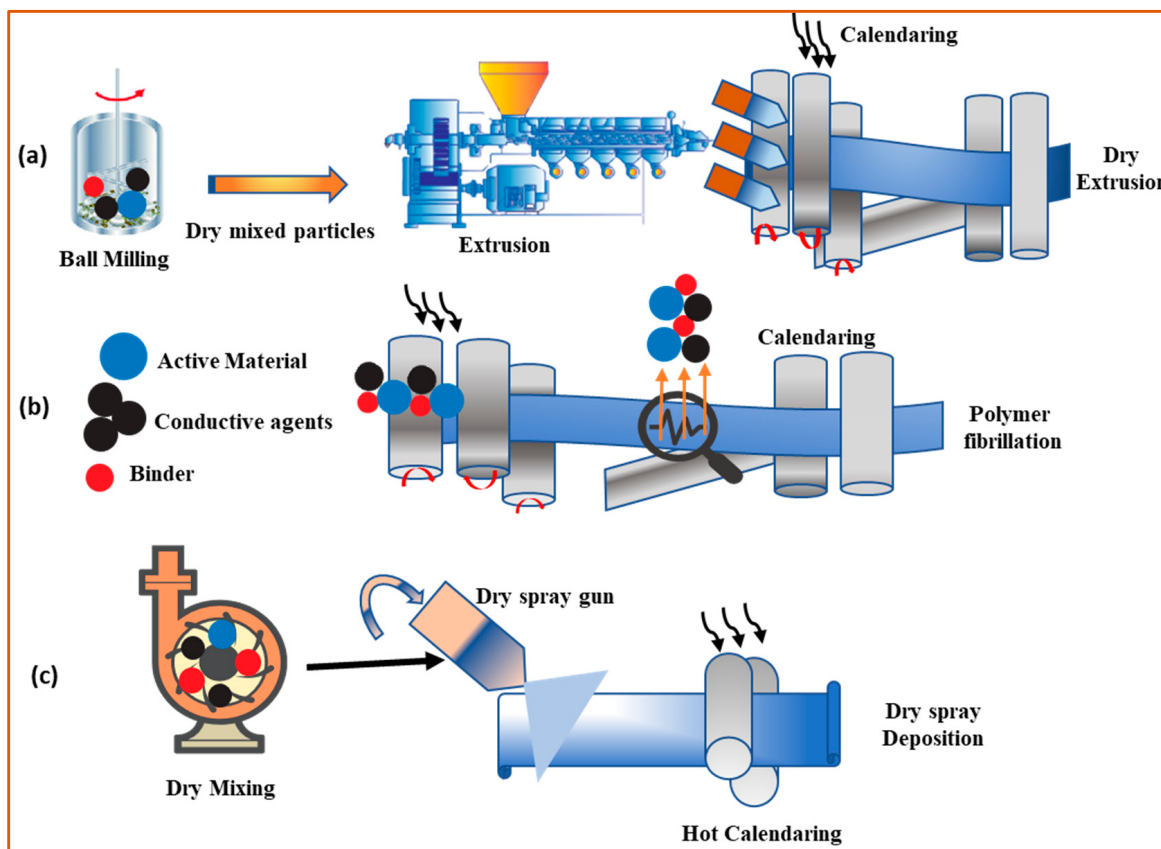


Figure 9. Methods for utilizing the dry process for electrode preparation: (a) dry extrusion, (b) polymer fibrillation, and (c) dry spray deposition [114].

For the LCO electrodes, the DP variant exhibits an initial discharge capacity of 114 mAh/g, with a capacity retention of 70% after 50 cycles at a rate of 0.5 C, cycling between voltage limits of 2.5 V and 4.2 V. On the other hand, the WP LCO electrode demonstrated a slightly higher initial discharge capacity of 115 mAh/g but a lower capacity retention of 58% under similar cycling conditions. For the NMC111 electrodes, the DP variant displayed a higher initial discharge capacity of 138 mAh/g, with a remarkable capacity retention of 87% after 50 cycles at 0.5 C between 2.8 V and 4.3 V. In contrast, the WP NMC111 electrode showed an initial discharge capacity of 138 mAh/g, with a slightly lower capacity retention of 84% after the same cycling conditions. The findings of this study demonstrate ESD's efficacy in fabricating high-performance LIB electrodes; the DP electrodes showed favorable electrochemical performance and improved mechanical strength compared to their WP counterpart, highlighting the potential benefits of this technique in advancing electrode manufacturing for LIBs.

Table 4 provides a comparative analysis of the electrochemical behavior of dry-painted and conventional electrodes using CV and EIS techniques. The painted electrodes demonstrate advantages in terms of rate capability and electrochemical polarization, which are critical factors for the performance of lithium-ion batteries.

In a study spearheaded by Ludwig et al. [24], the electrochemical performance of LIB electrodes was investigated using a specific active material composition of LCO combined with PVDF as the binder, and carbon black was used as a conductivity enhancer; the electrodes were evaluated in a full cell configuration with a graphite anode, the electrochemical performance of the DP LCO electrodes was characterized by an initial discharge capacity of 127 mAh/g, with capacity retention of 77% after 100 cycles at a rate of 0.5 C while cycling between voltage limits of 2.5 V and 4.2 V. The study also assessed the mechanical strength of the DP electrodes, which was measured at 93.8 KPa. The study was designed to

examine the effects of reduced binder and CB levels in the electrode composition by using a significantly high ratio of LCO binder and CB (98:1:1); we aimed to understand how reducing the amount of binder and CB impacts the electrode's electrochemical performance and mechanical strength. The results demonstrated that the DP electrodes with reduced binder and CB content exhibited favorable electrochemical performance, promising initial discharge capacities, and satisfactory capacity retention after cycling.

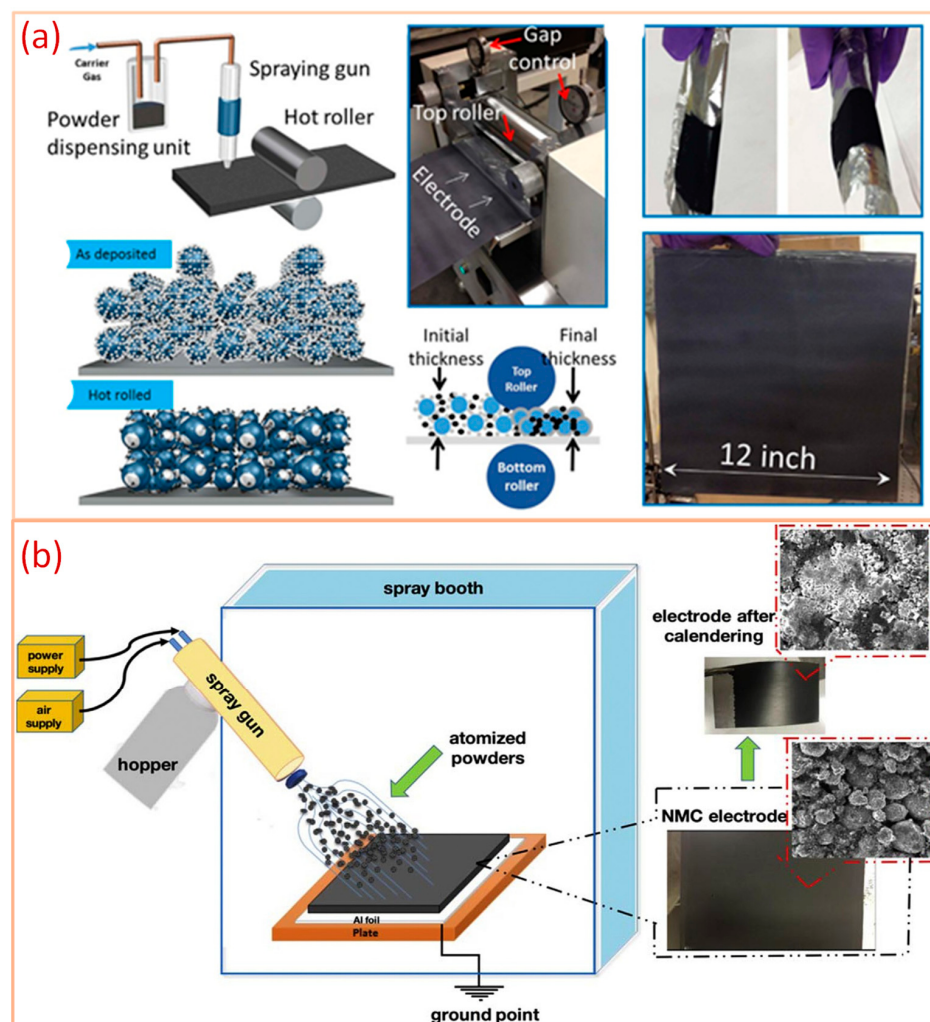


Figure 10. (a) The dry spray deposition process for electrode fabrication typically involves the following steps: the fluidization of the dry mixture, the charging and deposition of particles, calendering and hot rolling, and dry painting the electrode on Al foils. (b) The electrostatic spray deposition process for an LIB cathode, with permission from Ludwig et al. [22] and AL Shroofy et al. [319], respectively.

The study compared the DP and two WPs with higher and lower mass loadings by AL Shroofy et al. [319] by using NMC 111 as the active material, PVDF as the binder, and CB as a conductive additive; the electrodes were tested in Li half-cells, and their porosity ranged from 31 to 41%. The investigation involved various electrode configurations with different thicknesses and mass loadings:

- a. Wet (lower loading): the electrode had a thickness of 32.6 μm , and it carried a mass loading value of 7.65 mg/cm^2 ;
- b. Wet (higher loading): the electrode had a thickness of 52 μm , with a mass loading of 14.27 mg/cm^2 ;
- c. Dry: the dry electrode had a thickness of 40.5 μm , with a mass loading of 10.07 mg/cm^2 .

The electrode's electrochemical behavior was analyzed through their initial discharge capacity retention after 300 cycles, and the results were as follows:

- a. Wet (lower loading): the electrodes exhibited an initial discharge capacity of 156 mAh/g, with a capacity retention of 60% after 300 cycles when cycled between 3 V and 4.3 V at a rate of 0.5 C;
- b. Wet (higher loading): the electrode demonstrated an initial discharge capacity of 157 mAh/g, with a capacity retention of 65% after the same cycling conditions;
- c. Dry: the dry electrode displayed a primary discharge capability retention of 80% after the same cycling conditions.

Table 4. Summarizing the Electrochemical Impedance Spectroscopy (EIS) analysis for understanding the performance differences between dry-painted and conventional wet electrodes in lithium-ion batteries (LCO) [22].

Parameter	Dry-Painted Electrodes	Conventional Wet Electrodes	Implications
Cyclic voltammetry (CV) at 0.025 mV/s	Single pair of oxidation and reduction peaks (reduction at ~3.8 V, oxidation at ~4 V)	Single pair of oxidation and reduction peaks (reduction at ~3.8 V, oxidation at ~4 V)	Both types of electrodes show good reversibility of lithium insertion and extraction from LCO
CV peak symmetry at higher scan rates	Maintain symmetrical shape of cathodic and anodic peaks	Significant change in the shape of cathodic and anodic peaks	Dry-painted electrodes exhibit better rate capabilities and stability under rapid charge/discharge conditions
Potential difference between peaks	Smaller potential difference between cathodic and anodic peaks	The larger potential difference between cathodic and anodic peaks	Dry-painted electrodes have lower electrochemical polarization, indicating more efficient electrochemical reactions
EIS analysis	Show lower impedance characteristics	Show higher impedance characteristics	Lower impedance in dry-painted electrodes suggests better conductivity and lower internal resistance
Charge transfer resistance	Lower	Higher	Lower charge transfer resistance in dry-painted electrodes implies more efficient electron transfer during electrochemical reactions
Lithium-ion diffusion	Potentially more favorable	Potentially less favorable	Better lithium-ion diffusion in painted electrodes could contribute to their enhanced performance

The findings highlight the impact of electrode fabrication techniques and mass loading on the electrochemical performance of LIB electrodes; the DP electrode exhibits competitive electrochemical performance, with the highest capacity retention after cycling.

In a study spearheaded by Liu et al. [23] using NMC 111 with PVDF and CB, the electrodes were evaluated in full-cell configuration with a graphite anode, and their porosity was 29–30%. Both wet and dry electrode preparation methods were employed, resulting in electrodes with a thickness of 55–56 µm and mass loading of approximately 2.45 mAh/cm². For the DP, different thicknesses were investigated, namely 100 µm, 150 µm, and 200 µm, relating to an area capacity of 5.8 mAh/cm², 6.52 mAh/cm², and 9.11 mAh/cm², respectively. The electrochemical performance of the electrodes was analyzed through their initial discharge capacity and capacity retention after 500 cycles at a rate of 0.5 C. The results were as follows:

- a. Wet (55 µm): the electrode showed a primary discharge of 145 mAh/g, with a capacity retention of 65% after 500 cycles;
- b. Dry (55 µm): the electrode exhibited an initial discharge capacity of 150 mAh/g, with capacity retention of over 80% after the same cycling conditions;

- c. Dry (55 μm): the electrode displayed a discharge capacity of 120 mAh/g at a high rate of 3 C;
- d. Dry (100 μm , 150 μm , and 200 μm): the electrode exhibited a discharge capacity of less than 20 mAh/g at the same high rate of 3 C.

By comparing the different thicknesses of the dry-coated electrodes, the study found that the thin DP electrodes showed superior rate performance compared to the thick versions.

In a study spearheaded by Wang et al. [328], ESD was employed to investigate a PVDF binder's molecular weight (MW) by using NMC 111 combined with PVDF and CB; the electrodes were tested in Li half-cells, specifically a coin cell, and the porosity was measured at 31%; the electrode thickness was 59 μm , with a mass loading of approximately 2.4 mAh/cm². Two PVDFs were utilized: low MW and high MW PVDF.

The examination of the electrode's electrochemical behavior was conducted through their initial discharge capacity and capacity retention following 50 cycles at a rate of 0.5 C; the electrode was also subjected to cycling at a higher rate of 5 C to assess its performance under rapid charging/discharging conditions, and the results were as follows:

- a. Low MW PVDF: the electrode displayed an initial discharge capacity of 160 mAh/g at a rate of 0.2 C, with capacity retention of 93% after 50 cycles at 0.5 C; however, at a higher rate of 5 C, the capacity retention dropped to 16.7%;
- b. High MW PVDF: the electrode exhibits a primary discharge capacity of 160 mAh/g at 0.2 C, with a capacity retention of 91% following 50 cycles.

This meticulous study sheds light on the pivotal role of PVDF binder MW in influencing the electrochemical performance of the fabricated dry electrodes, providing insight into their behavior across varying cycling rates.

Dry spraying deposition offers several advantages, including its solvent-free nature, potential for upscaling, and uniform coating capability. However, challenges concerning equipment compatibility, efficiency, and thickness control need to be addressed for its successful integration into industrial LIB production.

3.4. Polymer Fibrillation

Maxwell Technologies pioneered an innovative methodology for creating electrode-harnessing polymer fibrillation. This cutting-edge approach is tailored to craft activated carbon electrodes designed explicitly for supercapacitor application. This ground-breaking technique has achieved remarkable results and secured a patent, solidifying its status as a pioneering advancement in the field [341–343]. The process of binder fibrillation garnered global recognition following Tesla's acquisition of Maxwell in 2019, and this innovation held particular significance, as it constituted the primary technology employed by Maxwell for the fabrication of supercapacitor electrodes. Notably, this technique has the remarkable capability of preparing electrode/electrolyte membranes for a spectrum of energy storage devices, including supercapacitors, LIBs, and ASSBs [344,345]. One of the critical requirements of the Maxwell DP is the use of binders with considerable plasticity, mechanical deformability (fibrillation), and polymerization temperature (25–80 °C) to achieve electrodes with a very high loading density of 6.8 mAh/cm², such as polytetrafluoroethylene (PTFE) [31,346,347].

Fibrillation significantly influences the particular surface area and accessibility of active material sites, which are crucial for electrochemical reactions. Inadequate fibrillation limits these reaction sites, resulting in lower capacity, poorer rate capability, and reduced cycling stability [348].

Weiliang Yao et al. developed a PTFE-based dry electrode fabrication method for high-voltage spinel oxide LNMO electrodes. This technique, surpassing the constraints of slurry-coated electrodes, allows for ultra-high loadings and remarkable cycling stability. Even at 1000 cycles, electrodes with a 3.0 mA h cm⁻² level maintain 68% capacity retention, demonstrating effectiveness with both baseline and high-performance fluorinated electrolytes [349].

Zhou et al. [350] crafted SF electrodes that were effectively produced through an uncomplicated three-SF approach at the pilot stage. As shown in Figure 11a, this method seamlessly integrates a high-speed air-blowing process to fiberize the PTFE. It uses hot rolling and hot overlying processes to fabricate the LFP cathode and LTO anode. Remarkably, the SF electrode's compact densities reached an impressive 1.3 g/cm^3 , surpassing the wet coating electrode's value by 1.6 times. This signifies a notable enhancement in electrode density, highlighting the efficacy of the SF fabrication technique.

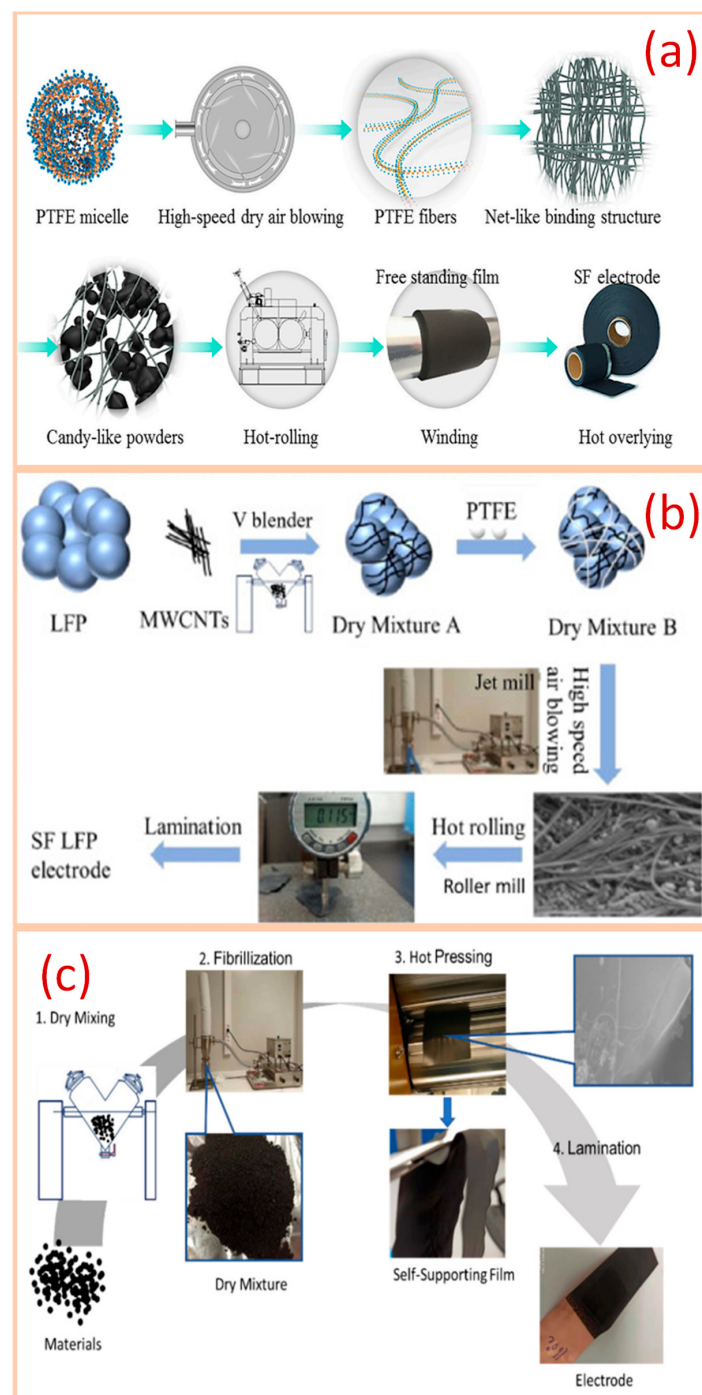


Figure 11. (a) Diagrammatic outline of the SF-electrode fabrication pathway, with permission from Zhou et al. [350]; (b) illustration of SF LFP electrode production via PTFE fibrillation, encompassing dry mixing, fibrillation, hot-rolling, and lamination, with permission from Zhang et al. [330]; (c) illustration of SF graphite anode production, with permission from Zhang et al. [351].

The successful fabrication of PTFE fibrillation-based (SF) LFP electrodes, as shown in Figure 11b, was achieved by Zhang et al. [330], facilitated by the incorporation of carbon nanotubes (CNTs). In this approach, CNTs serve a dual role as a conductive additive and a matrix, effectively binding LFP particles. This matrix function ensures the sustained fibrillation of PTFE when subjected to calendaring machine pressure. The outcome is a remarkable SF LFP electrode characterized by notable stability and enhanced rate capability compared to its counterparts produced using a wet process. This advantageous performance can be attributed to the excellent conductivity of CNTs, which promotes efficient electron transport. Additionally, the presence of PTFE fibrils establishes localized contacts with LFP particles, further contributing to improved electrochemical performance. In PTFE, the energy level of the LUMO, or lowest unoccupied molecular orbitals, is notably low, suggesting its propensity to readily accept electrons, rendering it electrochemically unstable in the anodes.

Zhang et al. [351] effectively expanded the application of PTEF for SF-fabricated anodes, as shown in Figure 11c. This advancement was manifested through successfully fabricating anodes utilizing distinct carbon-based active substances such as graphite, hard carbon, and soft carbon. In order to evaluate the stability of these anodes, the researchers gauged the volume changes in the active materials throughout charge/discharge cycling; both the DP hard carbon anode and the DP soft carbon anode exhibited commendable cycle stability during the charge/discharge regimen. The SF hard carbon anode demonstrated comparable long-term cycling stability and equivalent performance at various C-rates compared to an anode fabricated using the WP. PTFE is widely used, yet the selection of binders for Maxwell-type manufacturing still needs to be improved, constraining the technique's widespread adoption across various battery systems. There is a significant need to explore and develop binder materials with fibrillization effects to broaden the applicability of this method.

3.5. Extrusion and Melt Processing

In extrusion, materials are continuously pushed through restricted or confined spaces. As part of these processes, the materials are generally thoroughly mixed [352]. Extrusion is a versatile manufacturing method that is used to manufacture various products, including, but not limited to, shopping bags, food items, pharmaceuticals, and, more recently, co-crystals and metal–organic frameworks. Extrusion encompasses a range of processing techniques, including single-screw and twin-screw extrusion [353], as depicted in Figure 12, for the manufacturing and processing of various materials for electrode preparation.

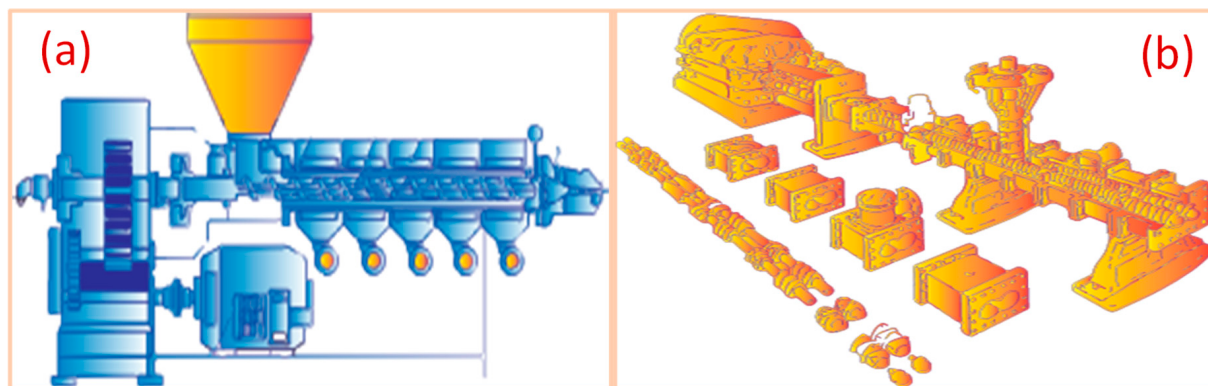


Figure 12. (a) Single screw extruder and (b) twin screw extruder for manufacturing and processing of various materials for electrode preparation.

Melt extrusion without solvents is a manufacturing process that has gained attention for producing the specific components of LIBs. This process offers advantages regarding environmental impact, efficiency, and cost-effectiveness. Melt extrusion is a manufacturing

technique where raw materials are combined and heated until they reach a molten state. This molten mixture is then forced through a mold to produce a particular form, like a film, sheet, or electrode. The critical feature of melt extrusion is that it does not require solvents, unlike the traditional methods used in LIB production.

Several vital parameters determine the success of the extrusion process. Temperature control is central, as it governs the material's behavior by ensuring it reaches an optimal state for extrusion. Concurrently, the choice of screw configuration, type, and size significantly influences material handling and mixing within the extruder. These factors dictate how effectively the material is processed. Lastly, the screw speed, or the rate of screw rotation, directly impacts the production output and product quality. Additionally, the feeding mechanism plays a crucial role in introducing and controlling the flow of raw material into the extruder. Striking the right balance between these parameters is essential for achieving precise control, efficiency, and the desired extrusion results across various industrial applications [354]. Polymer composition is significantly influenced by heat and shear rate. In electrode production, it is essential to explore how dispersing, particularly during extrusion and calendaring, affects the properties of the resulting electrode [355], illustrating various steps using powder extrusion for electrode preparation as shown in Figure 13. Bolloré Technologies submitted a patent application in 1997 that described the utilization of an extrusion technique to fabricate electrodes, which were combined with a solid polymer electrolyte (SPE) that was also produced through extrusion. The cathodes manufactured via this method generally consist of MnO₂, amorphous carbon, polyethylene oxide (PEO), and lithium triflate (LiCF₃SO₃) [356].

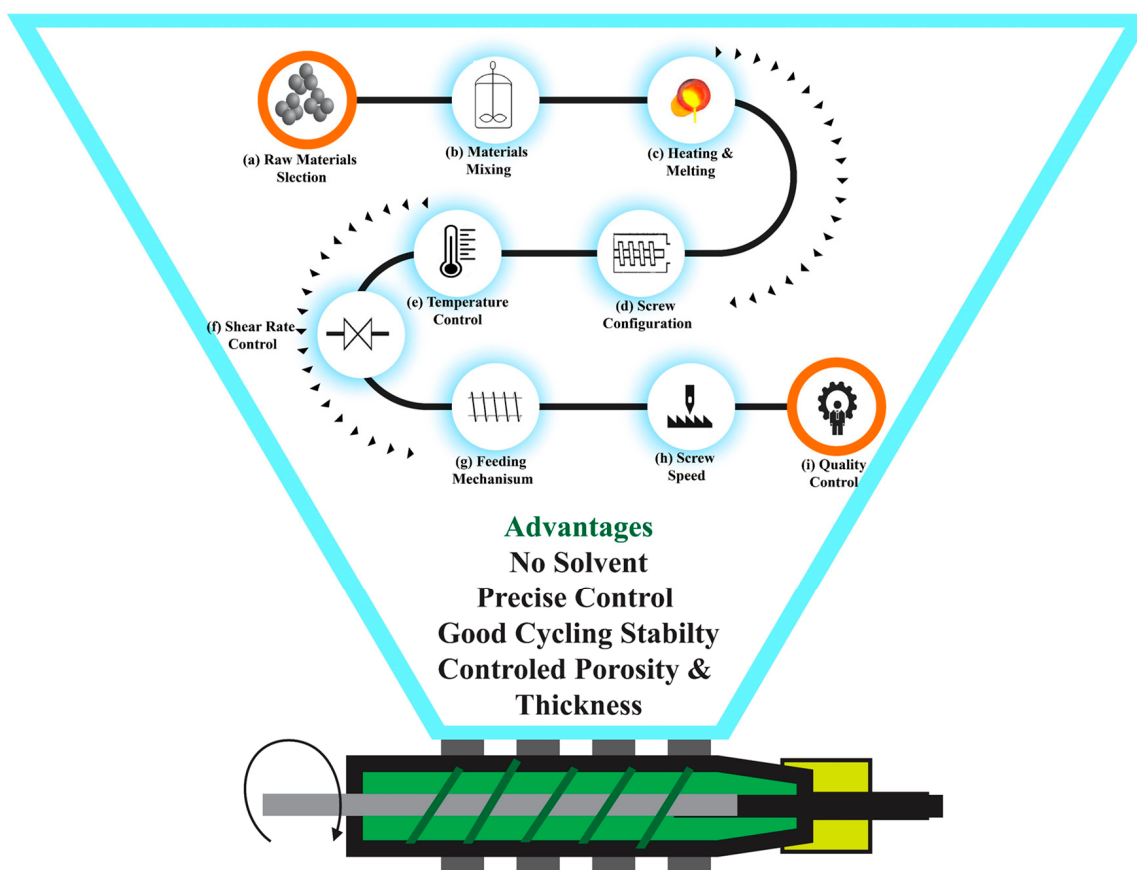


Figure 13. Diagram illustrating the various steps using powder extrusion for electrode preparation.

For the production of yttria-stabilized zirconia (YSZ) samples by injection molding, a high-solid-loading polymer-based system was developed, resulting in high-density, homogeneous microstructures and conductivities that were comparable to those of uniaxially

compacted samples. The binder formulation, comprising 50 vol% (PP), 46 vol% paraffin wax (PW), and 4 vol% stearic acid (SA), along with 55 vol% powder loading, proved optimal. The surface treatment of YSZ powder with SA significantly reduced the feedstock viscosity, facilitating the injection molding process with a moderate wax content. The resulting injected-molded bars exhibited electrical properties akin to uniaxially compacted samples, with a conductivity of around 0.10 S/cm at $900\text{ }^{\circ}\text{C}$, showcasing the potential for use as high-temperature solid fuel cell electrolytes [357]. The advancement entailed substituting the conventional PVDF binder with a blend suited for direct extrusion, comprising thermoplastic polymers like PP, paraffin wax, and SA [358].

Sotomayor et al. devised a highly scalable method using powder extrusion molding technology to craft robust ceramic LIB electrodes using LTO. This method allows for the creation of self-standing LTO electrodes with impressive attributes. These LTO-sintered anodes exhibit exceptional thickness, reaching approximately $500\text{ }\mu\text{m}$, ensuring mechanical consistency, and boasting porous and uniformly structured micro-components. These electrodes are characterized by their substantial thickness, high density (about 2.9 g cm^{-3}), remarkable volumetric capacity (around 349 mAh/cm^{-3}), and, most notably, an impressive areal capacity, exceeding 15.2 mAh/cm^2 [359]. Sotomayor et al. pioneered the utilization of extrusion as a solid-state shear-induced mixing SF technique to produce electrodes incorporating LTO and LFP as active materials. This innovative approach facilitated the creation of electrodes characterized by a high packing density, strong interaction between the particles of the active material, and a conductive carbon matrix, resulting in enhanced electrochemical performance. Their study successfully demonstrated the fabrication of LIBs featuring thick, self-supported LTO and LFP electrodes, all achieved without the need for additives. These batteries exhibited exceptional electrochemical performance, boasting a substantial mass loading of approximately 100 mg/cm^{-2} , translating to an increased volumetric capacity of 340 mAh/cm^{-3} and an impressive areal capacity exceeding 13 mAh/cm^2 [360].

In their experimental work, Gamarra et al. systematically optimized the powder extrusion molding (PEM) process to manufacture thick LFP electrodes with a thickness of approximately $500\text{ }\mu\text{m}$. In their study, they investigated multiple parameters, such as the composition of the active material in the feedstock, the thickness of the samples, the sintering temperature, and the viscosity of the electrolytes.

Despite the substantial thickness of these ceramic electrodes, they demonstrated remarkable electrochemical performance, especially at relatively low C-rates, spanning from C/10 to C/24. This exceptional outcome was attributed to the electrodes' high porosity, reaching 35%, facilitating the efficient infiltration of the liquid electrolyte through the thick substance. LFP cathodes come without additives (no binder and no additional carbon black) and have a thickness of 0.5 mm , achieving a very high area capacity (13.7 mAh/cm^{-2}). These innovative thick electrodes demonstrate excellent electrochemical performance and non-flammable characteristics, making them highly promising for various applications [361].

Utilizing Hutchinson's France patents [362,363], El Khakani et al. most recently documented the use of SF extrusion for producing Li-ion battery electrodes [364]. The binder formulation used was a combination of hydrogenated nitrile butadiene rubber (HNBR) and polypropylene carbonate (PPC), as depicted in Figure 14. The process involved introducing HNBR and PPC into an internal mixer at $90\text{ }^{\circ}\text{C}$ until a homogeneous molten blend was achieved. Following that, the active components, like LTO, LFP, or NMC, along with conductive additives, were integrated into the polymer mixture and stirred until uniformly distributed. The composite mixture was laminated repeatedly to form self-supporting electrode films until the desired thickness was attained. Finally, the electrode was laminated to a current collector with a carbon coating. This original approach aims to utilize affordable polymers, reduce solvent handling costs, introduce a circular economy with PPC recycling, and enable the precise control of porosity and thickness.

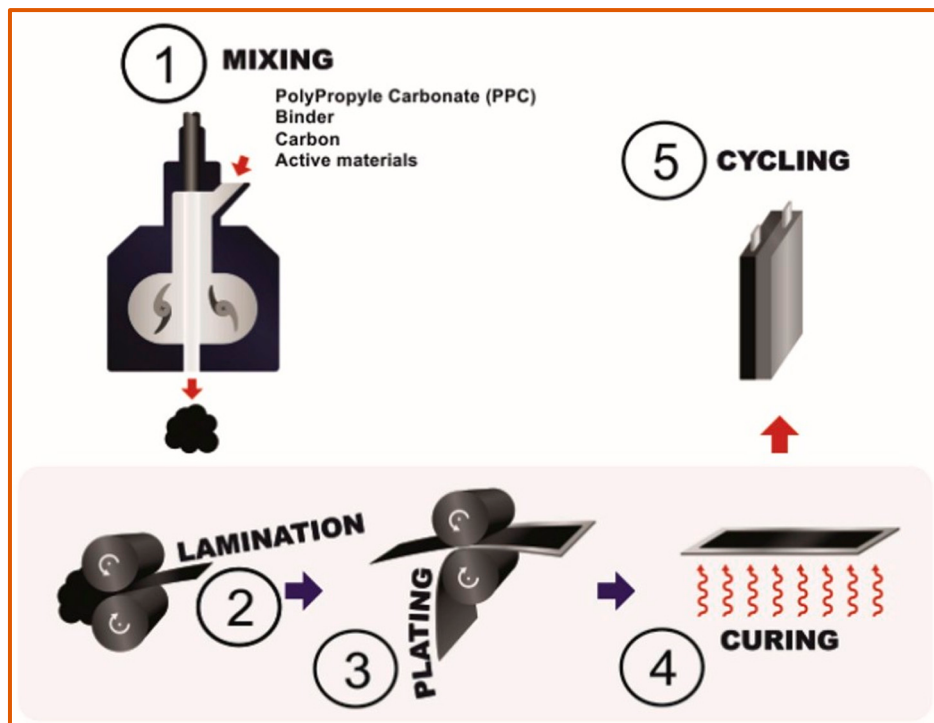


Figure 14. Schematic of dry extrusion steps in LIBs with permission from El Khakani et al. [364].

In producing LIB electrodes through SF extrusion, diverse, active materials like LTO, LFP, and NMC, along with conductive additives, can be integrated into the polymer mixture without the need for solvents. This creates a homogeneous mixture and promotes strong interaction between the active material particles and the conductive carbon matrix, ultimately enhancing electrochemical performance. Moreover, using specific binder systems (PPC or HNBR) in SF extrusion ensures precise control over porosity and thickness. The absence of solvents in the binder system contributes to LIB components' overall consistency and quality.

From a chemical perspective, SF extrusion in LIB component manufacturing is of the utmost importance. It allows for the precise control over materials and their interactions, improving electrochemical performance and producing high-quality, environmentally friendly LIBs. Below is a Table 5 that outlines the differences between melt extrusion with and without a solvent, highlighting why solvent-free extrusion might be considered superior.

Table 5. Differences between melt extrusion with and without solvent in manufacturing LIBs.

Criteria	With Solvent [89,365]	Without Solvent [332,358,364]
Manufacturing process	Involves slurry-casting procedure	Utilizes melt extrusion technique
Active materials	Limited option	Diverse (LFP, NMC, LTO, NCA, ...)
Binders	Conventional binders	PPC, HNRP,...
Thickness	Varies	Up to 500 μm
Density	-	$\sim 2.9 \text{ g/cm}^3$
Volumetric capacity	-	$\sim 349 \text{ mAh/cm}^3$
Areal capacity	-	$>15.2 \text{ mAh/cm}^2$
Porosity	Uncontrolled	Controlled
Electrochemical performance	Varies	Enhanced

The extrusion method is profoundly influenced by particle dimensions, requiring careful management and control. A critical aspect that demands precision is the shear rate and temperature [366]. Temperature is a pivotal element; it not only influences the melt viscosity but also affects the flow rate of materials, directly impacting the electrochemical

properties and structural integrity of the LIB's electrodes. The optimal temperature ensures that the active materials and binders meld effectively, ensuring enhanced electrical conductivity and structural cohesion.

The screw configuration is another critical aspect, especially in LIBs. The design and settings of the screw determine the mixing efficiency of the active materials, binders, and conductive additives. A well-optimized screw configuration ensures the uniform distribution of these components, leading to consistent electrochemical performance across the entire electrode surface. The feeding mechanism's role is accentuated in LIB production. A precisely calibrated feeding system is essential to ensure that the correct proportions of active materials, binders, and additives are consistently introduced into the extrusion process. This precision is crucial for maintaining the desired electrochemical properties and ensuring the reliability of the LIBs.

Each technique has its unique advantages and challenges. DSD is noted for its uniform binder distribution and flexibility, polymer fibrillation is known for its compatibility with current commercial LIBs production, and electrodes produced via melt extrusion have good cycling stability, as shown in Table 6.

Table 6. Overview of the processes of polymer fibrillation, dry spray deposition, and extrusion, and their respective characteristics when applied in LIBs. (AC: activated carbon).

Dry Method	Process Description	Active Materials	Binder and Properties	Temperature	Chief Performance	References	Advantages	Disadvantages
Dry spray deposition	Utilizes a spraying gun	NMC, LCO	PVDF Thermoplastic	100–190 °C 250 °C	Increased bonding strength	[22,24]	- Solvent-free	-
		NMC	PVDF Thermoplastic	170 °C	80%: highest capacity retention after 300 cycles (>650 cycles) at a standard thickness of 56 µm.	[319]	- Flexibility	- Equipment compatibility
		NMC	PVDF Thermoplastic	180 °C	Electrodes (up to 200 µm)	[23]	- Uniform coating	- Thickness control
		NMC	PVDF Thermoplastic	200 °C	High molecular weight: PVDF is preferred	[329]	- Favourable electrochemical performance	
Polymer fibrillation	Utilization of fibrillizable PTFE	Graphite	FEP/THV	170–300 °C	New binders. High electrochemical performance	[29]		
		LFP, LTO + 40% AC.	PTFE	160–180 °C	Higher capacity and energy density	[350]	- Solventless	- Binder limitation
		NMC, graphite	PTFE	120 °C	High loading: 5 mAh/cm ² , thick electrode, high-rate capability	[28]	- High loading density	- Electrochemical stability (LUMO)
		Silicon/graphite	PTFE	160–180 °C	Excellent cycle life and high stability of hard and soft carbon	[351]	- Enhanced rate capability	- in PTFE unstable in anodes
		Graphite, hard carbon, soft carbon	PTFE	320–330 °C	100 charge-discharge cycles without artificial pressure, high areal 6.5 mAh/cm ² .	[31]	- Commercial compatibility	
Extrusion and melt process	Extruded to form a continuous, uniform electrode film	LFP	PP PW SA Thermoplastic	160–190 °C	Cathode exhibits good cyclability across 20 cycles at a C/10 rate—high areal capacity (13.7 mAh/cm ⁻²) with 500 µm thickness.	[361]	- No solvent	- Temperature control
		LFP, NMC LTO	PPC elastomeric HNBR	40–90 °C	A new binder, such as HNBR, decreases the viscosity, control of thickness, and porosity.	[364]	- Precise control over porosity and thickness	- Material handling
		NCA, graphite	PPC elastomeric	50–250 °C	Areal capacities over 5 mAh/cm ² at a C/5 rate, large loading range from 4–40 mg/cm ² .	[367]	- Good cycling stability	- The choice of screw configuration

4. Summary

Battery research has increasingly concentrated on the development of electrode materials, reflecting the growing emphasis on LIB production. As the anticipated demand for LIBs escalates, it becomes crucial to ensure that their production is both cost-effective and sustainable. Achieving this goal involves reducing the energy required for battery manufacturing. Consequently, there has been a concerted effort to explore alternatives to conventional wet slurry methods for electrode fabrication, with the aim of finding more energy-efficient and environmentally benign processes. A highly effective strategy for cutting down energy usage in electrode manufacturing is to do away with the use of the NMP solvent, transitioning instead to a dry electrode processing technique. The dry electrode process technology is increasingly recognized as a pivotal advancement for the next generation of batteries, particularly LIBs. The dry-film-production approach streamlines the manufacturing of LIBs by eliminating the traditional solvent mixing, coating, drying, and solvent recovery steps. This reduction in process complexity also results in significant energy and equipment expense savings. As a result, this has greatly improved the efficiency of battery production. Dry process technology is recognized as a transformative innovation in battery manufacturing, offering cost and performance benefits. This review focuses on the development and assessments of this solvent-free technology and also its advantages and disadvantages. A comprehensive comparison of conventional wet and emerging dry processes is presented. While there are more than three distinct solvent-free methods for electrode fabrication, not all of them are suitable for large-scale production. Among these methods, melt extrusion emerges as the most promising alternative to the wet process due to its scalability and compatibility with existing production lines. Melt extrusion solvent-free methods are emerging as a preferred choice for LIB manufacturing, balancing cost, quality, and environmental considerations. The technique's adaptability and efficiency make it a favorable answer to cater to the escalating requirement for high-performance, eco-friendly LIBs. Solid-state batteries represent a promising direction in the quest to achieve higher energy densities, such as the target of 400 Wh/kg. These batteries can be broadly categorized into two types based on the solid electrolyte used: inorganic solid-state batteries and polymer solid-state batteries. Each type has distinct characteristics and strategies for integration into battery systems, especially when considering the implementation of thick electrodes through dry processing techniques. The dry process in LIB manufacturing presents several challenges that need to be addressed to ensure its viability as a replacement for the wet process. Here are some of the key issues:

1. Binder selection: The choice of binder in the dry process is critical because it must provide sufficient cohesion to hold the active materials together without the aid of a solvent. Finding binders that can perform effectively in a dry environment is challenging, as they need to ensure structural integrity and maintain electrical contact between particles.
2. Homogeneity of dry mixtures: Achieving a uniform mixture when combining materials of varying densities and particle sizes is more difficult in a dry process. The absence of a liquid medium can lead to segregation, making it challenging to obtain a consistent and homogenous mix, which is essential for the battery's performance.
3. Cohesion and adhesion: The dry process must ensure that the particles not only stick together (cohesion) but also adhere well to the current collectors (adhesion). Without the use of solvents, which often act as adhesives, maintaining the balance between cohesion and adhesion becomes a complex task.
4. Equipment: Dry processing requires specialized equipment that can handle and mix particulate materials without causing damage or loss regarding material properties. This equipment must also be capable of pressing the mixture into a dense, uniform electrode film, which is a different technical challenge compared to the wet process.
5. Compatibility with existing production lines: One of the significant hurdles is integrating the dry process with current production lines designed for wet processing. The infrastructure for wet processes is well established, and transitioning to dry methods

may require substantial modifications or entirely new manufacturing lines, entailing significant investment and technical redesign.

Author Contributions: M.D.B. and K.Z. designed the structure of the review. M.D.B., K.Z. and A.K.M.R.R. collected the papers related to the topic of the review. M.D.B. and A.K.M.R.R. wrote the review manuscript and Graphics. K.Z., X.L. and S.D. finished the language polishing and corrections. H.L. and A.K.M.R.R. review & editing, figures design. All authors have read and agreed to the published version of the manuscript.

Funding: Concordia University, AI-Moguel and Innove.

Data Availability Statement: Not applicable.

Acknowledgments: We extend our deepest gratitude to AI-Moguel (Montreal, QC, Canada) and Innove (Montreal, QC, Canada) for their generous support, which was instrumental in the realization of this work. We would also like to express our special thanks to Sarah Sajedi, whose significant contributions to the graphic design elements of the project were invaluable and greatly enhanced the quality of our presentation.

Conflicts of Interest: The authors declare that this study received funding from Concordia University, AI-Moguel and Innove that is mentioned in our manuscript. The funder had the following involvement with the study of English editing and graphical design.

Abbreviation

LIBs	Lithium-ion batteries
AM	Active materials
CA	Conductive additives
EVs	Electric vehicles
WP	Wet process
DP	Dry process
NMP	N-Methyl Pyrrolidone
SF	Solvent-free
ASSBs	All-solid-state batteries
NCA	Lithium Nickel Cobalt Aluminum Oxide
LNMO	Lithium Nickel Manganese Oxide
SiO _x	Silicon Oxide
PE	Polyethylene
PP	Polypropylene
ESD	Electrostatic dry spraying deposition
NMC	Lithium-Nickel-Manganese-Cobalt Oxide
DSD	Dry spray deposition
LCO	Lithium-Cobalt-Oxide
MW	Molecular weight
PVDF	Polyvinylidene Fluoride
PTFE	Polytetrafluoroethylene
LFP	Lithium Iron Phosphate
LTO	Lithium titanate oxide
PPC	propylene carbonate
HNBR	Hydrogenated nitrile butadiene rubber
T _g	Glass transition temperature
T _m	Melting temperature
PW	Paraffin wax
SA	Stearic acid
LUMO	Lowest unoccupied molecular orbitals
CNTs	Carbon nanotubes

References

- Toro, L.; Moscardini, E.; Baldassari, L.; Forte, F.; Falcone, I.; Coletta, J.; Toro, L. A Systematic Review of Battery Recycling Technologies: Advances, Challenges, and Future Prospects. *Energies* **2023**, *16*, 6571. [[CrossRef](#)]
- Zheng, M.; Salim, H.; Liu, T.; Stewart, R.A.; Lu, J.; Zhang, S. Intelligence-Assisted Predesign for the Sustainable Recycling of Lithium-Ion Batteries and Beyond. *Energy Environ. Sci.* **2021**, *14*, 5801–5815. [[CrossRef](#)]
- Shu, X.; Guo, Y.; Yang, W.; Wei, K.; Zhu, G. Life-cycle assessment of the environmental impact of the batteries used in pure electric passenger cars. *Energy Rep.* **2021**, *7*, 2302–2315. [[CrossRef](#)]
- Nagaura, T. Lithium ion rechargeable battery. *Prog. Batteries Sol. Cells* **1990**, *9*, 209.
- Broadhead, J.; Gibbard, H.F.; Kuo, H.; Chi, I.; Bowden, W. High-Energy, High-Power Lithium-Ion Rechargeable Cells. In Proceedings of the Symposium on Rechargeable Lithium and Lithium-Ion Batteries; The Electrochemical Society: Pennington, NJ, USA, 1995; Volume 94, p. 370.
- Ram, M.; Aghahosseini, A.; Breyer, C. Job creation during the global energy transition towards 100% renewable power system by 2050. *Technol. Forecast. Soc. Change* **2020**, *151*, 119682. [[CrossRef](#)]
- Degen, F.; Krätzig, O. Future in Battery Production: An Extensive Benchmarking of Novel Production Technologies as Guidance for Decision Making in Engineering. *IEEE Trans. Eng. Manag.* **2022**, *71*, 1038–1056. [[CrossRef](#)]
- Global EV Outlook 2023. Available online: <https://iea.blob.core.windows.net/assets/dacf14d2-eabc-498a-8263-9f97fd5dc327/GEVO2023.pdf> (accessed on 5 May 2023).
- World Economic Forum. A Vision for a Sustainable Battery Value Chain in 2030. Available online: https://www3.weforum.org/docs/WEF_A_Vision_for_a_Sustainable_Battery_Value_Chain_in_2030_Report.pdf (accessed on 9 May 2023).
- Degen, F. Lithium-Ion Battery Cell Production in Europe: Scenarios for Reducing Energy Consumption and Greenhouse Gas Emissions Until 2030. *J. Ind. Ecol.* **2023**, *27*, 964–976. [[CrossRef](#)]
- Musk, E. Tesla Battery Day 2020; Tesla, Inc.: Fremont, CA, USA, 2020. Available online: <https://www.tesla.com/2020/shareholdermeeting> (accessed on 10 May 2023).
- Wang, M.; Dong, X.; Escobar, I.C.; Cheng, Y.T. Lithium Ion Battery Electrodes Made Using Dimethyl Sulfoxide (DMSO) A Green Solvent. *ACS Sustain. Chem. Eng.* **2020**, *8*, 11046–11051. [[CrossRef](#)]
- Haufroid, V.; Jaeger, V.K.; Jeggli, S.; Eisenegger, R.; Bernard, A.; Friedli, D.; Lison, D.; Hotz, P. Biological Monitoring and Health Effects of Low-Level Exposure to N-Methyl-2-Pyrrolidone: A Cross-Sectional Study. *Int. Arch. Occup. Environ. Health* **2014**, *87*, 663–674. [[CrossRef](#)]
- Zhang, R.; Shi, X.; Esan, O.C.; An, L. Organic Electrolytes Recycling From Spent Lithium-Ion Batteries. *Glob. Chall.* **2022**, *6*, 2200050. [[CrossRef](#)]
- Ryu, M.; Hong, Y.K.; Lee, S.Y.; Park, J.H. Ultrahigh Loading Dry-Process for Solvent-Free Lithium-Ion Battery Electrode Fabrication. *Nat. Commun.* **2023**, *14*, 1316. [[CrossRef](#)]
- Chordia, M.; Nordelöf, A.; Ellingsen, L.A.W. Environmental Life Cycle Implications of Upscaling Lithium-Ion Battery Production. *Int. J. Life Cycle Assess.* **2021**, *26*, 2024–2039. [[CrossRef](#)]
- Fernandez-Diaz, L.; Castillo, J.; Sasieta-Barrutia, E.; Arnaiz, M.; Cabello, M.; Judez, X.; Villaverde, A. Mixing Methods for Solid State Electrodes: Techniques, Fundamentals, Recent Advances, and Perspectives. *Chem. Eng. J.* **2023**, *464*, 142469. [[CrossRef](#)]
- Valikangas, J.; Sliz, R.; Silva Santos, H.; Vilmi, P.; Rieppo, L.; Hu, T.; Fabritius, T. Suitable Cathode NMP Replacement for Efficient Sustainable Printed Li-Ion Batteries. *ACS Appl. Energy Mater.* **2022**, *5*, 4047–4058.
- Daniel, C.; Li, J.; Mohanty, D.; Wood, D.L., III. Thick Low-Cost, High-Power Lithium-Ion Electrodes via Aqueous Processing. In Proceedings of the US Department of Energy Hydrogen and Fuel Cells Program Annual Merit Review and Peer Evaluation Meeting, Washington, DC, USA, 6–10 June 2016; Office of Energy Efficiency & Renewable Energy: Washington, DC, USA, 2016.
- Lyckfeldt, O.; Orlenius, J.; Kasvayee, K.A.; Johander, P. Water Based Processing of LiFePO₄/C Cathode Material for Li-Ion Batteries Utilizing Freeze Granulation. *J. Power Sources* **2012**, *213*, 119–127.
- Chen, C.F.; Stein, M., IV; Robles, D.J.; Rhodes, C.; Mukherjee, P.P. Non-Aqueous Electrode Processing and Construction of Lithium-Ion Coin Cells. *JoVE (J. Vis. Exp.)* **2016**, *108*, e53490.
- Ludwig, B.; Zheng, Z.; Shou, W.; Wang, Y.; Pan, H. Solvent-Free Manufacturing of Electrodes for Lithium-Ion Batteries. *Sci. Rep.* **2016**, *6*, 23150. [[CrossRef](#)]
- Liu, J.; Ludwig, B.; Liu, Y.; Zheng, Z.; Wang, F.; Tang, M.; Wang, Y. Scalable Dry Printing Manufacturing to Enable Long-Life and High Energy Lithium-Ion Batteries. *Adv. Mater. Technol.* **2017**, *2*, 1700106. [[CrossRef](#)]
- Ludwig, B.; Liu, J.; Chen, I.M.; Liu, Y.; Shou, W.; Wang, Y.; Pan, H. Understanding Interfacial-Energy-Driven Dry Powder Mixing for Solvent-Free Additive Manufacturing of Li-Ion Battery Electrodes. *Adv. Mater. Interfaces* **2017**, *4*, 1700570. [[CrossRef](#)]
- Wood, D.L., III; Wood, M.; Li, J.; Du, Z.; Ruther, R.E.; Hays, K.A.; Belharouak, I. Perspectives on the Relationship Between Materials Chemistry and Roll-to-Roll Electrode Manufacturing for High-Energy Lithium-Ion Batteries. *Energy Storage Mater.* **2020**, *29*, 254–265. [[CrossRef](#)]
- Kato, Y.; Shiotani, S.; Morita, K.; Suzuki, K.; Hirayama, M.; Kanno, R. All-Solid-State Batteries with Thick Electrode Configurations. *J. Phys. Chem. Lett.* **2018**, *9*, 607–613. [[CrossRef](#)] [[PubMed](#)]
- Shin, J.; Duong, H. Electrochemical Performance of Dry Battery Electrode. *ECS Meet. Abstr.* **2018**, *233*, 365. [[CrossRef](#)]
- Duong, H.; Shin, J.; Yudi, Y. Dry Electrode Coating Technology. In Proceedings of the 48th Power Sources Conference, Denver, CO, USA, 11–14 June 2018; Volume 3, pp. 34–37.

29. Schälicke, G.; Landwehr, I.; Dinter, A.; Pettinger, K.H.; Haselrieder, W.; Kwade, A. Solvent-Free Manufacturing of Electrodes for Lithium-Ion Batteries via Electrostatic Coating. *Energy Technol.* **2020**, *8*, 1900309. [[CrossRef](#)]
30. Shin, J.; Yudi, Y.; Magsino, P.; Wong, W.; Duong, H. Dry Processed Nickel-Rich Layered Transition Metal Oxide Cathode Electrode. *ECS Meet. Abstr.* **2019**, *235*, 317. [[CrossRef](#)]
31. Hippauf, F.; Schumm, B.; Doerfler, S.; Althues, H.; Fujiki, S.; Shiratsuchi, T.; Kaskel, S. Overcoming Binder Limitations of Sheet-Type Solid-State Cathodes Using a Solvent-Free Dry-Film Approach. *Energy Storage Mater.* **2019**, *21*, 390–398. [[CrossRef](#)]
32. Sahore, R.; Wood, D.L., III; Kukay, A.; Grady, K.M.; Li, J.; Belharouak, I. Towards Understanding of Cracking During Drying of Thick Aqueous-Processed LiNi_{0.8}Mn_{0.1}Co_{0.1}O₂ Cathodes. *ACS Sustain. Chem. Eng.* **2020**, *8*, 3162–3169. [[CrossRef](#)]
33. Lacey, S.D.; Walsh, E.D.; Hitz, E.; Dai, J.; Connell, J.W.; Hu, L.; Lin, Y. Highly Compressible, Binderless and Ultrathick Holey Graphene-Based Electrode Architectures. *Nano Energy* **2017**, *31*, 386–392. [[CrossRef](#)]
34. Hawley, W.B.; Parejiya, A.; Bai, Y.; Meyer, H.M., III; Wood, D.L., III; Li, J. Lithium and Transition Metal Dissolution Due to Aqueous Processing in Lithium-Ion Battery Cathode Active Materials. *J. Power Sources* **2020**, *466*, 228315. [[CrossRef](#)]
35. Wu, X.; Xia, S.; Huang, Y.; Hu, X.; Yuan, B.; Chen, S.; Liu, W. High-Performance, Low-Cost, and Dense-Structure Electrodes with High Mass Loading for Lithium-Ion Batteries. *Adv. Funct. Mater.* **2019**, *29*, 1903961. [[CrossRef](#)]
36. Sun, H.; Zhu, J.; Baumann, D.; Peng, L.; Xu, Y.; Shakir, I.; Huang, Y.; Duan, X. Hierarchical 3D Electrodes for Electrochemical Energy Storage. *Nat. Rev. Mater.* **2019**, *4*, 45–60. [[CrossRef](#)]
37. Peng, H.J.; Huang, J.Q.; Cheng, X.B.; Zhang, Q. Review on High-Loading and High-Energy Lithium–Sulfur Batteries. *Adv. Energy Mater.* **2017**, *7*, 1700260. [[CrossRef](#)]
38. Lin, Z.; Liu, T.; Ai, X.; Liang, C. Aligning Academia and Industry for Unified Battery Performance Metrics. *Nat. Commun.* **2018**, *9*, 5262. [[CrossRef](#)] [[PubMed](#)]
39. Duffner, F.; Kronemeyer, N.; Tübke, J.; Leker, J.; Winter, M.; Schmuck, R. Post-Lithium-Ion Battery Cell Production and Its Compatibility with Lithium-Ion Cell Production Infrastructure. *Nat. Energy* **2021**, *6*, 123–134. [[CrossRef](#)]
40. Kim, H.M.; Yoo, B.I.; Yi, J.W.; Choi, M.J.; Yoo, J.K. Solvent-Free Fabrication of Thick Electrodes in Thermoplastic Binders for High Energy Density Lithium-Ion Batteries. *Nanomaterials* **2022**, *12*, 3320. [[CrossRef](#)] [[PubMed](#)]
41. Zhang, M.; Chouchane, M.; Shojaee, S.A.; Winiarski, B.; Liu, Z.; Li, L.; Meng, Y.S. Coupling of Multiscale Imaging Analysis and Computational Modeling for Understanding Thick Cathode Degradation Mechanisms. *Joule* **2023**, *7*, 201–220. [[CrossRef](#)]
42. Liu, K.; Liu, Y.; Lin, D.; Pei, A.; Cui, Y. Materials for Lithium-Ion Battery Safety. *Sci. Adv.* **2018**, *4*, eaas9820. [[CrossRef](#)]
43. Chen, Y.; Kang, Y.; Zhao, Y.; Wang, L.; Liu, J.; Li, Y.; Li, B. A Review of Lithium-Ion Battery Safety Concerns: The Issues, Strategies, and Testing Standards. *J. Energy Chem.* **2021**, *59*, 83–99. [[CrossRef](#)]
44. Li, H.; Peng, L.; Wu, D.; Wu, J.; Zhu, Y.J.; Hu, X. Ultrahigh-Capacity and Fire-Resistant LiFePO₄-Based Composite Cathodes for Advanced Lithium-Ion Batteries. *Adv. Energy Mater.* **2019**, *9*, 1802930. [[CrossRef](#)]
45. Kaur, S.; Santra, S. Application of Guar Gum and its Derivatives as Green Binder/Separator for Advanced Lithium-Ion Batteries. *ChemistryOpen* **2022**, *11*, e202100209. [[CrossRef](#)]
46. Park, C.W.; Lee, J.H.; Seo, J.K.; Ran, W.T.A.; Whang, D.; Hwang, S.M.; Kim, Y.J. Graphene/PVDF Composites for Ni-Rich Oxide Cathodes Toward High-Energy Density Li-Ion Batteries. *Materials* **2021**, *14*, 2271. [[CrossRef](#)]
47. Gaikwad, A.M.; Khau, B.V.; Davies, G.; Hertzberg, B.; Steingart, D.A.; Arias, A.C. A High Areal Capacity Flexible Lithium-Ion Battery with a Strain-Compliant Design. *Adv. Energy Mater.* **2015**, *5*, 1401389. [[CrossRef](#)]
48. Dunn, B.; Kamath, H.; Tarascon, J.M. Electrical Energy Storage for the Grid: A Battery of Choices. *Science* **2011**, *334*, 928–935. [[CrossRef](#)] [[PubMed](#)]
49. Vanpeene, V.; Heitz, A.; Herkendaal, N.; Soucy, P.; Douillard, T.; Roué, L. Transforming Silicon Slag into High-Capacity Anode Material for Lithium-Ion Batteries. *Battery Energy* **2022**, *1*, 20220016. [[CrossRef](#)]
50. Ma, J.; Zhang, H.; Liu, R.; Zhang, W.; Han, S.; Han, J.; Ma, Z.F. In-Situ Processing Nano-Porous Silicon into 3D Conductive Structure as High-Capacity Anode for Lithium-Ion Batteries. *Sci. China Mater.* **2023**, *66*, 493–504. [[CrossRef](#)]
51. Li, J.; Fan, S.; Xiu, H.; Wu, H.; Huang, S.; Wang, S.; Xiong, C. TiO₂-Coated Silicon Nanoparticle Core-Shell Structure for High-Capacity Lithium-Ion Battery Anode Materials. *Nanomaterials* **2023**, *13*, 1144. [[CrossRef](#)] [[PubMed](#)]
52. Peng, J.; Wu, D.; Li, H.; Chen, L.; Wu, F. Long-Life High-Capacity Lithium Battery with Liquid Organic Cathode and Sulfide Solid Electrolyte. *Battery Energy* **2023**, *2*, 20220059. [[CrossRef](#)]
53. Zuluaga-Gómez, C.C.; Plaza-Rivera, C.O.; Tripathi, B.; Katiyar, R.K.; Pradhan, D.K.; Morell, G.; Katiyar, R.S. Holey Graphene/Ferroelectric/Sulfur Composite Cathodes for High-Capacity Lithium–Sulfur Batteries. *ACS Omega* **2023**, *8*, 13097–13108. [[CrossRef](#)]
54. Park, S.H.; King, P.J.; Tian, R.; Boland, C.S.; Coelho, J.; Zhang, C.; Nicolosi, V. High Areal-Capacity Battery Electrodes Enabled by Segregated Nanotube Networks. *Nat. Energy* **2019**, *4*, 560–567. [[CrossRef](#)]
55. Kim, J.H.; Kim, J.M.; Cho, S.K.; Kim, N.Y.; Lee, S.Y. Redox-Homogeneous, Gel Electrolyte-Embedded High-Mass-Loading Cathodes for High-Energy Lithium Metal Batteries. *Nat. Commun.* **2022**, *13*, 2541. [[CrossRef](#)]
56. Sawada, S.; Yoshida, H.; Luski, S.; Markevich, E.; Salitra, G.; Elias, Y.; Aurbach, D. Stable High-Capacity Elemental Sulfur Cathodes with Simple Process for Lithium Sulfur Batteries. *Molecules* **2023**, *28*, 4568. [[CrossRef](#)]
57. Kang, H.J.; Lee, T.G.; Kim, H.; Park, J.W.; Hwang, H.J.; Hwang, H.; Jun, Y.S. Thick Free-Standing Electrode Based on Carbon–Carbon Nitride Microspheres with Large Mesopores for High-Energy-Density Lithium–Sulfur Batteries. *Carbon Energy* **2021**, *3*, 410–423. [[CrossRef](#)]

58. McCloskey, B.D. Attainable Gravimetric and Volumetric Energy Density of Li–S and Li Ion Battery Cells with Solid Separator-Protected Li Metal Anodes. *J. Phys. Chem. Lett.* **2015**, *6*, 4581–4588. [[CrossRef](#)] [[PubMed](#)]
59. Elango, R.; Demortière, A.; De Andrade, V.; Morcrette, M.; Seznec, V. Thick Binder-Free Electrodes for Li-Ion Battery Fabricated Using Templating Approach and Spark Plasma Sintering Reveals High Areal Capacity. *Adv. Energy Mater.* **2018**, *8*, 1703031. [[CrossRef](#)]
60. Hu, L.; La Mantia, F.; Wu, H.; Xie, X.; McDonough, J.; Pasta, M.; Cui, Y. Lithium-Ion Textile Batteries with Large Areal Mass Loading. *Adv. Energy Mater.* **2011**, *1*, 1012–1017. [[CrossRef](#)]
61. Wang, J.S.; Liu, P.; Sherman, E.; Verbrugge, M.; Tataria, H. Formulation and characterization of ultra-thick electrodes for high energy lithium-ion batteries employing tailored metal foams. *J. Power Sources* **2011**, *196*, 8714–8718. [[CrossRef](#)]
62. Peled, E.; Patolsky, F.; Golodnitsky, D.; Freedman, K.; Davidi, G.; Schneier, D. Tissue-like silicon nanowires-based three-dimensional anodes for high-capacity lithium ion batteries. *Nano Lett.* **2015**, *15*, 3907–3916. [[CrossRef](#)]
63. Higgins, T.M.; Park, S.H.; King, P.J.; Zhang, C.; McEvoy, N.; Berner, N.C.; Coleman, J.N. A commercial conducting polymer as both binder and conductive additive for silicon nanoparticle-based lithium-ion battery negative electrodes. *ACS Nano* **2016**, *10*, 3702–3713. [[CrossRef](#)] [[PubMed](#)]
64. Choi, M.J.; Xiao, Y.; Hwang, J.Y.; Belharouak, I.; Sun, Y.K. Novel strategy to improve the Li-storage performance of micro silicon anodes. *J. Power Sources* **2017**, *348*, 302–310. [[CrossRef](#)]
65. Hong, H.; Salem, D.R.; Christensen, G.L.; Yang, R.; Younes, H.A. High Capacity Electrodes. U.S. Patent 11,626,584, 11 April 2023.
66. Wang, M.J.; Kazyak, E.; Dasgupta, N.P.; Sakamoto, J. Transitioning solid-state batteries from lab to market: Linking electro-chemo-mechanics with practical considerations. *Joule* **2021**, *5*, 1371–1390. [[CrossRef](#)]
67. Ye, G.; Zhao, M.; Hou, L.P.; Chen, W.J.; Zhang, X.Q.; Li, B.Q.; Huang, J.Q. Evaluation on a 400 Wh kg^{−1} lithium–sulfur pouch cell. *J. Energy Chem.* **2022**, *66*, 24–29. [[CrossRef](#)]
68. Cerbelaud, M.; Lestriez, B.; Videcoq, A.; Ferrando, R.; Guyomard, D. Understanding the structure of electrodes in Li-ion batteries: A numerical study. *J. Electrochem. Soc.* **2015**, *162*, A1485. [[CrossRef](#)]
69. Zhong, Y.; Yang, M.; Zhou, X.; Zhou, Z. Structural design for anodes of lithium-ion batteries: Emerging horizons from materials to electrodes. *Mater. Horiz.* **2015**, *2*, 553–566. [[CrossRef](#)]
70. Shodiev, A.; Chouchane, M.; Gaberscek, M.; Arcelus, O.; Xu, J.; Oularbi, H.; Franco, A.A. Deconvoluting the benefits of porosity distribution in layered electrodes on the electrochemical performance of Li-ion batteries. *Energy Storage Mater.* **2022**, *47*, 462–471. [[CrossRef](#)]
71. Santoki, J.; Daubner, S.; Schneider, D.; Kamlah, M.; Nestler, B. Effect of tortuosity, porosity, and particle size on phase-separation dynamics of ellipsoid-like particles of porous electrodes: Cahn–Hilliard-type phase-field simulations. *Modell. Simul. Mater. Sci. Eng.* **2021**, *29*, 06501. [[CrossRef](#)]
72. Ragones, H.; Menkin, S.; Kamir, Y.; Gladkikh, A.; Mukra, T.; Kosa, G.; Golodnitsky, D. Towards smart free form-factor 3D printable batteries. *Sustain. Energy Fuels* **2018**, *2*, 1542–1549. [[CrossRef](#)]
73. Tjaden, B.; Brett, D.J.; Shearing, P.R. Tortuosity in electrochemical devices: A review of calculation approaches. *Int. Mater. Rev.* **2018**, *63*, 47–67. [[CrossRef](#)]
74. Nguyen, T.T.; Demortière, A.; Fleutot, B.; Delobel, B.; Delacourt, C.; Cooper, S.J. The electrode tortuosity factor: Why the conventional tortuosity factor is not well suited for quantifying transport in porous Li-ion battery electrodes and what to use instead. *NPJ Comput. Mater.* **2020**, *6*, 123. [[CrossRef](#)]
75. Kuang, Y.; Chen, C.; Kirsch, D.; Hu, L. Thick electrode batteries: Principles, opportunities, and challenges. *Adv. Energy Mater.* **2019**, *9*, 1901457. [[CrossRef](#)]
76. Kaiser, N.; Spannenberger, S.; Schmitt, M.; Cronau, M.; Kato, Y.; Roling, B. Ion transport limitations in all-solid-state lithium battery electrodes containing a sulfide-based electrolyte. *J. Power Sources* **2018**, *396*, 175–181. [[CrossRef](#)]
77. Kehrwald, D.; Shearing, P.R.; Brandon, N.P.; Sinha, P.K.; Harris, S.J. Local tortuosity inhomogeneities in a lithium battery composite electrode. *J. Electrochem. Soc.* **2011**, *158*, A1393. [[CrossRef](#)]
78. Vijayaraghavan, B.; Ely, D.R.; Chiang, Y.M.; García-García, R.; García, R.E. An analytical method to determine tortuosity in rechargeable battery electrodes. *J. Electrochem. Soc.* **2012**, *159*, A548. [[CrossRef](#)]
79. Ebrahimi, A.; Bazylak, A. Lattice Boltzmann Simulation of Tortuous Flow within Stochastic Porous Media and the Examination of the Tortuosity–Porosity Relationship. In Proceedings of the 224th ECS Meeting, San Francisco, CA, USA, 27 October–1 November 2013; Volume 224, p. 1228.
80. Thorat, I.V.; Stephenson, D.E.; Zacharias, N.A.; Zaghib, K.; Harb, J.N.; Wheeler, D.R. Quantifying tortuosity in porous Li-ion battery materials. *J. Power Sources* **2009**, *188*, 592–600. [[CrossRef](#)]
81. Röder, F.; Sonntag, S.; Schröder, D.; Kreuer, U. Simulating the impact of particle size distribution on the performance of graphite electrodes in lithium-ion batteries. *Energy Technol.* **2016**, *4*, 1588–1597. [[CrossRef](#)]
82. Lestaringsih, T.; Sabrina, Q.; Ratri, C.R.; Subhan, A.; Priyono, S. The Effect of LiBOB Addition on Solid Polymer Electrolyte (SPE) Production based PVDF-HFP/TiO₂/LiTFSI on Ionic Conductivity for Lithium-Ion Battery Applications. *J. Kimia Sains Apl.* **2022**, *25*, 13–19. [[CrossRef](#)]
83. Dyartanti, E.R.; Purwanto, A.; Widiasa, I.N.; Susanto, H. Ionic conductivity and cycling stability improvement of PVdF/nano-clay using PVP as polymer electrolyte membranes for LiFePO₄ batteries. *Membranes* **2018**, *8*, 36. [[CrossRef](#)] [[PubMed](#)]

84. Gonçalves, R.; Lanceros-Méndez, S.; Costa, C.M. Electrode fabrication process and its influence in lithium-ion battery performance: State of the art and future trends. *Electrochim. Commun.* **2022**, *135*, 107210. [[CrossRef](#)]
85. Yonaga, A.; Kawauchi, S.; Mori, Y.; Xuanchen, L.; Ishikawa, S.; Nunoshita, K.; Matsunaga, T. Effects of dry powder mixing on electrochemical performance of lithium-ion battery electrode using solvent-free dry forming process. *J. Power Sources* **2023**, *581*, 233466. [[CrossRef](#)]
86. Erabhoina, H.; Thelakkat, M. Tuning of composition and morphology of LiFePO₄ cathode for applications in all solid-state lithium metal batteries. *Sci. Rep.* **2022**, *12*, 5454. [[CrossRef](#)]
87. Keppeler, M.; Tran, H.Y.; Braunwarth, W. The Role of Pilot Lines in Bridging the Gap Between Fundamental Research and Industrial Production for Lithium-Ion Battery Cells Relevant to Sustainable Electromobility: A Review. *Energy Technol.* **2021**, *9*, 2100132. [[CrossRef](#)]
88. Duquesnoy, M.; Liu, C.; Dominguez, D.Z.; Kumar, V.; Ayerbe, E.; Franco, A.A. Machine learning-assisted multi-objective optimization of battery manufacturing from synthetic data generated by physics-based simulations. *Energy Storage Mater.* **2023**, *56*, 50–61. [[CrossRef](#)]
89. Grant, P.S.; Greenwood, D.; Pardikar, K.; Smith, R.; Entwistle, T.; Middlemiss, L.A.; Cumming, D.J. Roadmap on Li-ion battery manufacturing research. *J. Phys. Energy* **2022**, *4*, 042006. [[CrossRef](#)]
90. Chae, B.J.; Song, H.J.; Mun, J.; Yim, T. Effect of Sulfate-based Cathode-Electrolyte Interphases on Electrochemical Performance of Ni-rich Cathode Material. *J. Electrochem. Sci. Technol.* **2020**, *11*, 361–367. [[CrossRef](#)]
91. Liu, Y.; Zhang, R.; Wang, J.; Wang, Y. Current and future lithium-ion battery manufacturing. *iScience* **2021**, *24*, 102332. [[CrossRef](#)] [[PubMed](#)]
92. Wood, D.L.; Quass, J.D.; Li, J.; Ahmed, S.; Ventola, D.; Daniel, C. Technical and economic analysis of solvent-based lithium-ion electrode drying with water and NMP. *Dry. Technol.* **2018**, *36*, 234–244. [[CrossRef](#)]
93. Hawley, W.B.; Meyer, H.M., III; Li, J. Enabling aqueous processing for LiNi_{0.80}Co_{0.15}Al_{0.05}O₂ (NCA)-based lithium-ion battery cathodes using polyacrylic acid. *Electrochim. Acta* **2021**, *380*, 138203. [[CrossRef](#)]
94. Zackrisson, M.; Avellán, L.; Orlenius, J. Life cycle assessment of lithium-ion batteries for plug-in hybrid electric vehicles—Critical issues. *J. Clean. Prod.* **2010**, *18*, 1519–1529. [[CrossRef](#)]
95. N-Methyl-2-Pyrrolidone NMP Solvents for Lithium Battery Applications. Available online: <https://nanografi.com/battery-equipment/n-methyl-2-pyrrolidone-nmp-solvent-for-lithium-battery-cathode-materials-purity-99-90/> (accessed on 9 June 2023).
96. Nelson, P.A.; Ahmed, S.; Gallagher, K.G.; Dees, D.W. *Modeling the Performance and Cost of Lithium-Ion Batteries for Electric-Drive Vehicles*; ANL/CSE-19/2; Argonne National Laboratory: Argonne, IL, USA, 2019.
97. Emilsson, E.; Dahllöf, L. *Lithium-Ion Vehicle Battery Production—Status 2019 on Energy Use, CO₂ Emissions, Use of Metals, Products Environmental Footprint, and Recycling*; IVL Swedish Environmental Research Institute: Stockholm, Sweden, 2019.
98. Sitarek, K.; Stetkiewicz, J.; Wasowicz, W. Evaluation of reproductive disorders in female rats exposed to N-methyl-2-pyrrolidone. *Birth Defects Res. Part B Dev. Reprod. Toxicol.* **2012**, *95*, 195–201. [[CrossRef](#)]
99. Sitarek, K.; Stetkiewicz, J. Assessment of reproductive toxicity and gonadotoxic potential of N-methyl-2-pyrrolidone in male rats. *Int. J. Occup. Med. Environ. Health* **2008**, *21*, 73–80. [[CrossRef](#)]
100. Erakca, M.; Baumann, M.; Bauer, W.; de Biasi, L.; Hofmann, J.; Bold, B.; Weil, M. Energy flow analysis of laboratory scale lithium-ion battery cell production. *iScience* **2021**, *24*, 102437. [[CrossRef](#)]
101. Pettinger, K.H.; Dong, W. When does the operation of a battery become environmentally positive? *J. Electrochem. Soc.* **2016**, *164*, A6274. [[CrossRef](#)]
102. Yuan, C.; Deng, Y.; Li, T.; Yang, F. Manufacturing energy analysis of lithium ion battery pack for electric vehicles. *CIRP Ann.* **2017**, *66*, 53–56. [[CrossRef](#)]
103. Ahmed, S.; Nelson, P.A.; Gallagher, K.G.; Dees, D.W. Energy impact of cathode drying and solvent recovery during lithium-ion battery manufacturing. *J. Power Sources* **2016**, *322*, 169–178. [[CrossRef](#)]
104. Guerfi, A.; Kaneko, M.; Petitclerc, M.; Mori, M.; Zaghib, K. LiFePO₄ water-soluble binder electrode for Li-ion batteries. *J. Power Sources* **2007**, *163*, 1047–1052. [[CrossRef](#)]
105. Cetinkaya, T.; Akbulut, A.; Guler, M.O.; Akbulut, H. A different method for producing a flexible LiMn₂O₄/MWCNT composite electrode for lithium-ion batteries. *J. Appl. Electrochem.* **2014**, *44*, 209–214. [[CrossRef](#)]
106. Huttner, F.; Haselrieder, W.; Kwade, A. The influence of different post-drying procedures on remaining water content and physical and electrochemical properties of lithium-ion batteries. *Energy Technol.* **2020**, *8*, 1900245. [[CrossRef](#)]
107. Bryntesen, S.N.; Kahrom, A.; Lamb, J.J.; Tolstorebров, I.; Burheim, O.S. Experimental Analysis of Drying Kinetics and Quality Aspects of Convection-Dried Cathodes at Laboratory Scale. *Batteries* **2023**, *9*, 96. [[CrossRef](#)]
108. Bryntesen, S.N.; Strømman, A.H.; Tolstorebrov, I.; Shearing, P.R.; Lamb, J.J.; Stokke Burheim, O. Opportunities for the state-of-the-art production of LiB electrodes—A review. *Energies* **2021**, *14*, 1406. [[CrossRef](#)]
109. Rollag, K.; Juarez-Robles, D.; Du, Z.; Wood, D.L., III; Mukherjee, P.P. Drying temperature and capillarity-driven crack formation in aqueous processing of Li-ion battery electrodes. *ACS Appl. Energy Mater.* **2019**, *2*, 4464–4476. [[CrossRef](#)]
110. Du, Z.; Rollag, K.M.; Li, J.; An, S.J.; Wood, M.; Sheng, Y.; Wood, D.L., III. Enabling aqueous processing for crack-free thick electrodes. *J. Power Sources* **2017**, *354*, 200–206. [[CrossRef](#)]

111. Marks, T.; Trussler, S.; Smith, A.J.; Xiong, D.; Dahn, J.R. A guide to Li-ion coin-cell electrode making for academic researchers. *J. Electrochem. Soc.* **2010**, *158*, A51. [[CrossRef](#)]
112. Jaiser, S.; Müller, M.; Baunach, M.; Bauer, W.; Scharfer, P.; Schabel, W. Investigation of film solidification and binder migration during drying of Li-Ion battery anodes. *J. Power Sources* **2016**, *318*, 210–219. [[CrossRef](#)]
113. Stein, M.; Mistry, A.; Mukherjee, P.P. Mechanistic understanding of the role of evaporation in electrode processing. *J. Electrochem. Soc.* **2017**, *164*, A1616. [[CrossRef](#)]
114. Lu, Y.; Zhao, C.Z.; Yuan, H.; Hu, J.K.; Huang, J.Q.; Zhang, Q. Dry electrode technology, the rising star in solid-state battery industrialization. *Mater.* **2022**, *5*, 876–898. [[CrossRef](#)]
115. Li, Y.; Wu, Y.; Wang, Z.; Xu, J.; Ma, T.; Chen, L.; Wu, F. Progress in solvent-free dry-film technology for batteries and supercapacitors. *Mater. Today* **2022**, *55*, 92–109. [[CrossRef](#)]
116. Hood, Z.D.; Mane, A.U.; Sundar, A.; Tepavcevic, S.; Zapol, P.; Eze, U.D.; Connell, J.G. Multifunctional Coatings on Sulfide-Based Solid Electrolyte Powders with Enhanced Processability, Stability, and Performance for Solid-State Batteries. *Adv. Mater.* **2023**, *35*, 2300673. [[CrossRef](#)] [[PubMed](#)]
117. Karabelli, D.; Birke, K.P.; Weeber, M. A performance and cost overview of selected solid-state electrolytes: Race between polymer electrolytes and inorganic sulfide electrolytes. *Batteries* **2021**, *7*, 18. [[CrossRef](#)]
118. Lee, J.; Lee, T.; Char, K.; Kim, K.J.; Choi, J.W. Issues and advances in scaling up sulfide-based all-solid-state batteries. *Acc. Chem. Res.* **2021**, *54*, 3390–3402. [[CrossRef](#)] [[PubMed](#)]
119. Dreger, H.; Bockholt, H.; Haselrieder, W.; Kwade, A. Discontinuous and continuous processing of low-solvent battery slurries for lithium nickel cobalt manganese oxide electrodes. *J. Electron. Mater.* **2015**, *44*, 4434–4443. [[CrossRef](#)]
120. Lopez, J.; Pletscher, S.; Aemisegger, A.; Bucher, C.; Gallou, F. N-butyrylpyrrolidinone as an alternative solvent for solid-phase peptide synthesis. *Org. Process Res. Dev.* **2018**, *22*, 494–503. [[CrossRef](#)]
121. Voropaeva, D.; Novikova, S.; Xu, T.; Yaroslavtsev, A. Polymer electrolytes for LIBs based on perfluorinated sulfocationic Nepem-117 membrane and aprotic solvents. *J. Phys. Chem. B* **2019**, *123*, 10217–10223. [[CrossRef](#)]
122. Zhou, C.; Bag, S.; Lv, B.; Thangadurai, V. Understanding the role of solvents on the morphological structure and Li-ion conductivity of poly(vinylidene fluoride)-based polymer electrolytes. *J. Electrochem. Soc.* **2020**, *167*, 070552. [[CrossRef](#)]
123. Dolzhenko, A.V. Ethyl lactate and its aqueous solutions as sustainable media for organic synthesis. *Sustain. Chem. Pharm.* **2020**, *18*, 100322. [[CrossRef](#)]
124. Sarkar, A.; May, R.; Valmonte, Z.; Marbella, L.E. PolarClean & dimethyl isosorbide: Green matches in formulating cathode slurry. *Energy Adv.* **2022**, *1*, 671–676.
125. Bottino, A.; Capannelli, G.; Munari, S.; Turturro, A. Solubility parameters of poly(vinylidene fluoride). *J. Polym. Sci. Part B Polym. Phys.* **1988**, *26*, 785–794. [[CrossRef](#)]
126. Pastore, B.M.; Savelski, M.J.; Slater, C.S.; Richetti, F.A. Life cycle assessment of N-methyl-2-pyrrolidone reduction strategies in the manufacture of resin precursors. *Clean Technol. Environ. Policy* **2016**, *18*, 2635–2647.
127. Bresser, D.; Buchholz, D.; Moretti, A.; Varzi, A.; Passerini, S. Alternative binders for sustainable electrochemical energy storage—The transition to aqueous electrode processing and bio-derived polymers. *Energy Environ. Sci.* **2018**, *11*, 3096–3127. [[CrossRef](#)]
128. Larcher, D.; Tarascon, J.M. Towards greener and more sustainable batteries for electrical energy storage. *Nat. Chem.* **2015**, *7*, 19–29. [[CrossRef](#)]
129. Doberdò, I.; Löffler, N.; Laszczyński, N.; Cericola, D.; Penazzi, N.; Bodoardo, S.; Passerini, S. Enabling aqueous binders for lithium battery cathodes Carbon coating of aluminum current collector. *J. Power Sources* **2014**, *248*, 1000–1006. [[CrossRef](#)]
130. Wood, D.L., III; Li, J.; Daniel, C. Prospects for reducing the processing cost of lithium-ion batteries. *J. Power Sources* **2015**, *275*, 234–242. [[CrossRef](#)]
131. Hofmann, M.; Kapuschinski, M.; Guntow, U.; Giffin, G.A. Implications of aqueous processing for high energy density cathode materials: Part I. Ni-rich layered oxides. *J. Electrochem. Soc.* **2020**, *167*, 140512. [[CrossRef](#)]
132. Li, C.C.; Lin, Y.S. Interactions between organic additives and active powders in water-based lithium iron phosphate electrode slurries. *J. Power Sources* **2012**, *220*, 413–421. [[CrossRef](#)]
133. Li, J.; Daniel, C.; Wood, D. Materials processing for lithium-ion batteries. *J. Power Sources* **2011**, *196*, 2452–2460. [[CrossRef](#)]
134. Kuenzel, M.; Bresser, D.; Diemant, T.; Carvalho, D.V.; Kim, G.T.; Behm, R.J.; Passerini, S. Complementary strategies toward the aqueous processing of high-voltage LiNi_{0.5}Mn_{1.5}O₄ lithium-ion cathodes. *ChemSusChem* **2018**, *11*, 562–573. [[CrossRef](#)] [[PubMed](#)]
135. Li, J.; Du, Z.; Ruther, R.E.; An, S.J.; David, L.A.; Hays, K.; Wood, D.L. Toward low-cost, high-energy density, and high-power density lithium-ion batteries. *JOM* **2017**, *69*, 1484–1496. [[CrossRef](#)]
136. Radloff, S.; Carbonari, G.; Scurtu, R.G.; Hözlé, M.; Wohlfahrt-Mehrens, M. Advances in the Aqueous Processing of Ni-Rich Positive Electrodes. *Electrochim. Soc. Meet. Abstr.* **2022**, *242*, 284. [[CrossRef](#)]
137. Bauer, W.; Çetinel, F.A.; Müller, M.; Kaufmann, U. Effects of pH control by acid addition at the aqueous processing of cathodes for lithium-ion batteries. *Electrochim. Acta* **2019**, *317*, 112–119. [[CrossRef](#)]
138. Loeffler, N.; Kim, G.T.; Mueller, F.; Diemant, T.; Kim, J.K.; Behm, R.J.; Passerini, S. In situ coating of Li[Ni_{0.33}Mn_{0.33}Co_{0.33}]O₂ particles to enable aqueous electrode processing. *ChemSusChem* **2016**, *9*, 1112–1117. [[CrossRef](#)]
139. Carvalho, D.V.; Loeffler, N.; Kim, G.T.; Marinaro, M.; Wohlfahrt-Mehrens, M.; Passerini, S. Study of water-based lithium titanate electrode processing: The role of pH and binder molecular structure. *Polymers* **2016**, *8*, 276. [[CrossRef](#)]

140. Bichon, M.; Sotta, D.; Dupré, N.; De Vito, E.; Boulineau, A.; Porcher, W.; Lestriez, B. Study of immersion of $\text{LiNi}_{0.5}\text{Mn}_{0.3}\text{Co}_{0.2}\text{O}_2$ material in water for aqueous processing of positive electrode for Li-ion batteries. *ACS Appl. Mater. Interfaces* **2019**, *11*, 18331–18341. [[CrossRef](#)]
141. Belboom, S.; Szöcs, C.; Léonard, A. Environmental impacts of phosphoric acid production using di-hemihydrate process: A Belgian case study. *J. Clean. Prod.* **2015**, *108*, 978–986. [[CrossRef](#)]
142. Liu, J.; Xu, C.; Chen, Z.; Ni, S.; Shen, Z.X. Progress in aqueous rechargeable batteries. *Green Energy Environ.* **2018**, *3*, 20–41. [[CrossRef](#)]
143. Chen, L.; Cao, L.; Ji, X.; Hou, S.; Li, Q.; Chen, J.; Yang, C.; Eidson, N.; Wang, C. Enabling safe aqueous lithium-ion open batteries by suppressing the oxygen reduction reaction. *Nat. Commun.* **2020**, *11*, 2638. [[CrossRef](#)] [[PubMed](#)]
144. Lin, J.; Lin, L.; Qu, S.; Deng, D.; Wu, Y.; Yan, X.; Peng, D. Promising electrode and electrolyte materials for high-energy-density thin-film lithium batteries. *Energy Environ. Mater.* **2022**, *5*, 133–156. [[CrossRef](#)]
145. Bates, J.B.; Dudney, N.J.; Neudecker, B.; Ueda, A.; Evans, C.D. Thin-film lithium and lithium-ion batteries. *Solid State Ion.* **2000**, *135*, 33–45. [[CrossRef](#)]
146. Chiu, K.F. Lithium cobalt oxide thin films deposited at low temperature by ionized magnetron sputtering. *Thin Solid Films* **2007**, *515*, 4614–4618. [[CrossRef](#)]
147. Patil, A.; Patil, V.; Shin, D.W.; Choi, J.W.; Paik, D.S.; Yoon, S.J. Issues and challenges facing rechargeable thin-film lithium batteries. *Mater. Res. Bull.* **2008**, *43*, 1913–1942. [[CrossRef](#)]
148. Reyes Jiménez, A.; Klöpsch, R.; Wagner, R.; Rodehorst, U.C.; Kolek, M.; Nöolle, R.; Placke, T. A step toward high-energy silicon-based thin film lithium-ion batteries. *ACS Nano* **2017**, *11*, 4731–4744. [[CrossRef](#)]
149. Maximov, M.; Nazarov, D.; Rumyantsev, A.; Koshtyai, Y.; Ezhov, I.; Mitrofanov, I.; Popovich, A. Atomic layer deposition of lithium–nickel–silicon oxide cathode material for thin-film lithium-ion batteries. *Energies* **2020**, *13*, 2345. [[CrossRef](#)]
150. Maurel, A.; Grugeon, S.; Armand, M.; Fleutot, B.; Courty, M.; Prashantha, K.; Dupont, L. Overview on lithium-ion battery 3D-printing by means of material extrusion. *ECS Trans.* **2020**, *98*, 3. [[CrossRef](#)]
151. Fu, K.; Wang, Y.; Yan, C.; Yao, Y.; Chen, Y.; Dai, J.; Hu, L. Graphene oxide-based electrode inks for 3D-printed lithium-ion batteries. *Adv. Mater.* **2016**, *28*, 2587–2594. [[CrossRef](#)]
152. Sun, K.; Wei, T.S.; Ahn, B.Y.; Seo, J.Y.; Dillon, S.J.; Lewis, J.A. 3D printing of interdigitated Li-Ion microbattery architectures. *Adv. Mater.* **2013**, *25*, 4539–4543. [[CrossRef](#)] [[PubMed](#)]
153. Foster, C.W.; Down, M.P.; Zhang, Y.; Ji, X.; Rowley-Neale, S.J.; Smith, G.C.; Banks, C.E. 3D printed graphene-based energy storage devices. *Sci. Rep.* **2017**, *7*, 42233. [[CrossRef](#)] [[PubMed](#)]
154. Reyes, C.; Somogyi, R.; Niu, S.; Cruz, M.A.; Yang, F.; Catenacci, M.J.; Wiley, B.J. Three-dimensional printing of a complete lithium-ion battery with fused filament fabrication. *ACS Appl. Energy Mater.* **2018**, *1*, 5268–5279. [[CrossRef](#)]
155. Trembacki, B.; Duoss, E.; Oxberry, G.; Stadermann, M.; Murthy, J. Mesoscale electrochemical performance simulation of 3D interpenetrating lithium-ion battery electrodes. *J. Electrochem. Soc.* **2019**, *166*, A923. [[CrossRef](#)]
156. Wang, Y.; Chen, C.; Xie, H.; Gao, T.; Yao, Y.; Pastel, G.; Hu, L. 3D-printed all-fiber Li-ion battery toward wearable energy storage. *Adv. Funct. Mater.* **2017**, *27*, 1703140. [[CrossRef](#)]
157. Yang, K.; Xie, X.; Du, X.; Zuo, Y.; Zhang, Y. Research on Micromechanical Behavior of Current Collector of Lithium-Ion Batteries Battery Cathode during the Calendering Process. *Processes* **2023**, *11*, 1800. [[CrossRef](#)]
158. Schmitt, M. *Slot Die Coating of Lithium-Ion Battery Electrodes*; KIT Scientific Publishing: Karlsruhe, Germany, 2016.
159. Schmitt, M.; Baunach, M.; Wengeler, L.; Peters, K.; Junges, P.; Scharfer, P.; Schabel, W. Slot-die processing of lithium-ion battery electrodes—Coating window characterization. *Chem. Eng. Process.* **2013**, *68*, 32–37. [[CrossRef](#)]
160. Schmitt, M.; Scharfer, P.; Schabel, W. Slot die coating of lithium-ion battery electrodes: Investigations on edge effect issues for stripe and pattern coatings. *J. Coat. Technol. Res.* **2014**, *11*, 57–63. [[CrossRef](#)]
161. Dahn, J.R.; Zheng, T.; Liu, Y.; Xue, J.S. Mechanisms for lithium insertion in carbonaceous materials. *Science* **1995**, *270*, 590–593. [[CrossRef](#)]
162. Guyomard, D.; Tarascon, J.M. Rechargeable $\text{Li}_{1+x}\text{Mn}_2\text{O}_4/\text{Carbon}$ cells with a new electrolyte composition: Potentiostatic studies and application to practical cells. *J. Electrochem. Soc.* **1993**, *140*, 3071. [[CrossRef](#)]
163. Liu, Z.; Yu, A.; Lee, J.Y. Cycle life improvement of LiMn_2O_4 cathode in rechargeable lithium batteries. *J. Power Sources* **1998**, *74*, 228–233. [[CrossRef](#)]
164. Chen, J.M.; Tsai, C.L.; Yao, C.Y.; Sheu, S.P.; Shih, H.C. Experimental design method applied to Li/LiCoO₂ rechargeable cells. *Mater. Chem. Phys.* **1997**, *51*, 190–194. [[CrossRef](#)]
165. Wentker, M.; Greenwood, M.; Leker, J. A bottom-up approach to lithium-ion battery cost modeling with a focus on cathode active materials. *Energy* **2019**, *12*, 504. [[CrossRef](#)]
166. Manthiram, A. A reflection on lithium-ion battery cathode chemistry. *Nat. Commun.* **2020**, *11*, 1550. [[CrossRef](#)] [[PubMed](#)]
167. Kiemel, S.; Glöser-Chahoud, S.; Waltersmann, L.; Schutzbach, M.; Sauer, A.; Miehe, R. Assessing the application-specific substitutability of lithium-ion battery cathode chemistries based on material criticality, performance, and price. *Resources* **2021**, *10*, 87. [[CrossRef](#)]
168. Torres-Rodríguez, J.S. Reversing Planar Gliding, Microcracking Enhances Performance of Single-Crystalline Ni-Rich Cathode. *MRS Bull.* **2021**, *46*, 560. [[CrossRef](#)]

169. Yi, M.; Li, J.; Fan, X.; Bai, M.; Zhang, Z.; Hong, B.; Lai, Y. Single crystal Ni-rich layered cathodes enabling superior performance in all-solid-state batteries with PEO-based solid electrolytes. *J. Mater. Chem. A* **2021**, *9*, 16787–16797. [[CrossRef](#)]
170. Trevisanello, E.; Ruess, R.; Conforto, G.; Richter, F.H.; Janek, J. Polycrystalline and single crystalline NCM cathode materials—Quantifying particle cracking, active surface area, and lithium diffusion. *Adv. Energy Mater.* **2021**, *11*, 2003400. [[CrossRef](#)]
171. Yu, F.; Wang, Y.; Guo, C.; Liu, H.; Bao, W.; Li, J.; Wang, F. Spinel LiMn₂O₄ cathode materials in wide voltage window: Single-crystalline versus polycrystalline. *Crystals* **2022**, *12*, 317. [[CrossRef](#)]
172. He, S.; Mian, J. The Progress of Carbon Coating Modification on the Surface of Lithium Iron Phosphate Cathode Materials. *Highlights Sci. Eng. Technol.* **2022**, *3*, 43–49. [[CrossRef](#)]
173. Ramasubramanian, B.; Sundarrajan, S.; Chellappan, V.; Reddy, M.V.; Ramakrishna, S.; Zaghib, K. Recent development in carbon-LiFePO₄ cathodes for lithium-ion batteries: A mini review. *Batteries* **2022**, *8*, 133. [[CrossRef](#)]
174. Li, J.; Fleetwood, J.; Hawley, W.B.; Kays, W. From materials to cell: State-of-the-art and prospective technologies for lithium-ion battery electrode processing. *Chem. Rev.* **2021**, *122*, 903–956. [[CrossRef](#)]
175. Chu, B.; Guo, Y.J.; Shi, J.L.; Yin, Y.X.; Huang, T.; Su, H.; Yu, A.; Guo, Y.G.; Li, Y. Cobalt in high-energy-density layered cathode materials for lithium ion batteries. *J. Power Sources* **2022**, *544*, 231873. [[CrossRef](#)]
176. Nitta, N.; Wu, F.; Lee, J.T.; Yushin, G. Li-ion battery materials: Present and future. *Mater. Today* **2015**, *18*, 252–264. [[CrossRef](#)]
177. Sun, H.H.; Ryu, H.H.; Kim, U.H.; Weeks, J.A.; Heller, A.; Sun, Y.K.; Mullins, C.B. Beyond doping and coating: Prospective strategies for stable high-capacity layered Ni-rich cathodes. *ACS Energy Lett.* **2020**, *5*, 1136–1146. [[CrossRef](#)]
178. Ren, Y.; Fan, J.S.; Fu, Y.Z. Recent strategies for improving the performances of rechargeable lithium batteries with sulfur-and oxygen-based conversion cathodes. *Energy Mater.* **2023**, *3*, 300015. [[CrossRef](#)]
179. Yang, X.; Luo, J.; Sun, X. Towards high-performance solid-state Li–S batteries: From fundamental understanding to engineering design. *Chem. Soc. Rev.* **2020**, *49*, 2140–2195. [[CrossRef](#)]
180. Zhou, G.; Chen, H.; Cui, Y. Formulating energy density for designing practical lithium–sulfur batteries. *Nat. Energy* **2022**, *7*, 312–319. [[CrossRef](#)]
181. Zhu, J.; Zou, J.; Cheng, H.; Gu, Y.; Lu, Z. High energy batteries based on sulfur cathode. *Green Energy Environ.* **2019**, *4*, 345–359. [[CrossRef](#)]
182. Lee, J.; Ko, B.; Kang, J.; Chung, Y.; Kim, Y.; Halim, W.; Lee, J.H.; Joo, Y.L. Facile and scalable fabrication of highly loaded sulfur cathodes and lithium–sulfur pouch cells via air-controlled electrospray. *Mater. Today Energy* **2017**, *6*, 255–263. [[CrossRef](#)]
183. Liu, Y.T.; Liu, S.; Li, G.R.; Yan, T.Y.; Gao, X.P. High volumetric energy density sulfur cathode with heavy and catalytic metal oxide host for lithium–sulfur battery. *Adv. Sci.* **2020**, *7*, 1903693. [[CrossRef](#)] [[PubMed](#)]
184. Gao, Y.; Pan, Z.; Sun, J.; Liu, Z.; Wang, J. High-energy batteries: Beyond lithium-ion and their long road to commercialisation. *Nano-Micro Lett.* **2022**, *14*, 94. [[CrossRef](#)]
185. Ye, C.; Zhang, L.; Guo, C.; Li, D.; Vasileff, A.; Wang, H.; Qiao, S.Z. A 3D hybrid of chemically coupled nickel sulfide and hollow carbon spheres for high performance lithium–sulfur batteries. *Adv. Funct. Mater.* **2017**, *27*, 1702524. [[CrossRef](#)]
186. Wei Seh, Z.; Li, W.; Cha, J.J.; Zheng, G.; Yang, Y.; McDowell, M.T.; Hsu, P.C.; Cui, Y. Sulphur–TiO₂ yolk–shell nanoarchitecture with internal void space for long-cycle lithium–sulphur batteries. *Nat. Commun.* **2013**, *4*, 1331. [[CrossRef](#)] [[PubMed](#)]
187. Yang, X.; Yan, N.; Zhou, W.; Zhang, H.; Li, X.; Zhang, H. Sulfur embedded in one-dimensional French fries-like hierarchical porous carbon derived from a metal–organic framework for high performance lithium–sulfur batteries. *J. Mater. Chem. A* **2015**, *3*, 15314–15323. [[CrossRef](#)]
188. Das, D.; Manna, S.; Puravankara, S. Electrolytes, Additives and Binders for NMC Cathodes in Li-Ion Batteries—A Review. *Batteries* **2023**, *9*, 193. [[CrossRef](#)]
189. Muralidharan, N.; Essehli, R.; Hermann, R.P.; Amin, R.; Jafta, C.; Zhang, J.; Belharouak, I. Lithium Iron Aluminum Nickelate, LiNi_xFeyAlzO₂—New Sustainable Cathodes for Next-Generation Cobalt-Free Li-Ion Batteries. *Adv. Mater.* **2020**, *32*, 2002960. [[CrossRef](#)]
190. Sim, R.; Lee, S.; Li, W.; Manthiram, A. Influence of calendering on the electrochemical performance of LiNi_{0.9}Mn_{0.05}Al_{0.05}O₂ cathodes in lithium-ion cells. *ACS Appl. Mater. Interfaces* **2021**, *13*, 42898–42908. [[CrossRef](#)]
191. Li, W.; Lee, S.; Manthiram, A. High-nickel NMA: A cobalt-free alternative to NMC and NCA cathodes for lithium-ion batteries. *Adv. Mater.* **2020**, *32*, 2002718. [[CrossRef](#)]
192. Wood, M.; Li, J.; Ruther, R.E.; Du, Z.; Self, E.C.; Meyer, H.M., III; Deniel, C.; Belharouak, I.; Wood, D.L., III. Chemical stability and long-term cell performance of low-cobalt, Ni-Rich cathodes prepared by aqueous processing for high-energy Li-Ion batteries. *Energy Storage Mater.* **2020**, *24*, 188–197. [[CrossRef](#)]
193. Murdock, B.E.; Toghill, K.E.; Tapia-Ruiz, N. A perspective on the sustainability of cathode materials used in lithium-ion batteries. *Adv. Energy Mater.* **2021**, *11*, 2102028. [[CrossRef](#)]
194. Zeng, W.; Xia, F.; Tian, W.; Cao, F.; Chen, J.; Wu, J.; Song, R.; Mu, S. Single-crystal high-nickel layered cathodes for lithium-ion batteries: Advantages, mechanism, challenges and approaches. *Curr. Opin. Electrochem.* **2022**, *31*, 100831. [[CrossRef](#)]
195. Langdon, J.; Manthiram, A. A perspective on single-crystal layered oxide cathodes for lithium-ion batteries. *Energy Storage Mater.* **2021**, *37*, 143–160. [[CrossRef](#)]
196. Nzereogu, P.U.; Omah, A.D.; Ezema, F.I.; Iwuoha, E.I.; Nwanya, A.C. Anode materials for lithium-ion batteries: A review. *Appl. Surf. Sci. Adv.* **2022**, *9*, 100233. [[CrossRef](#)]

197. Armand, M.; Axmann, P.; Bresser, D.; Copley, M.; Edström, K.; Ekberg, C.; Guyomard, D.; Lestriez, B.; Novák, P.; Zhang, H. Lithium-ion batteries—Current state of the art and anticipated developments. *J. Power Sources* **2020**, *479*, 228708. [[CrossRef](#)]
198. Takada, K.; Inada, T.; Kajiyama, A.; Sasaki, H.; Kondo, S.; Watanabe, M.; Murayama, M.; Kanno, R. Solid-state lithium battery with graphite anode. *Solid State Ion.* **2003**, *158*, 269–274. [[CrossRef](#)]
199. Goldman, A.R.; Rotondo, F.S.; Swallow, J.G. *Lithium ion Battery Industrial Base in the US and Abroad*; Institute for Defense Analyses: Alexandria, VA, USA, 2019; p. 67.
200. Asenbauer, J.; Eisenmann, T.; Kuenzel, M.; Kazzazi, A.; Chen, Z.; Bresser, D. The success story of graphite as a lithium-ion anode material—fundamentals, remaining challenges, and recent developments including silicon (oxide) composites. *Sustain. Energy Fuels* **2020**, *4*, 5387–5416. [[CrossRef](#)]
201. Zhang, H.; Yang, Y.; Ren, D.; Wang, L.; He, X. Graphite as anode materials: Fundamental mechanism, recent progress and advances. *Energy Storage Mater.* **2021**, *36*, 147–170. [[CrossRef](#)]
202. Ghanooni Ahmadabadi, V.; Rahman, M.M.; Chen, Y. A Study on High-Rate Performance of Graphite Nanostructures Produced by Ball Milling as Anode for Lithium-Ion Batteries. *Micromachines* **2023**, *14*, 191. [[CrossRef](#)]
203. Franco Gonzalez, A.; Yang, N.H.; Liu, R.S. Silicon anode design for lithium-ion batteries: Progress and perspectives. *J. Phys. Chem. C* **2017**, *121*, 27775–27787. [[CrossRef](#)]
204. Liang, B.; Liu, Y.; Xu, Y. Silicon-based materials as high capacity anodes for next generation lithium ion batteries. *J. Power Sources* **2014**, *267*, 469–490. [[CrossRef](#)]
205. Li, M.; Gu, J.; Feng, X.; He, H.; Zeng, C. Amorphous-silicon@ silicon oxide/chromium/carbon as an anode for lithium-ion batteries with excellent cyclic stability. *Electrochim. Acta* **2015**, *164*, 163–170. [[CrossRef](#)]
206. Huo, H.; Janek, J. Silicon as emerging anode in solid-state batteries. *ACS Energy Lett.* **2022**, *7*, 4005–4016. [[CrossRef](#)]
207. Zhao, J.; Lu, Z.; Wang, H.; Liu, W.; Lee, H.W.; Yan, K.; Zhuo, D.; Lin, D.; Liu, N.; Cui, Y. Artificial solid electrolyte interphase-protected Li_xSi nanoparticles: An efficient and stable prelithiation reagent for lithium-ion batteries. *J. Am. Chem. Soc.* **2015**, *137*, 8372–8375. [[CrossRef](#)] [[PubMed](#)]
208. Ashuri, M.; He, Q.; Shaw, L.L. Silicon as a potential anode material for Li-ion batteries: Where size, geometry and structure matter. *Nanoscale* **2016**, *8*, 74–103. [[CrossRef](#)] [[PubMed](#)]
209. Chen, T.; Wu, J.; Zhang, Q.; Su, X. Recent advancement of SiO_x based anodes for lithium-ion batteries. *J. Power Sources* **2017**, *363*, 126–144. [[CrossRef](#)]
210. Tzeng, Y.; Chen, R.; He, J.L. Silicon-based anode of lithium ion battery made of nano silicon flakes partially encapsulated by silicon dioxide. *Nanomaterials* **2020**, *10*, 2467. [[CrossRef](#)]
211. Li, Z.; Du, M.; Guo, X.; Zhang, D.; Wang, Q.; Sun, H.; Wang, B.; Wu, Y.A. Research progress of SiO_x-based anode materials for lithium-ion batteries. *Chem. Eng. J.* **2023**, *473*, 145294. [[CrossRef](#)]
212. Sun, M.; Ma, J.; Xu, M.; Yang, H.; Zhang, J.; Wang, C. A Low-Cost SiO_x/C@ Graphite Composite Derived from Oat Husk as an Advanced Anode for High-Performance Lithium-Ion Batteries. *ACS Omega* **2022**, *7*, 15123–15131. [[CrossRef](#)]
213. Kirkaldy, N.; Samieian, M.A.; Offer, G.J.; Marinescu, M.; Patel, Y. Lithium-Ion Battery Degradation: Measuring Rapid Loss of Active Silicon in Silicon–Graphite Composite Electrodes. *ACS Appl. Energy Mater.* **2022**, *5*, 13367–13376. [[CrossRef](#)]
214. Andersen, H.F.; Foss, C.E.L.; Voje, J.; Tronstad, R.; Mokkelbost, T.; Vullum, P.E.; Ulvestad, A.; Kirkengen, M.; Mæhlen, J.P. Silicon-Carbon Composite Anodes from Industrial Battery Grade Silicon. *Sci. Rep.* **2019**, *9*, 14814. [[CrossRef](#)]
215. Hays, K.A.; Ruther, R.E.; Kukay, A.J.; Cao, P.; Saito, T.; Wood, D.L., III; Li, J. What Makes Lithium Substituted Polyacrylic Acid a Better Binder than Polyacrylic Acid for Silicon-Graphite Composite Anodes? *J. Power Sources* **2018**, *384*, 136–144. [[CrossRef](#)]
216. Ratyński, M.; Hamankiewicz, B.; Krajewski, M.; Boczar, M.; Czerwiński, A. The Effect of Compressive Stresses on a Silicon Electrode’s Cycle Life in a Li-Ion Battery. *RSC Adv.* **2018**, *8*, 22546–22551. [[CrossRef](#)] [[PubMed](#)]
217. Moon, J.; Lee, H.C.; Jung, H.; Wakita, S.; Cho, S.; Yoon, J.; Lee, J.; Ueda, A.; Choi, B.; Han, I.T.; et al. Interplay between Electrochemical Reactions and Mechanical Responses in Silicon–Graphite Anodes and Its Impact on Degradation. *Nat. Commun.* **2021**, *12*, 2714. [[CrossRef](#)]
218. Minseong, K.O.; Sujong, C.H.A.E.; Jaephil, C.H.O. Challenges in Accommodating Volume Change of Si Anodes for Li-ion Batteries. *ChemElectroChem* **2015**, *2*, 1645–1651.
219. Wang, H.; Lu, S.H.; Wang, X.; Xia, S.; Chew, H.B. A Review of the Multiscale Mechanics of Silicon Electrodes in High-Capacity Lithium-Ion Batteries. *J. Phys. D Appl. Phys.* **2021**, *55*, 063001. [[CrossRef](#)]
220. Casimir, A.; Zhang, H.; Ogoke, O.; Amine, J.C.; Lu, J.; Wu, G. Silicon-based Anodes for Lithium-Ion Batteries: Effectiveness of Materials Synthesis and Electrode Preparation. *Nano Energy* **2016**, *27*, 359–376. [[CrossRef](#)]
221. Sandhya, C.P.; John, B.; Gouri, C. Lithium Titanate as Anode Material for Lithium-Ion Cells: A Review. *Ionics* **2014**, *20*, 601–620. [[CrossRef](#)]
222. Zaghib, K.; Simoneau, M.; Armand, M.; Gauthier, M. Electrochemical Study of Li₄Ti₅O₁₂ as Negative Electrode for Li-ion Polymer Rechargeable Batteries. *J. Power Sources* **1999**, *81*, 300–305. [[CrossRef](#)]
223. Behi, H.; Karimi, D.; Kalogiannis, T.; He, J.; Patil, M.S.; Muller, J.D.; Berecibar, M. Advanced Hybrid Thermal Management System for LTO Battery Module Under Fast Charging. *Case Stud. Therm. Eng.* **2022**, *33*, 101938. [[CrossRef](#)]
224. Chen, J.; Yang, L.; Fang, S.; Tang, Y. Synthesis of Sawtooth-like Li₄Ti₅O₁₂ Nanosheets as Anode Materials for Li-ion Batteries. *Electrochim. Acta* **2010**, *55*, 6596–6600. [[CrossRef](#)]

225. Jin, X.; Han, Y.; Zhang, Z.; Chen, Y.; Li, J.; Yang, T.; Wang, X.; Li, W.; Han, X.; Jiao, S.; et al. Mesoporous Single-Crystal Lithium Titanate Enabling Fast-Charging Li-Ion Batteries. *Adv. Mater.* **2022**, *34*, 2109356. [[CrossRef](#)] [[PubMed](#)]
226. Tang, Y.; Yang, L.; Fang, S.; Qiu, Z. $\text{Li}_4\text{Ti}_5\text{O}_{12}$ Hollow Microspheres Assembled by Nanosheets as an Anode Material for High-Rate Lithium-Ion Batteries. *Electrochim. Acta* **2009**, *54*, 6244–6249. [[CrossRef](#)]
227. Qasim, K.F.; Mousa, M.A. Physicochemical Properties of Oriented Crystalline Assembled Polyaniline/Metal Doped $\text{Li}_4\text{Ti}_5\text{O}_{12}$ Composites for Li-ion Storage. *J. Inorg. Organomet. Polym. Mater.* **2023**, *33*, 2601–2617. [[CrossRef](#)]
228. Wen, Z.; Huang, S.; Yang, X.; Lin, B. High Rate Electrode Materials for Lithium Ion Batteries. *Solid State Ion.* **2008**, *179*, 1800–1805. [[CrossRef](#)]
229. Ouyang, C.Y.; Zhong, Z.Y.; Lei, M.S. Ab Initio Studies of Structural and Electronic Properties of $\text{Li}_4\text{Ti}_5\text{O}_{12}$ Spinel. *Electrochim. Commun.* **2007**, *9*, 1107–1112. [[CrossRef](#)]
230. Sun, X.; Radovanovic, P.V.; Cui, B. Advances in Spinel $\text{Li}_4\text{Ti}_5\text{O}_{12}$ Anode Materials for Lithium-Ion Batteries. *New J. Chem.* **2015**, *39*, 38–63. [[CrossRef](#)]
231. Xiao, X.; Liu, L.; Zhang, L.; Wang, Q.; Yan, H.; Zhao, B.; An, H. Electrochemical and Transport Properties of Te-Doped $\text{Li}_4\text{Ti}_5\text{O}_{12}$ as Anode Material for Lithium-Ion Half/Full Batteries. *J. Alloys Compd.* **2022**, *897*, 162744. [[CrossRef](#)]
232. Annisa, N.; Orlando, I.; Syahrial, A.Z. Effect of Activated Carbon Addition on Electrochemical Performance of $\text{Li}_4\text{Ti}_5\text{O}_{12}$ /Nano Si Composite as Anode Material for LiB. *IOP Conf. Ser. Mater. Sci. Eng.* **2019**, *553*, 012057. [[CrossRef](#)]
233. Chen, C.; Agrawal, R.; Wang, C. High Performance $\text{Li}_4\text{Ti}_5\text{O}_{12}$ /Si Composite Anodes for Li-ion Batteries. *Nanomaterials* **2015**, *5*, 1469–1480. [[CrossRef](#)]
234. Selinis, P.; Farmakis, F. A Review on the Anode and Cathode Materials for Lithium-Ion Batteries with Improved Subzero Temperature Performance. *J. Electrochem. Soc.* **2022**, *169*, 010526. [[CrossRef](#)]
235. Marinow, A.; Katcharava, Z.; Binder, W.H. Self-Healing Polymer Electrolytes for Next-Generation Lithium Batteries. *Polymers* **2023**, *15*, 1145. [[CrossRef](#)] [[PubMed](#)]
236. Peled, E.; Menkin, S. SEI: Past, Present, and Future. *J. Electrochem. Soc.* **2017**, *164*, A1703. [[CrossRef](#)]
237. Li, Q.; Chen, J.; Fan, L.; Kong, X.; Lu, Y. Progress in Electrolytes for Rechargeable Li-Based Batteries and Beyond. *Green Energy Environ.* **2016**, *1*, 18–42. [[CrossRef](#)]
238. Yao, P.; Yu, H.; Ding, Z.; Liu, Y.; Lu, J.; Lavorgna, M.; Liu, X. Review on Polymer-Based Composite Electrolytes for Lithium Batteries. *Front. Chem.* **2019**, *7*, 522. [[CrossRef](#)] [[PubMed](#)]
239. Goodenough, J.B.; Kim, Y. Challenges for Rechargeable Li Batteries. *Chem. Mater.* **2010**, *22*, 587–603. [[CrossRef](#)]
240. Chattopadhyay, J.; Pathak, T.S.; Santos, D.M. Applications of Polymer Electrolytes in Lithium-Ion Batteries: A Review. *Polymers* **2023**, *15*, 3907. [[CrossRef](#)] [[PubMed](#)]
241. Salado, M.; Lizundia, E. Advances, Challenges, and Environmental Impacts in Metal–Air Battery Electrolytes. *Mater. Today Energy* **2022**, *28*, 101064. [[CrossRef](#)]
242. Barbosa, J.C.; Gonçalves, R.; Costa, C.M.; Lanceros-Méndez, S. Toward Sustainable Solid Polymer Electrolytes for Lithium-Ion Batteries. *ACS Omega* **2022**, *7*, 14457–14464. [[CrossRef](#)]
243. Hall, D.S.; Self, J.; Dahn, J.R. Dielectric Constants for Quantum Chemistry and Li-Ion Batteries: Solvent Blends of Ethylene Carbonate and Ethyl Methyl Carbonate. *J. Phys. Chem. C* **2015**, *119*, 22322–22330. [[CrossRef](#)]
244. Lv, W.; Zhu, C.; Chen, J.; Ou, C.; Zhang, Q.; Zhong, S. High Performance of Low-Temperature Electrolyte for Lithium-Ion Batteries Using Mixed Additives. *Chem. Eng. J.* **2021**, *418*, 129400. [[CrossRef](#)]
245. Bushkova, O.V.; Yaroslavtseva, T.V.; Dobrovolsky, Y.A. New Lithium Salts in Electrolytes for Lithium-Ion Batteries. *Russ. J. Electrochim.* **2017**, *53*, 677–699. [[CrossRef](#)]
246. Younesi, R.; Veith, G.M.; Johansson, P.; Edström, K.; Vegge, T. Lithium Salts for Advanced Lithium Batteries: Li–Metal, Li– O_2 , and Li–S. *Energy Environ. Sci.* **2015**, *8*, 1905–1922. [[CrossRef](#)]
247. Sharova, V. Enhancing the Performance of Lithium Batteries through the Development of Improved Electrolyte Formulation, Formation Protocol, and Graphite Surface Modification. Ph.D. Dissertation, Karlsruher Institut für Technologie (KIT), Karlsruhe, Germany, 2017.
248. Aurbach, D.; Markovsky, B.; Levi, M.D.; Levi, E.; Schechter, A.; Moshkovich, M.; Cohen, Y. New Insights into the Interactions Between Electrode Materials and Electrolyte Solutions for Advanced Nonaqueous Batteries. *J. Power Sources* **1999**, *81*, 95–111. [[CrossRef](#)]
249. Bonilla, M.R.; Daza, F.A.G.; Cortés, H.A.; Carrasco, J.; Akhmatkaya, E. On the Interfacial Lithium Dynamics in $\text{Li}_7\text{La}_3\text{Zr}_2\text{O}_{12}$: Poly(ethylene oxide)(LiTFSI) Composite Polymer-Ceramic Solid Electrolytes Under Strong Polymer Phase Confinement. *J. Colloid Interface Sci.* **2022**, *623*, 870–882. [[CrossRef](#)] [[PubMed](#)]
250. Rodrigo, N.D.; Jayawardhana, C.; Rynearson, L.; Hu, E.; Yang, X.Q.; Lucht, B.L. Use of Ethylene Carbonate Free Ester Solvent Systems with Alternative Lithium Salts for Improved Low-Temperature Performance in $\text{NCM}622\|\text{Graphite}$ Li-ion Batteries. *J. Electrochim. Soc.* **2022**, *169*, 110504. [[CrossRef](#)]
251. Zhang, S.; Xu, K.; Jow, T. Low-Temperature Performance of Li-ion Cells with a LiBF_4 -Based Electrolyte. *J. Solid State Electrochem.* **2003**, *7*, 147–151. [[CrossRef](#)]
252. Zhang, S.S.; Xu, K.; Jow, T.R. Study of LiBF_4 as an Electrolyte Salt for a Li-ion Battery. *J. Electrochim. Soc.* **2002**, *149*, A586. [[CrossRef](#)]

253. Ulihin, A.; Novozhilov, D.; Uvarov, N. Solid Electrolytes in the N-Propyl-N-methyl-pyrrolidinium Tetrafluoroborate—Lithium Tetrafluoroborate System. *Batteries* **2023**, *9*, 167. [CrossRef]
254. Ndruru, S.T.C.L.; Wahyuningrum, D.; Bundjali, B.; Arcana, I.M. Preparation and Characterization of Biopolymer Electrolyte Membranes Based on LiClO₄-Complexed Methyl Cellulose as Lithium-Ion Battery Separator. *J. Eng. Technol. Sci.* **2020**, *52*, 28–50. [CrossRef]
255. Chen, H.P.; Fergus, J.W.; Jang, B.Z. The Effect of Ethylene Carbonate and Salt Concentration on the Conductivity of Propylene Carbonate | Lithium Perchlorate Electrolytes. *J. Electrochem. Soc.* **2000**, *147*, 399. [CrossRef]
256. Maddu, A.; Sulaiman, A.S.; Wahyudi, S.T.; Rifai, A. Enhancing Ionic Conductivity of Carboxymethyl Cellulose-Lithium Perchlorate with Crosslinked Citric Acid as Solid Polymer Electrolytes for Lithium Polymer Batteries. *Int. J. Renew. Energy Dev.* **2022**, *11*. [CrossRef]
257. Schmidt, M.; Heider, U.; Kuehner, A.; Oesten, R.; Jungnitz, M.; Ignat'ev, N.; Sartori, P. Lithium Fluoroalkylphosphates: A New Class of Conducting Salts for Electrolytes for High Energy Lithium-Ion Batteries. *J. Power Sources* **2001**, *97*, 557–560. [CrossRef]
258. Koch, V.R.; Goldman, J.L.; Mattos, C.J.; Mulvaney, M. Specular Lithium Deposits from Lithium Hexafluoroarsenate/Diethyl Ether Electrolytes. *J. Electrochem. Soc.* **1982**, *129*, 1. [CrossRef]
259. Aurbach, D.; Markovsky, B.; Shechter, A.; Ein-Eli, Y.; Cohen, H. A Comparative Study of Synthetic Graphite and Li Electrodes in Electrolyte Solutions Based on Ethylene Carbonate-Dimethyl Carbonate Mixtures. *J. Electrochem. Soc.* **1996**, *143*, 3809. [CrossRef]
260. Nazri, G.; Muller, R.H. Stability of Nonaqueous Electrolytes for Ambient Temperature Rechargeable Lithium Cells. *Chem. Eng. Commun.* **1985**, *38*, 383–391. [CrossRef]
261. Zakiyyah, S.; Lestariningsih, T.; Rifai, A.; Ratri, C.; Sabrina, Q.; Subhan, A.; Slamet, P.; Muhammad, D.; Izha, M.Y. Modification of Lithium Source in LiBOB Salt of LiTFSI-LiBOB Electrolyte to Improve Lithium-Ion Battery Performance. In *AIP Conference Proceedings*; AIP Publishing: New York, NY, USA, 2022; Volume 2652.
262. Liu, Z.; Chai, J.; Xu, G.; Wang, Q.; Cui, G. Functional Lithium Borate Salts and Their Potential Application in High-Performance Lithium Batteries. *Coord. Chem. Rev.* **2015**, *292*, 56–73. [CrossRef]
263. Xue, Z.M.; Sun, B.B.; Zhou, W.; Chen, C.H. A New Lithium Salt with Dihydroxybenzene and Lithium Tetrafluoroborate for Lithium Battery Electrolytes. *J. Power Sources* **2011**, *196*, 8710–8713. [CrossRef]
264. Azeez, F.; Fedkiw, P.S. Conductivity of LiBOB-Based Electrolyte for Lithium-Ion Batteries. *J. Power Sources* **2010**, *195*, 7627–7633. [CrossRef]
265. Tan, S.; Ji, Y.J.; Zhang, Z.R.; Yang, Y. Recent Progress in Research on High-Voltage Electrolytes for Lithium-Ion Batteries. *ChemPhysChem* **2014**, *15*, 1956–1969. [CrossRef]
266. Zhang, S.S.; Jow, T.R.; Amine, K.; Henriksen, G.L. LiPF₆–EC–EMC Electrolyte for Li-ion Battery. *J. Power Sources* **2002**, *107*, 18–23. [CrossRef]
267. Hayamizu, K. Direct Relations Between Ion Diffusion Constants and Ionic Conductivity for Lithium Electrolyte Solutions. *Electrochim. Acta* **2017**, *254*, 101–111. [CrossRef]
268. Zhang, S.S. A Review on the Separators of Liquid Electrolyte Li-ion Batteries. *J. Power Sources* **2007**, *164*, 351–364. [CrossRef]
269. Deimede, V.; Elmasides, C. Separators for Lithium-Ion Batteries: A Review on the Production Processes and Recent Developments. *Energy Technol.* **2015**, *3*, 453–468. [CrossRef]
270. Costa, C.M.; Lee, Y.H.; Kim, J.H.; Lee, S.Y.; Lanceros-Méndez, S. Recent Advances on Separator Membranes for Lithium-Ion Battery Applications: From Porous Membranes to Solid Electrolytes. *Energy Storage Mater.* **2019**, *22*, 346–375. [CrossRef]
271. Heidari, A.A.; Mahdavi, H. Recent Development of Polyolefin-Based Microporous Separators for Li-Ion Batteries: A Review. *Chem. Rec.* **2020**, *20*, 570–595. [CrossRef] [PubMed]
272. Kaimai, N.; Takita, K.; Kono, K.; Funakoa, H. Method of Producing Highly Permeable Microporous Polyolefin Membrane. U.S. Patent 6,153,133, 28 November 2000.
273. Hashimoto, A.; Yagi, K.; Mantoku, H. Porous Film of High Molecular Weight Polyolefin and Process for Producing Same. U.S. Patent 6,048,607, 11 April 2000.
274. Mahdavi, H.; Enayati Nook, M. Commercial, High-Impact Polypropylenes: Composition and Chain Structure as Revealed by Temperature-Gradient Extraction Fractionation. *J. Appl. Polym. Sci.* **2012**, *125*, 1606–1615. [CrossRef]
275. Mahdavi, H.; Nook, M.E. Structure and Morphology of a Commercial High-Impact Polypropylene In-Reactor Alloy Synthesized Using a Spherical Ziegler–Natta Catalyst. *Polymer Int.* **2010**, *59*, 1701–1708. [CrossRef]
276. Xie, Y.; Chen, X.; Han, K.; Xiong, X. Natural Halloysite Nanotubes-Coated Polypropylene Membrane as Dual-Function Separator for Highly Safe Li-ion Batteries with Improved Cycling and Thermal Stability. *Electrochim. Acta* **2021**, *379*, 138182. [CrossRef]
277. Arora, P.; Zhang, Z. Battery Separators. *Chem. Rev.* **2004**, *104*, 4419–4462. [CrossRef]
278. Ji, W.; Jiang, B.; Ai, F.; Yang, H.; Ai, X. Temperature-Responsive Microspheres-Coated Separator for Thermal Shutdown Protection of Lithium Ion Batteries. *RSC Adv.* **2015**, *5*, 172–176. [CrossRef]
279. Santhanagopalan, S.; Zhang, Z. Separators for Lithium-Ion Batteries. In *Lithium-Ion Batteries: Advanced Materials and Technologies*; CRC Press: Boca Raton, FL, USA, 2011; Chapter 197.
280. Lagadec, M.F.; Zahn, R.; Wood, V. Characterization and Performance Evaluation of Lithium-Ion Battery Separators. *Nat. Energy* **2019**, *4*, 16–25. [CrossRef]
281. Gor, G.Y.; Cannarella, J.; Leng, C.Z.; Vishnyakov, A.; Arnold, C.B. Swelling and Softening of Lithium-Ion Battery Separators in Electrolyte Solvents. *J. Power Sources* **2015**, *294*, 167–172. [CrossRef]

282. Parikh, D.; Christensen, T.; Hsieh, C.T.; Li, J. Elucidation of Separator Effect on Energy Density of Li-ion Batteries. *J. Electrochem. Soc.* **2019**, *166*, A3377. [[CrossRef](#)]
283. Peabody, C.; Arnold, C.B. The Role of Mechanically Induced Separator Creep in Lithium-Ion Battery Capacity Fade. *J. Power Sources* **2011**, *196*, 8147–8153. [[CrossRef](#)]
284. Yang, M.; Hou, J. Membranes in Lithium Ion Batteries. *Membranes* **2012**, *2*, 367–383. [[CrossRef](#)]
285. Shi, C.; Zhang, P.; Chen, L.; Yang, P.; Zhao, J. Effect of a Thin Ceramic-Coating Layer on Thermal and Electrochemical Properties of Polyethylene Separator for Lithium-Ion Batteries. *J. Power Sources* **2014**, *270*, 547–553. [[CrossRef](#)]
286. Lee, T.; Kim, W.K.; Lee, Y.; Ryou, M.H.; Lee, Y.M. Effect of Al_2O_3 Coatings Prepared by RF Sputtering on Polyethylene Separators for High-Power Lithium Ion Batteries. *Macromol. Res.* **2014**, *22*, 1190–1195. [[CrossRef](#)]
287. Liu, H.; Xu, J.; Guo, B.; He, X. Effect of $\text{Al}_2\text{O}_3/\text{SiO}_2$ Composite Ceramic Layers on Performance of Polypropylene Separator for Lithium-Ion Batteries. *Ceram. Int.* **2014**, *40*, 14105–14110. [[CrossRef](#)]
288. Greiner, A.; Wendorff, J.H. Electrospinning: A Fascinating Method for the Preparation of Ultrathin Fibers. *Angew. Chem. Int. Ed.* **2007**, *46*, 5670–5703. [[CrossRef](#)]
289. Golodnitsky, D.; Strauss, E.; Peled, E.; Greenbaum, S. On Order and Disorder in Polymer Electrolytes. *J. Electrochem. Soc.* **2015**, *162*, A2551. [[CrossRef](#)]
290. Zhang, X.; Sahraei, E.; Wang, K. Deformation and Failure Characteristics of Four Types of Lithium-Ion Battery Separators. *J. Power Sources* **2016**, *327*, 693–701. [[CrossRef](#)]
291. Lee, Y.; Park, J.; Jeon, H.; Yeon, D.; Kim, B.H.; Cho, K.Y.; Lee, Y.M. In-depth Correlation of Separator Pore Structure and Electrochemical Performance in Lithium-Ion Batteries. *J. Power Sources* **2016**, *325*, 732–738. [[CrossRef](#)]
292. Kalnaus, S.; Wang, Y.; Turner, J.A. Mechanical Behavior and Failure Mechanisms of Li-ion Battery Separators. *J. Power Sources* **2017**, *348*, 255–263. [[CrossRef](#)]
293. Greene, J.P. *Automotive Plastics and Composites: Materials and Processing*; William Andrew: Norwich, UK, 2021.
294. Barbosa, J.C.; Costa, C.M.; Lanceros-Méndez, S. *Polymer-Based Separators for Lithium-Ion Batteries*; In Nanomaterials for Electrochemical Energy Storage Devices; Wiley: Hoboken, NJ, USA, 2019; p. 429.
295. Chang, W.; Dayong, W. LIB Separators and the Recent Technical Progress. *Energy Storage Sci. Technol.* **2016**, *5*, 120.
296. Zhou, X.; Liao, Q.; Bai, T.; Yang, J. Nitrogen-Doped Microporous Carbon from Polyaspartic Acid Bonding Separator for High Performance Lithium-Sulfur Batteries. *J. Electroanal. Chem.* **2017**, *791*, 167–174. [[CrossRef](#)]
297. Zhang, K.; Xiao, W.; Liu, J.; Yan, C. A Novel Self-Binding Composite Separator Based on Poly (Tetrafluoroethylene) Coating for Li-ion Batteries. *Polymers* **2018**, *10*, 1409. [[CrossRef](#)]
298. Zhou, Q.; Zhang, J.; Cui, G. Rigid–Flexible Coupling Polymer Electrolytes toward High-Energy Lithium Batteries. *Macromol. Mater. Eng.* **2018**, *303*, 1800337. [[CrossRef](#)]
299. Saxena, P.; Shukla, P. A Comprehensive Review on Fundamental Properties and Applications of Poly (Vinylidene Fluoride) (PVDF). *Adv. Compos. Hybrid Mater.* **2021**, *4*, 8–26. [[CrossRef](#)]
300. Kim, K.J.; Kim, J.H.; Park, M.S.; Kwon, H.K.; Kim, H.; Kim, Y.J. Enhancement of Electrochemical and Thermal Properties of Polyethylene Separators Coated with Polyvinylidene Fluoride–Hexafluoropropylene Co-Polymer for Li-ion Batteries. *J. Power Sources* **2012**, *198*, 298–302. [[CrossRef](#)]
301. Sousa, R.E.; Kundu, M.; Gören, A.; Silva, M.M.; Liu, L.; Costa, C.M.; Lanceros-Mendez, S. Poly (vinylidene fluoride-co-chlorotrifluoroethylene)(PVDF-CTFE) Lithium-ion Battery Separator Membranes Prepared by Phase Inversion. *RSC Adv.* **2015**, *5*, 90428–90436. [[CrossRef](#)]
302. Pan, J.L.; Zhang, Z.; Zhang, H.; Zhu, P.P.; Wei, J.C.; Cai, J.X.; Yang, Z.Y. Ultrathin and Strong Electrospun Porous Fiber Separator. *ACS Appl. Energy Mater.* **2018**, *1*, 4794–4803. [[CrossRef](#)]
303. Othman, N.; Azahari, N.A.; Ismail, H. Thermal Properties of Polyvinyl Alcohol (PVOH)/Corn Starch Blend Film. *Malays. Polym. J.* **2011**, *6*, 147–154.
304. Xiao, W.; Zhao, L.; Gong, Y.; Liu, J.; Yan, C. Preparation and Performance of Poly (Vinyl Alcohol) Porous Separator for Lithium-Ion Batteries. *J. Membr. Sci.* **2015**, *487*, 221–228. [[CrossRef](#)]
305. Calleja, G.; Jourdan, A.; Ameduri, B.; Habas, J.P. Where is the Glass Transition Temperature of Poly (Tetrafluoroethylene)? A New Approach by Dynamic Rheometry and Mechanical Tests. *Eur. Polym. J.* **2013**, *49*, 2214–2222. [[CrossRef](#)]
306. Xiong, M.; Tang, H.; Wang, Y.; Lin, Y.; Sun, M.; Yin, Z.; Pan, M. Expanded Polytetrafluoroethylene Reinforced Polyvinylidene-fluoride–Hexafluoropropylene Separator with High Thermal Stability for Lithium-Ion Batteries. *J. Power Sources* **2013**, *241*, 203–211. [[CrossRef](#)]
307. Kim, B.G.; Kim, J.S.; Min, J.; Lee, Y.H.; Choi, J.H.; Jang, M.C.; Choi, J.W. A Moisture-and Oxygen-Impermeable Separator for Aprotic Li-O₂ Batteries. *Adv. Funct. Mater.* **2016**, *26*, 1747–1756. [[CrossRef](#)]
308. Luo, H.F.; Qiao, Y.D. Preparation and Characterization of Cellulose Acetate-based Separator for Lithium-ion Batteries. *J. Electrochem.* **2017**, *23*, 9.
309. Jeong, H.S.; Kim, J.H.; Lee, S.Y. A Novel Poly (Vinylidene Fluoride-Hexafluoropropylene)/Poly (Ethylene Terephthalate) Composite Nonwoven Separator with Phase Inversion-Controlled Microporous Structure for a Lithium-Ion Battery. *J. Mater. Chem.* **2010**, *20*, 9180–9186. [[CrossRef](#)]

310. Choi, E.S.; Lee, S.Y. Particle size-dependent, tunable porous structure of a SiO_2 /poly(vinylidene fluoride-hexafluoropropylene)-coated poly(ethylene terephthalate) nonwoven composite separator for a lithium-ion battery. *J. Mater. Chem.* **2011**, *21*, 14747–14754. [[CrossRef](#)]
311. Bierenbaum, H.S.; Isaacson, R.B.; Druin, M.L.; Plovan, S.G. Microporous polymeric films. *Ind. Eng. Chem. Prod. Res. Dev.* **1974**, *13*, 2–9. [[CrossRef](#)]
312. Mun, S.C.; Won, J.H. Manufacturing processes of microporous polyolefin separators for lithium-ion batteries and correlations between mechanical and physical properties. *Crystals* **2021**, *11*, 1013. [[CrossRef](#)]
313. Dai, X.; Zhang, X.; Wen, J.; Wang, C.; Ma, X.; Yang, Y.; Huang, G.; Ye, H.M.; Xu, S. Research progress on high-temperature resistant polymer separators for lithium-ion batteries. *Energy Storage Mater.* **2022**, *51*, 638–659. [[CrossRef](#)]
314. Takita, K.; Kono, K.; Takashima, T.; Okamoto, K. Microporous Polyolefin Membrane and Method of Producing Same. U.S. Patent 5,051,183, 24 September 1991.
315. Yamada, K.; Nakamura, T. Microporous Membranes and Methods for Producing and Using Such Membranes, Assigned to Toray Tonen Specialty. U.S. Patent Application 20110117439A1, 19 May 2011.
316. DeMeuse, M.T. *Polymer-based Separators for Lithium-ion Batteries: Production, Processing, and Properties*; Elsevier: Amsterdam, The Netherlands, 2021.
317. Wu, T.; Wang, K.; Xiang, M.; Fu, Q. Progresses in manufacturing techniques of lithium-ion battery separators in China. *Chin. J. Chem.* **2019**, *37*, 1207–1215. [[CrossRef](#)]
318. Hawley, W.B.; Li, J. Electrode manufacturing for lithium-ion batteries—Analysis of current and next generation processing. *J. Energy Storage* **2019**, *25*, 100862. [[CrossRef](#)]
319. Al-Shroofy, M.; Zhang, Q.; Xu, J.; Chen, T.; Kaur, A.P.; Cheng, Y.T. Solvent-free dry powder coating process for low-cost manufacturing of $\text{LiNi}_{1/3}\text{Mn}_{1/3}\text{Co}_{1/3}\text{O}_2$ cathodes in lithium-ion batteries. *J. Power Sources* **2017**, *352*, 187–193. [[CrossRef](#)]
320. Wang, C.; Yu, R.; Duan, H.; Lu, Q.; Li, Q.; Adair, K.R.; Sun, X. Solvent-free approach for interweaving freestanding and ultrathin inorganic solid electrolyte membranes. *ACS Energy Lett.* **2021**, *7*, 410–416. [[CrossRef](#)]
321. Aranmala, K.; Chanhaew, A.; Rahmawati, M.; Ikhsanudin, M.N.; Meethong, N. Effects of Conductive Agents on Electrochemical Performance of Water-Based $\text{LiNi}_{0.6}\text{Mn}_{0.2}\text{Co}_{0.2}\text{O}_2$ Cathodes for Cylindrical Cell Production of Lithium-Ion Batteries. *Defect Diffus. Forum* **2022**, *417*, 169–176. [[CrossRef](#)]
322. Bi, J.; Du, Z.; Sun, J.; Liu, Y.; Wang, K.; Du, H.; Huang, W. On the Road to the Frontiers of Lithium-Ion Batteries: A Review and Outlook of Graphene Anodes. *Adv. Mater.* **2023**, *35*, 2210734. [[CrossRef](#)]
323. Kirsch, D.J.; Lacey, S.D.; Kuang, Y.; Pastel, G.; Xie, H.; Connell, J.W.; Hu, L. Scalable dry processing of binder-free lithium-ion battery electrodes enabled by holey graphene. *ACS Appl. Energy Mater.* **2019**, *2*, 2990–2997. [[CrossRef](#)]
324. Yan, Z.; Jiang, J.; Zhang, Y.; Yang, D.; Du, N. Scalable and low-cost synthesis of porous silicon nanoparticles as high-performance lithium-ion battery anode. *Mater. Today Nano* **2022**, *18*, 100175. [[CrossRef](#)]
325. Chouchane, M.; Rucci, A.; Lombardo, T.; Ngandjong, A.C.; Franco, A.A. Lithium ion battery electrodes predicted from manufacturing simulations: Assessing the impact of the carbon-binder spatial location on the electrochemical performance. *J. Power Sources* **2019**, *444*, 227285. [[CrossRef](#)]
326. Jaiser, S.; Funk, L.; Baunach, M.; Scharfer, P.; Schabel, W. Experimental investigation into battery electrode surfaces: The distribution of liquid at the surface and the emptying of pores during drying. *J. Colloid Interface Sci.* **2017**, *494*, 22–31. [[CrossRef](#)] [[PubMed](#)]
327. Kallitsis, E.; Korre, A.; Kelsall, G.; Kupfersberger, M.; Nie, Z. Environmental life cycle assessment of the production in China of lithium-ion batteries with nickel-cobalt-manganese cathodes utilising novel electrode chemistries. *J. Clean. Prod.* **2020**, *254*, 120067. [[CrossRef](#)]
328. Zanotto, F.M.; Dominguez, D.Z.; Ayerbe, E.; Boyano, I.; Burmeister, C.; Duquesnoy, M.; Franco, A.A. Data specifications for battery manufacturing digitalization: Current status, challenges, and opportunities. *Batteries Supercaps* **2022**, *5*, e202200224. [[CrossRef](#)]
329. Wang, M.; Hu, J.; Wang, Y.; Cheng, Y.T. The influence of polyvinylidene fluoride (PVDF) binder properties on $\text{LiNi}_{0.33}\text{Co}_{0.33}\text{Mn}_{0.33}\text{O}_2$ (NMC) electrodes made by a dry-powder-coating process. *J. Electrochem. Soc.* **2019**, *166*, A2151. [[CrossRef](#)]
330. Zhang, Y.; Lu, S.; Lou, F.; Yu, Z. Solvent-free lithium iron phosphate cathode fabrication with fibrillation of polytetrafluoroethylene. *Electrochim. Acta* **2023**, *456*, 142469. [[CrossRef](#)]
331. Park, D.W.; Cañas, N.A.; Wagner, N.; Friedrich, K.A. Novel solvent-free direct coating process for battery electrodes and their electrochemical performance. *J. Power Sources* **2016**, *306*, 758–763. [[CrossRef](#)]
332. Helmers, L.; Froböse, L.; Friedrich, K.; Steffens, M.; Kern, D.; Michalowski, P.; Kwade, A. Sustainable Solvent-Free Production and Resulting Performance of Polymer Electrolyte-Based All-Solid-State Battery Electrodes. *Energy Technol.* **2021**, *9*, 2000923. [[CrossRef](#)]
333. Gyulai, A.; Bauer, W.; Ehrenberg, H. Dry Electrode Manufacturing in a Calender: The Role of Powder Premixing for Electrode Quality and Electrochemical Performance. *ACS Appl. Energy Mater.* **2023**, *6*, 5122–5134. [[CrossRef](#)]
334. Tao, R.; Steinhoff, B.; Sawicki, C.H.; Sharma, J.; Sardo, K.; Bishtawi, A.; Li, J. Unraveling the impact of the degree of dry mixing on dry-processed lithium-ion battery electrodes. *J. Power Sources* **2023**, *580*, 233379. [[CrossRef](#)]
335. Bauer, W.; Nötzel, D.; Wenzel, V.; Nirschl, H. Influence of dry mixing and distribution of conductive additives in cathodes for lithium ion batteries. *J. Power Sources* **2015**, *288*, 359–367. [[CrossRef](#)]

336. Bockholt, H.; Haselrieder, W.; Kwade, A. Intensive powder mixing for dry dispersing of carbon black and its relevance for lithium-ion battery cathodes. *Powder Technol.* **2016**, *297*, 266–274. [[CrossRef](#)]
337. Nam, Y.J.; Oh, D.Y.; Jung, S.H.; Jung, Y.S. Toward practical all-solid-state lithium-ion batteries with high energy density and safety: Comparative study for electrodes fabricated by dry-and slurry-mixing processes. *J. Power Sources* **2018**, *375*, 93–101. [[CrossRef](#)]
338. Wenzel, V.; Nirschl, H.; Nötzel, D. Challenges in lithium-ion-battery slurry preparation and potential of modifying electrode structures by different mixing processes. *Energy Technol.* **2015**, *3*, 692–698. [[CrossRef](#)]
339. Yang, J.; Sliva, A.; Banerjee, A.; Dave, R.N.; Pfeffer, R. Dry particle coating for improving the flowability of cohesive powders. *Powder Technol.* **2005**, *158*, 21–33. [[CrossRef](#)]
340. Wenzel, V.; Moeller, R.S.; Nirschl, H. Influence of Mixing Technology and the Potential to Modify the Morphological Properties of Materials used in the Manufacture of Lithium-Ion Batteries. *Energy Technol.* **2014**, *2*, 176–182. [[CrossRef](#)]
341. Mitchell, P.; Zhong, L.; Xi, X.; Zou, B. Dry Particle Based Adhesive and Dry Film and Methods of Making Same. U.S. Patent US20200152987A1, 14 May 2020.
342. Zou, B.; Zhong, L.; Mitchell, P.; Xi, X. Dry-Particle Packaging Systems and Methods of Making Same. U.S. Patent US20060137158A1, 29 June 2006.
343. Mitchell, P.; Zhong, L.; Xi, X. Recyclable Dry Particle Based Adhesive Electrode and Methods of Making Same. U.S. Patent US7342770B2, 11 March 2008.
344. Wu, Y.; Wang, S.; Li, H.; Chen, L.; Wu, F. Progress in thermal stability of all-solid-state-Li-ion-batteries. *InfoMat* **2021**, *3*, 827–853. [[CrossRef](#)]
345. Lu, P.; Liu, L.; Wang, S.; Xu, J.; Peng, J.; Yan, W.; Wang, Q.; Li, H.; Chen, L.; Wu, F. Superior all-solid-state batteries enabled by a gas-phase-synthesized sulfide electrolyte with ultrahigh moisture stability and ionic conductivity. *Adv. Mater.* **2021**, *33*, 2100921. [[CrossRef](#)]
346. Zhang, Z.; Wu, L.; Zhou, D.; Weng, W.; Yao, X. Flexible sulfide electrolyte thin membrane with ultrahigh ionic conductivity for all-solid-state lithium batteries. *Nano Lett.* **2021**, *21*, 5233–5239. [[CrossRef](#)]
347. Jiang, T.; He, P.; Wang, G.; Shen, Y.; Nan, C.W.; Fan, L.Z. Solvent-free synthesis of thin, flexible, nonflammable garnet-based composite solid electrolyte for all-solid-state lithium batteries. *Adv. Energy Mater.* **2020**, *10*, 1903376. [[CrossRef](#)]
348. Thieme, S.; Brückner, J.; Bauer, I.; Oschatz, M.; Borchardt, L.; Althues, H.; Kaskel, S. High capacity micro-mesoporous carbon-sulfur nanocomposite cathodes with enhanced cycling stability prepared by a solvent-free procedure. *J. Mater. Chem. A* **2013**, *1*, 9225–9234. [[CrossRef](#)]
349. Yao, W.; Chouchane, M.; Li, W.; Bai, S.; Liu, Z.; Li, L.; Sayahpour, B.; Shimizu, R.; Raghavendran, G.; Meng, Y.S. A 5 V-class cobalt-free battery cathode with high loading enabled by dry coating. *Energy Environ. Sci.* **2023**, *16*, 1620–1630. [[CrossRef](#)]
350. Zhou, H.; Liu, M.; Gao, H.; Hou, D.; Yu, C.; Liu, C.; Zhang, D.; Wu, J.C.; Yang, J.; Chen, D. Dense integration of solvent-free electrodes for Li-ion supercabattery with boosted low temperature performance. *J. Power Sources* **2020**, *473*, 228553. [[CrossRef](#)]
351. Zhang, Y.; Huld, F.; Lu, S.; Jektvik, C.; Lou, F.; Yu, Z. Revisiting polytetrafluoroethylene binder for solvent-free lithium-ion battery anode fabrication. *Batteries* **2022**, *8*, 57. [[CrossRef](#)]
352. Giles, H.F., Jr.; Mount, E.M., III; Wagner, J.R., Jr. *Extrusion: The Definitive Processing Guide and Handbook*; William Andrew: Norwich, UK, 2004.
353. Crawford, D.E.; Casabán, J. Recent developments in mechanochemical materials synthesis by extrusion. *Adv. Mater.* **2016**, *28*, 5747–5754. [[CrossRef](#)]
354. Thiry, J.; Krier, F.; Evrard, B. A review of pharmaceutical extrusion: Critical process parameters and scaling-up. *Int. J. Pharm.* **2015**, *479*, 227–240. [[CrossRef](#)]
355. Dreger, H.; Haselrieder, W.; Kwade, A. Influence of dispersing by extrusion and calendering on the performance of lithium-ion battery electrodes. *J. Energy Storage* **2019**, *21*, 231–240. [[CrossRef](#)]
356. Gueguen, M.; Billion, M.; Majastre, H. Method of Manufacturing a Multilayer Electrochemical Assembly Comprising an Electrolyte between Two Electrodes, and an Assembly Made Thereby. U.S. Patent US5593462A, 10 September 1997.
357. Jardiel, T.; Sotomayor, M.E.; Levenfeld, B.; Várez, A. Optimization of the Processing of 8-YSZ Powder by Powder Injection Molding for SOFC Electrolytes. *Int. J. Appl. Ceram. Technol.* **2008**, *5*, 574–581. [[CrossRef](#)]
358. Verdier, N.; Foran, G.; Lepage, D.; Prébé, A.; Aymé-Perrot, D.; Dollé, M. Challenges in solvent-free methods for manufacturing electrodes and electrolytes for lithium-based batteries. *Polymers* **2021**, *13*, 323. [[CrossRef](#)]
359. Sotomayor, M.E.; de La Torre-Gamarra, C.; Bucheli, W.; Amarilla, J.M.; Varez, A.; Levenfeld, B.; Sanchez, J.Y. Additive-free Li₄Ti₅O₁₂ thick electrodes for Li-ion batteries with high electrochemical performance. *J. Mater. Chem. A* **2018**, *6*, 5952–5961. [[CrossRef](#)]
360. Sotomayor, M.E.; de La Torre-Gamarra, C.; Levenfeld, B.; Sanchez, J.Y.; Varez, A.; Kim, G.T.; Passerini, S. Ultra-thick battery electrodes for high gravimetric and volumetric energy density Li-ion batteries. *J. Power Sources* **2019**, *437*, 226923. [[CrossRef](#)]
361. de La Torre-Gamarra, C.; Sotomayor, M.E.; Sanchez, J.Y.; Levenfeld, B.; Várez, A.; Laík, B.; Pereira-Ramos, J.P. High mass loading additive-free LiFePO₄ cathodes with 500 μm thickness for high areal capacity Li-ion batteries. *J. Power Sources* **2020**, *458*, 228033. [[CrossRef](#)]
362. Voillequin, B.; Ayme-Perrot, D.; Dufour, B.; Sonntag, P. Anode for a Cell of a Lithium-Ion Battery, Its Manufacturing Process and the Battery Incorporating It. U.S. Patent 9,112,200, 18 August 2015.

363. Voillequin, B.; Ayme-Perrot, D.; Dufour, B.; Sonntag, P. Cathode for a Cell of a Lithium-Ion Battery, Its Manufacturing Process and the Battery Incorporating it. U.S. Patent 9,484,571, 1 November 2016.
364. El Khakani, S.; Verdier, N.; Lepage, D.; Prébé, A.; Aymé-Perrot, D.; Rochefort, D.; Dollé, M. Melt-processed electrode for lithium-ion battery. *J. Power Sources* **2020**, *454*, 227884. [[CrossRef](#)]
365. Zhang, Y.; Lu, S.; Wang, Z.; Volkov, V.; Lou, F.; Yu, Z. Recent technology development in solvent-free electrode fabrication for lithium-ion batteries. *Renew. Sustain. Energy Rev.* **2023**, *183*, 113515. [[CrossRef](#)]
366. Hyvärinen, M.; Jabeen, R.; Kärki, T. The modelling of extrusion processes for polymers—A review. *Polymers* **2020**, *12*, 1306. [[CrossRef](#)]
367. Astafyeva, K.; Dousset, C.; Bureau, Y.; Stalmach, S.L.; Dufour, B. High Energy Li-Ion Electrodes Prepared via a Solventless Melt Process. *Batter. Supercaps* **2020**, *3*, 341–343. [[CrossRef](#)]

Disclaimer/Publisher's Note: The statements, opinions and data contained in all publications are solely those of the individual author(s) and contributor(s) and not of MDPI and/or the editor(s). MDPI and/or the editor(s) disclaim responsibility for any injury to people or property resulting from any ideas, methods, instructions or products referred to in the content.